

UNCLASSIFIED

AD 259 432

*Reproduced
by the*

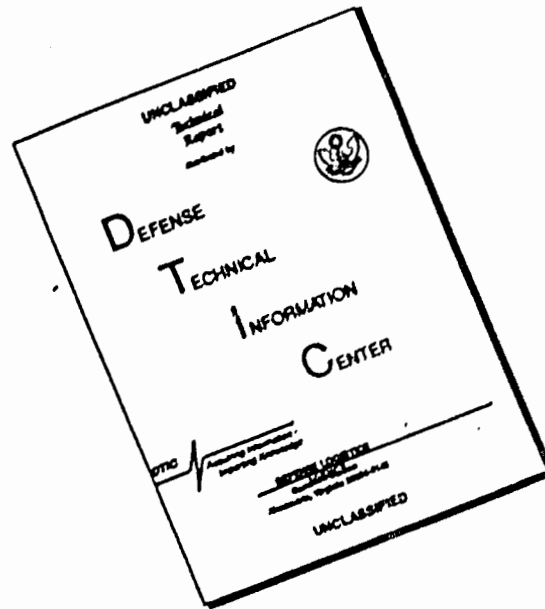
ARMED SERVICES TECHNICAL INFORMATION AGENCY
ARLINGTON HALL STATION
ARLINGTON 12, VIRGINIA



UNCLASSIFIED

NOTICE: When government or other drawings, specifications or other data are used for any purpose other than in connection with a definitely related government procurement operation, the U. S. Government thereby incurs no responsibility, nor any obligation whatsoever; and the fact that the Government may have formulated, furnished, or in any way supplied the said drawings, specifications, or other data is not to be regarded by implication or otherwise as in any manner licensing the holder or any other person or corporation, or conveying any rights or permission to manufacture, use or sell any patented invention that may in any way be related thereto.

DISCLAIMER NOTICE



THIS DOCUMENT IS BEST QUALITY AVAILABLE. THE COPY FURNISHED TO DTIC CONTAINED A SIGNIFICANT NUMBER OF PAGES WHICH DO NOT REPRODUCE LEGIBLY.

Ramjet Technology



NOX

THERMODYNAMICS OF RAMJET FLOW PROCESSES

by F. Bader and E. A. Bunt

Applied Physics Laboratory The Johns Hopkins University
Silver Spring, Maryland



APPLIED PHYSICS LABORATORY

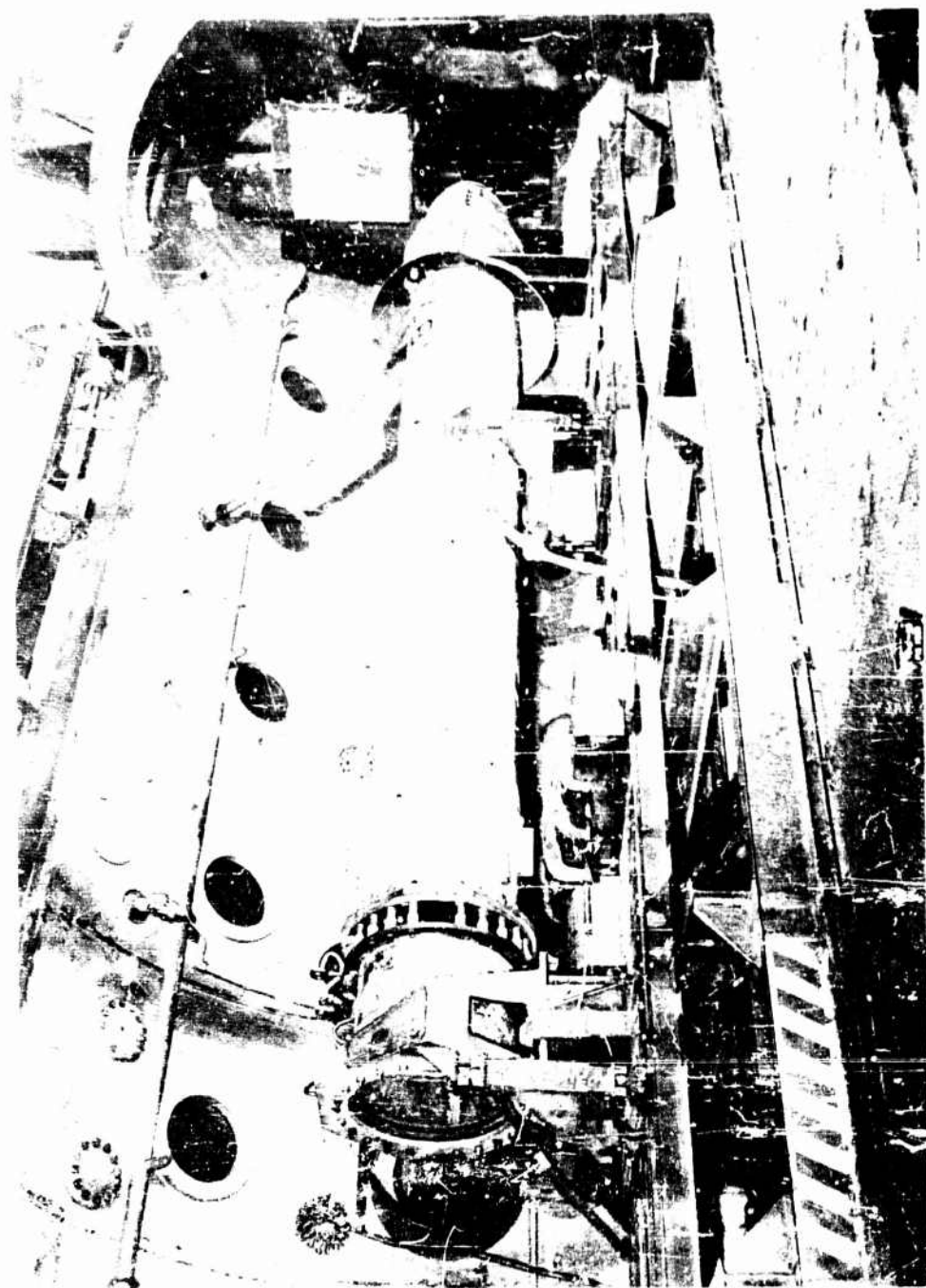
8621 GEORGIA AVENUE • SILVER SPRING, MARYLAND

Operating under Contract NOnr 266 with the Bureau of Naval Weapons, Department of the Navy

240 100

AD NO.
ASTIA 1350

4
1350



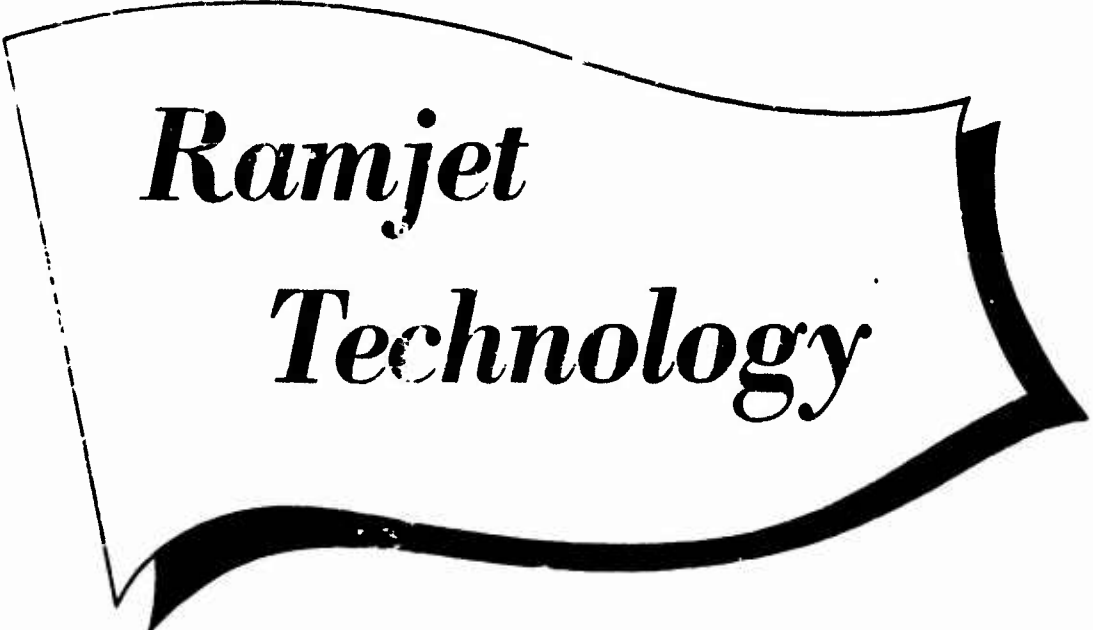
COMPLETE RAMJET ENGINE SET UP IN MACH 2.44 FREE JET TEST CELL

Rate spi shield around nose.

(Courtesy CONVAIR, Daingerfield, Texas)

TG 370-2

Copy No. 20



Ramjet
Technology

**THERMODYNAMICS OF RAMJET
FLOW PROCESSES**

by F. Bader and E. A. Bunt

Applied Physics Laboratory The Johns Hopkins University
Silver Spring, Maryland

Manuscript received for Publication, February 1960.

THE JOHNS HOPKINS UNIVERSITY

APPLIED PHYSICS LABORATORY

8621 GEORGIA AVENUE · SILVER SPRING, MARYLAND

Operating under Contract NOrd 7386 with the Bureau of Naval Weapons, Department of the Navy

TABLE OF CONTENTS

| | |
|---|------|
| List of Illustrations | vii |
| Nomenclature | xiii |
| 1. INTRODUCTION | 1 |
| 2. ONE-DIMENSIONAL GAS DYNAMICS | 5 |
| 2.1 Basic Thermodynamic Relationships | 5 |
| 2.2 The Speed of Sound | 11 |
| 2.3 The Mach Number | 14 |
| 2.4 Isentropic Compressible Flow | 17 |
| 2.5 The Normal Shock | 26 |
| 2.6 Steady Diabatic Flow | 34 |
| 2.7 Thrust and Drag | 41 |
| 3. TWO-DIMENSIONAL SUPERSONIC WAVE SYSTEMS | 51 |
| 3.1 Oblique Shock Waves | 51 |
| 3.2 Prandtl-Meyer Expansions | 58 |
| 3.3 Nozzle Flow and Jet Structure | 63 |
| 3.4 "Supersonic" Combustion | 68 |
| 4. RAMJET COMPONENT PERFORMANCE | 71 |
| 4.1 The Ramjet Thermodynamic Cycle | 71 |
| 4.2 The Diffuser | 75 |
| 4.3 The Combustor | 92 |
| 4.4 The Exit Nozzle | 110 |
| 5. RAMJET PERFORMANCE CALCULATIONS | 121 |
| 5.1 Thrust Performance | 121 |
| 5.2 Optimum Fuel Specific Impulse | 131 |
| 6. ENGINE OPTIMIZATION PROCEDURES | |
| 6.1 Typical Engine Design Calculations | 136 |
| 6.2 Typical Results of Engine Optimization Calculations | 141 |
| Appendix: Tabulation of Mach Number Functions | 153 |
| References | 173 |
| Bibliography | 175 |
| Acknowledgment | 177 |

LIST OF ILLUSTRATIONS

| Figure | | Page |
|--------|---|------|
| 1 | Schematic Diagram of Typical Ramjet Engine, Showing Station Locations | 1 |
| 2 | Variation of $\gamma = (c_p/c_v)$ with Temperature and Pressure | 10 |
| 3 | Definitions for Gas Flow through Weak Shock Wave | 11 |
| 4 | Mach Patterns Set Up by Small Pressure Disturbances Moving at Subsonic and Supersonic Velocities | 15 |
| 5 | Definition of Normal Shock Wave Relations | 27 |
| 6 | Normal Shock Functions (V_2/V_1) and (M_2/M_1), $\gamma = 1.4$ | 30 |
| 7 | Normal Shock Functions (P_2/P_1) and (ρ_2/ρ_1), $\gamma = 1.4$ | 31 |
| 8 | Normal Shock Function (T_2/T_1), $\gamma = 1.4$ | 32 |
| 9 | Normal Shock Function and Isentropic Flow Function of (P_2/P_1) versus (ρ_2/ρ_1), $\gamma = 1.4$ | 32 |
| 10 | Pitot Tube in Supersonic Stream | 33 |
| 11 | Analogy of Diabatic Flow of Air with that in a Duct Having Multiple (Geometric) Throats, Showing Unstable Nature of Decelerating Flow | 39 |
| 12 | Fanno and Rayleigh Lines | 41 |
| 13 | Duct Flow Variables | 42 |
| 14 | Definition of Velocity Vectors across Two-Dimensional Oblique Shock Wave | 52 |
| 15 | Variation of Shock Wave Angle with Upstream Mach Number for Various Flow Deflection Angles | 56 |
| 16 | Reflection and Intersection of Oblique Shock Waves | 59 |
| 17 | Prandtl-Meyer Expansion around Two-Dimensional Corner | 60 |
| 18 | Flow with Normal Shock in Air, $M = 3$ in Laval Nozzle. | 65 |

List of Illustrations

| | | |
|----|---|----|
| 19 | Two-Dimensional Supersonic Jet Structure | 66 |
| 20 | Heavily Underexpanded Nozzle Flow Case | 67 |
| 21 | Strong Standing Detonation Wave (Two-Dimensional Mach Reflected Shock) | 68 |
| 22 | Combustion in Open Jet from Underexpanded Axi- symmetric Nozzle | 68 |
| 23 | Combination Open-Shutter and Schlieren Flash Photo- graph of Flame and Associated Shock-Wave System in Stream below Surface of Wing, Mach Number 2.47; Angle of Attack, 2° | 69 |
| 24 | Thermodynamic Cycle of a Ramjet Engine | 72 |
| 25 | Ramjet Cycle on Ts Diagram | 74 |
| 26 | Pressure, Temperature, Velocity, and Density at Various Stations in a Ramjet Engine | 75 |
| 27 | Subcritical (a), Critical (b), and Supercritical (c) Diffuser Operation | 77 |
| 28 | Fastax Motion Picture Sequence of Flow Instability at Intake of 1/7-Scale Model Ramjet, Showing One-Half Cycle of the Oscillation | 79 |
| 29 | Supercritical Spillover and Additive Drag | 84 |
| 30 | Inlet Capture Area Ratio (A_0/A_1) for Supercritical Spillover, 20° Cone | 87 |
| 31 | Inlet Capture Area Ratio (A_0/A_1) for Supercritical Spillover, 25° Cone | 87 |
| 32 | Inlet Capture Area Ratio (A_0/A_1) for Supercritical Spillover, 30° Cone | 88 |
| 33 | Supercritical Additive Drag Coefficient for 20° Cone | 88 |
| 34 | Supercritical Additive Drag Coefficient for 25° Cone | 89 |
| 35 | Supercritical Additive Drag Coefficient for 30° Cone | 89 |
| 36 | Typical Diffuser Total Pressure Recovery for 25° Conical Diffuser | 91 |
| 37 | Typical Inlet Force Coefficient for 25° Conical Diffuser, (A_1/A_n) = 0.365, A_1 = 225 Square Inches . | 91 |

| | | |
|----|--|-----|
| 38 | Typical Correlation of Diffuser Exit Mach Number and Inlet Air Capture Ratio | 92 |
| 39 | Correlation of Combustor Inlet and Exit Mach Number for Can Combustor | 99 |
| 40 | Can Combustor Gas Dynamic Flow Correlation for Exit Nozzle Throat Area Equal to 65 Per Cent of Combustion Chamber Area | 100 |
| 41 | Can Combustor Gas Dynamic Flow Correlation for Exit Nozzle Throat Area Equal to 70 Per Cent of Combustion Chamber Area | 101 |
| 42 | Theoretical Effective Temperature Rise without Dissociation | 104 |
| 43 | Theoretical Air Specific Impulse, S_a , versus Equivalence Ratio, (E.R.) for Various Inlet Temperatures, T_t | 105 |
| 44 | Typical Combustion Efficiency Correlation for $T_t = 150^\circ\text{F}$ | 107 |
| 45 | Typical Combustion Efficiency Correlation for $T_t = 300^\circ\text{F}$ | 108 |
| 46 | Typical Combustion Efficiency Correlation for $T_t = 450^\circ\text{F}$ | 109 |
| 47 | Theoretical Exit Nozzle Efficiency η_e for Nozzles of Less Than Optimum Length. | 112 |
| 48 | Actual Variation of Thrust with Length of Conical Nozzle of Fixed Area Ratio | 113 |
| 49 | Actual Variation of Thrust of Conical Nozzle with Divergence Angle | 113 |
| 50 | Percentage Loss of Apparent Combustion Efficiency Due to Nonmixed Exit Jet | 119 |
| 51 | Effect of Freestream Mach Number and Engine Temperature Parameter on Thrust Coefficient | 123 |
| 52 | Effect of Freestream Mach Number and Engine Temperature Parameter on Thrust Coefficient and Airflow Capture Area Ratio | 123 |
| 53 | Relationship of Equivalence Ratio to Thrust Coefficient. | 125 |

List of Illustrations:

| | | |
|----|---|-----|
| 54 | Effect of Ambient Temperature on Thrust Coefficient at Constant Altitude of 30,000 Feet and Equivalence Ratio of 0.8 | 126 |
| 55 | Effect of Altitude on Thrust Coefficient for NACA Standard Day, at Constant Equivalent Ratio | 127 |
| 56 | Thrust Coefficient for Various Fuel Flows v_f at Constant Altitude | 128 |
| 57 | Fuel Specific Impulse for Typical Engine with Fixed Inlet and Exit Geometry | 129 |
| 58 | Fuel Specific Impulse for Typical Engine with Variable Inlet and Exit Geometry | 130 |
| 59 | Engine Exit Nozzle Stream Thrust Ratio at Specified Values of the Ratio of Combustion Chamber to Exit Nozzle Throat Areas | 134 |
| 60 | Effect of Burner Drag and Equivalence Ratio on Fuel Specific Impulse, $\eta_d = 0.9$ | 138 |
| 61 | Effect of Burner Drag and Equivalence Ratio on Fuel Specific Impulse, $\eta_d = 0.8$ | 138 |
| 62 | Effect of Burner Drag and Equivalence Ratio on Fuel Specific Impulse, $\eta_d = 0.7$ | 139 |
| 63 | Effect of Burner Drag and Equivalence Ratio on Fuel Specific Impulse, $\eta_d = 0.9$ | 142 |
| 64 | Effect of Burner Drag and Equivalence Ratio on Fuel Specific Impulse, $\eta_d = 0.8$ | 143 |
| 65 | Effect of Burner Drag and Equivalence Ratio on Fuel Specific Impulse, $\eta_d = 0.5$ | 143 |
| 66 | Effect of Flight Mach Number and Diffuser Efficiency on Fuel Specific Impulse | 144 |
| 67 | Experimental Diffuser Recovery Ratios | 145 |
| 68 | Comparison of Fuel Specific Impulse on Different Exit Nozzle Efficiencies | 146 |
| 69 | Optimum Inlet Area Variation with Diffuser Efficiency and Freestream Mach Number | 146 |
| 70 | Variation of Optimum Equivalence Ratio with Freestream Mach Number and Diffuser Efficiency | 147 |
| 71 | Effect of Burner Drag on Fuel Specific Impulse | 148 |

| | | |
|----|---|---------|
| 72 | Variation on Diffuser Mach Number with Burner Drag for Optimum Fuel Specific Impulse | 149 |
| 73 | Effect of Exit Nozzle Efficiency on Optimum Fuel Specific Impulse | 150 |
| 74 | Effect of Thrust Coefficient on Fuel Specific Impulse and Optimum Equivalence Ratio | 151 |
| | Appendix Figs. A-1 through A-17 | 157-174 |

NOMENCLATURE

| | | <u>Units</u> |
|-----------|--|---|
| | Speed of sound | ft sec^{-1} |
| | Gross sectional area | ft^2 |
| | Heat capacity (per unit mass) | $\text{ft}^2 \text{sec}^{-2} (^{\circ}\text{R})^{-1}$ |
| C | Coefficient | -- |
| d | Drain diameter | Lb; ft |
| f/R | Equivalence ratio, $(y_i/y_{i, \text{stoichiometric}})$ -- | -- |
| f | Stream thrust (per unit area) | Lb ft^{-2} |
| | Stream thrust | Lb |
| F | Force; thrust | Lb |
| g | Acceleration of gravity | ft sec^{-2} |
| G | Mass velocity | Lb $\text{ft}^{-2} \text{sec}^{-1}$ |
| H | Enthalpy (per unit mass) | $\text{ft}^2 \text{sec}^{-2}$ |
| I | (Fuel) specific impulse | sec |
| k | Constant | |
| l | Length | ft |
| m | Mass | slug |
| \dot{m} | Mass flow rate | slug sec^{-1} |
| M | Mach number | -- |
| n | Polytropic exponent | -- |
| P | Pressure intensity (static if without suffix) | Lb ft^{-2} |
| q | Dynamic pressure | Lb ft^{-2} |
| Q | Heat (per unit mass) | $\text{ft}^2 \text{sec}^{-2}$ |
| r | Radius | ft |
| R | Gas constant (R , universal--) | $\text{ft}^2 \text{sec}^{-2} (^{\circ}\text{R})^{-1}$ |
| S | Entropy (per unit mass) | $\text{ft}^2 \text{sec}^{-2} (^{\circ}\text{R})^{-1}$ |
| S | Specific impulse | sec |
| t | Time | sec |
| T | Temperature (static if without suffix) | $^{\circ}\text{F}$ or $^{\circ}\text{R}$ |

Nomenclature

| | | |
|---------------|--|---------------------------------------|
| u | Internal energy (per unit mass) | ft ² sec ⁻² |
| v | Specific volume, (1/ρ) | ft ³ slug ⁻¹ |
| V | Velocity | ft sec ⁻¹ |
| w | Weight (under constant gravitational attraction) | Lb |
| \dot{w} | Weight flow rate (under constant gravitational attraction) | Lb sec ⁻¹ |
| $\frac{O}{W}$ | Weight flow function, ($\dot{w} \sqrt{T_t}/AP$) | (OR) ^{1/2} sec ⁻¹ |
| W | Work | ft Lb |
| x | Degrees of freedom | -- |
| X | Distance along x-axis | ft |
| y | Ratio of fuel to air weight flows | -- |
| Z | Compressibility factor | -- |

GREEK

| | | |
|------|--|-----------------------|
| α | Nozzle half-divergence angle | -- |
| γ | Ratio of heat capacities, (c _p /c _v) | -- |
| η | Efficiency | -- |
| θ | Angle of oblique shock wave | -- |
| μ | Area ratio, (A _e /A ₂); Mach angle | -- |
| ν | Prandtl-Meyer turning angle | -- |
| ρ | Mass density | slug ft ⁻³ |
| σ | Fraction of engine throughput initially heated | -- |
| θ(M) | Stream thrust ratio, (f/f*) | -- |
| ω | Cone angle | -- |

SUBSCRIPTS

| | |
|--------|--|
| a | Air |
| actual | Actual |
| add | Additive |
| b | Burner (combustor) |
| c | Combustion; critical; constrictor (nozzle) |

| | |
|-----------------|---|
| d | Diffuser |
| D | Drag |
| e | Exit; exit nozzle (efficiency) |
| eff | Effective |
| ext | External |
| f | Fuel |
| h | Stream thrust |
| F | Thrust |
| G | Gross |
| i | Inlet; i th component |
| ideal | Ideal |
| int | Internal |
| n | Reference |
| N | Normal |
| net | Net |
| o | Over-all |
| ∞ | Freestream |
| out | Outlet |
| p | Constant pressure; propulsion; projected (of area) |
| r | Downstream of spike conical shock |
| s | Stoichiometric |
| t | Stagnation; thermodynamic |
| T | Tangential |
| uni | One-dimensional |
| v | Constant volume |
| w | Wedge |
| 1 | Upstream of shock; cowl lip |
| 2 | Downstream of shock; exit of subsonic diffuser |
| 0,1,2,a,2,b,c,e | Stations along ramjet engine (see Fig. 1) |

SUPERSCRIPTS

- * Throat condition ($M = 1$)
 † Value for iterative process
 A bar (̄) normalizes a velocity by division by a^* .

Nomenclature

STANDARD VALUES OF PARAMETERS

| | |
|----------|--|
| g | $32.174 \text{ ft sec}^{-2}$ |
| R | $1716 \text{ ft}^2 \text{ sec}^{-2} (\text{°R})^{-1}$ for air |
| | $1720 \text{ ft}^2 \text{ sec}^{-2} (\text{°R})^{-1}$ for combustion products (suggested) |
| γ | 7/5 for air |
| | 9/7 for combustion products (suggested) |

In stating units, the Stroud convention of using the abbreviation lb for pound mass, and Lb for pound weight (force) has been followed.

THERMODYNAMICS OF RAMJET FLOW PROCESSES

I. INTRODUCTION

In principle, the ramjet is an air-breathing jet propulsion heat engine which depends for its continued operation on ram compression of the entering air, since it contains no moving parts to effect this process. Figure 1 shows a schematic diagram of a conventional ramjet. However, the constructional simplicity of the fixed geometry

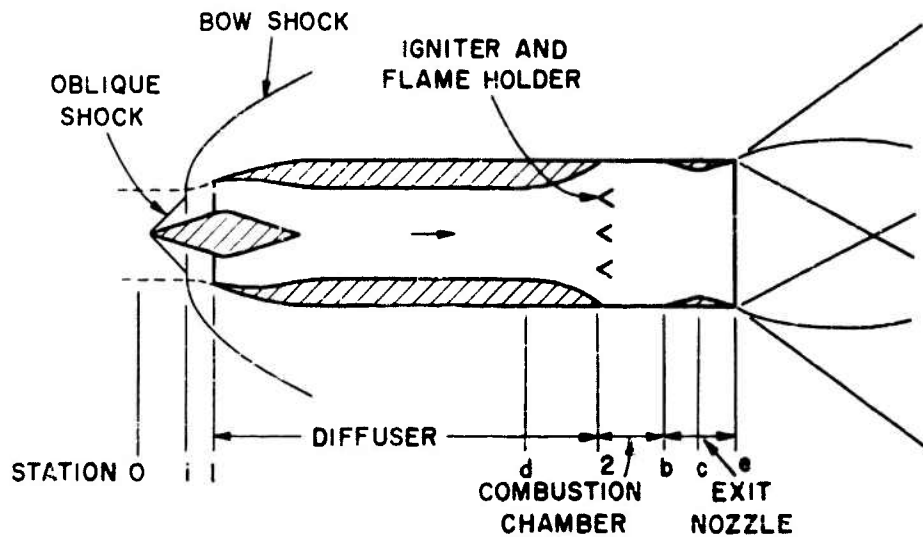


Fig. 1 Schematic Diagram of Typical Ramjet Engine, Showing Station Locations

ramjet somewhat belies the control complexity necessary to ensure successful operation over a wide range of flight speeds and altitudes, as will be emphasized by the various chapters of this volume. The ramjet is primarily a supersonic propulsion device, since at subsonic speeds

its efficiency of operation is very low. In addition, because of its inherent dependence on ram compression, the ramjet cannot produce usable thrust to enable it to start moving under its own power, and it suffers therefore from the disadvantage of needing to be boosted to flight speed by other means, such as by a rocket or turbojet. Thus it cannot form the sole power plant of an aircraft. At present ramjets operate at Mach numbers up to about 3, but it is confidently expected that future developments of hypersonic units may raise this figure to as high as 7 or above. Such a hypersonic ramjet is as yet in the design stage, but the indications are that it will look very different from designs now current. The principles of propulsion, however, will remain much the same.

The performance of a ramjet engine is analyzed by first making a force balance at the exit and inlet in order to find the net thrust. This is generally accomplished by determining the flow by the use of one-dimensional gas dynamic theory at both stations and then integrating the forces acting on corresponding areas. The net thrust is generally converted into a dimensionless coefficient (the thrust coefficient) by dividing it by the product of an engine reference area and the freestream dynamic pressure. Performance is also a function of compression, expansion, and temperature ratios. The use of a fixed exit design for an engine eliminates the variable of expansion ratio and makes possible a convenient plot of performance as a function of compression ratio as derived from the flight Mach number and the engine temperature function referred to later (this last quantity is not a dimensionless ratio). Analytical estimation of the performance of a ramjet engine and the determination of its optimum design cannot readily be accomplished. The flow of air through an engine is set by the parameters of heat addition to the combustion chamber and the exit nozzle throat area, and the equations relating exit and inlet conditions are usually of a complex implicit nature. Accordingly, calculations initially set out to relate conditions at the combustion chamber inlet to those at the exit nozzle throat, and diffuser performance characteristics are then used to determine the diffuser inlet conditions on the requirement that the flow at the diffuser exit match that at the combustion chamber inlet.

A certain amount of introductory thermodynamic theory is presented in Sections 2 and 3 of this TG since the application of this material is discussed in Section 3 onwards. Fuel and flow controls are discussed in more detail in TG 370-5 and -6 as fuel system design considerations are an outgrowth of propulsion requirements; such devices when properly designed are not subject to 'feedback' from the engine proper. Other aspects of component performance will be discussed in more detail in TG 370-4 on Diffusers, in TG 370-7 through -12 on Combustion Systems and in TG 370-13 on Exit Nozzles. In general, this TG will attempt to relate theory to practice, and engine performance to that of its components. (Unfortunately, however, much otherwise suitable material has had to be withheld as it has not yet been published in the open literature.) Consistent energy units are used throughout, so that use of the conversion factor J (the mechanical equivalent of heat) is not needed. The symbols used are in accord with the A.S.A. List of Preferred Symbols as far as possible.

II ONE-DIMENSIONAL GAS DYNAMICS

A brief and nonrigorous development of useful gas flow relationships is here presented, both for familiarization of the novice, and as a working reference. Such flow is first considered from the one-dimensional aspect, i.e., with constant properties across a plane perpendicular to the direction of flow. (More strictly, one-dimensional flow may be thought of as that in which the component of velocity at right angles to the direction of the average velocity at any cross section may be assumed to be negligible.) More rigorous treatment of one-dimensional flow does not appear justified as real flows are never truly one-dimensional, but are treated as such only to make the analysis tractable. Relevant flow phenomena that do not fall into the one-dimensional category are then considered in due course.

In general the treatment is concerned with ideal nonviscous flows, since these constitute a large part of the subject matter of fluid mechanics, and does not refer to the nonuniformities introduced by, for example, the growth of the more slowly moving boundary layers which form adjacent to a solid surface, and in which the fluid velocity is progressively reduced to zero. (It is usually possible to deal separately with such viscous effects, and then fit them into the main flow field.) Certain boundary layer effects will, however, be referred to later in connection with the subject of flow through nozzles.

2.1 Basic Thermodynamic Relationships

Any analysis of the working fluid requires consideration of the following fundamental laws:

1. Conservation of Matter: $\rho A V = \text{constant}$.

2. Newton's Laws of Motion:
 - (a) Matter at rest remains at rest or in uniform motion unless acted upon by external forces.
 - (b) The rate of change of momentum of a body is proportional to the applied force and takes place in the direction of that force. This definition is applicable to a fluid.
 - (c) To every action there is an equal and opposite reaction. (This implies that forces never occur singly, but that every force on a body is exerted by applying an equal and opposite force to another body.)
3. The First Law of Thermodynamics: All energy is conserved; when energy in one form disappears, an equal amount of energy reappears in another form.
4. The Second Law of Thermodynamics: Heat will not of its own accord flow from a cold to a hot body. Heat will therefore flow only where there is a favorable temperature differential. This law governs the behavior of all heat engines since these depend for their operation on the flow of heat into and out of a working fluid.
5. (a) The perfect gas law

$$P = \rho R T, \text{ and}$$

- (b) The adiabatic (and isentropic) law

$$P/\rho^\gamma = \text{constant}.$$

Both the perfect gas law and the adiabatic law are idealized representations of the observed behavior of gases. The departure from the perfect gas law is often taken care of by expressing

$$\frac{P}{\rho R T} = Z,$$

where Z is a compressibility factor which may differ from unity. R is used here in preference to the universal gas constant \mathcal{R} (to which it is related by the equation

$$R = \frac{\mathcal{R}}{\text{mol. weight}})$$

Since present applications deal essentially with the same fluid. For the case of nonisentropic flow of gases, the adiabatic law is considered to be a particular case of the polytropic law

$$P/\rho^n = \text{constant},$$

where n may have various values. When $n < \gamma$, heat flow takes place into the fluid during an expansion process, and when $n > \gamma$, heat flow takes place away from it. If $n = 1$, the equation represents an isothermal flow case.

The main problem to be considered in ramjet flow analysis is that of tracing the one-dimensional gas stream in terms of its state parameters through various flow transformations. If gas initially at a state A is transformed into a new state B, its final state will be a function both of its initial state and of the process through which it will have passed. Some processes are easy to follow because one can relate the initial and final stream states by equating the difference of state to the prescribed change; if there is no change of state this difference is zero. Analysis therefore depends upon the determination of the stream states for such processes at various points.

The obvious intrinsic properties of a gas are mass, volume, and pressure or temperature (since these latter may be related to each other by the perfect gas law). If the gas is in motion, it possesses kinetic energy; it also possesses potential energy by virtue of its pressure and volume, but its gravitational energy of position is normally negligible. Four independent variables are thus required to describe completely the state of the working fluid--the physical constants of the gas apart. The two familiar thermodynamic variables, pressure and temperature, may be replaced by point stream properties which are uniquely related to them. One may thus establish new thermodynamic state properties by manipulation of the equations stating the basic laws. For example, the First Law of Thermodynamics states

that in general a quantity Q of heat added to unit mass of a gas increases the internal thermal energy u and performs mechanical work W . This is expressed in differential form as

$$dQ = du + dW.$$

Mechanical work may be expressed in terms of force and distance as

$$dW = (\text{Force}) ds$$

$$\text{But Force} = PA.$$

$$\therefore dW = PA ds = P dv$$

$$\text{whence} \quad dQ = du + P dv \quad (1)$$

For ideal gases the internal energy u is a function of temperature only, yielding the relationship

$$dQ = c_v dT + P dv. \quad (2)$$

As it stands, this differential equation is not directly integrable, since it has not yet been established what portion of the added heat increases the internal energy of the body and what portion is converted to mechanical work. It may be shown from the Second Law, however, that the right hand side of the equation may be made an 'exact' differential by dividing by the temperature, i.e.,

$$\begin{aligned} \frac{dQ}{T} &= c_v \frac{dT}{T} + \frac{P}{T} dv. \\ \therefore \int_{Q_1}^{Q_2} \frac{dQ}{T} &= \int_{T_1}^{T_2} c_v \frac{dT}{T} + \int_{v_1}^{v_2} \frac{R}{v} dv = \int_{s_1}^{s_2} ds. \end{aligned} \quad (3)$$

This equation defines a quantity s , called entropy, which is thus shown to be a function of the thermodynamic state of the system, and

which in fact determines whether or not the flow may be regarded as reversible ($\Delta s = 0$). A reversible adiabatic process is therefore isentropic. Conversely, an irreversible adiabatic process is non-isentropic.

If the heat addition be specified to occur at constant pressure, Eq. (1) is directly integrable since P will not then be a function of v :

$$\int_{P \text{ constant}} dQ = \int_{u_1}^{u_2} du + \int_{v_1}^{v_2} P dv = \left[H \right]_{H_1}^{H_2} .$$

$$\therefore H = u + Pv. \quad (4)$$

The quantity H so defined is known as enthalpy, which thus represents the heat absorbed by a body at constant pressure. By definition, $c_p = \left(\frac{\partial H}{\partial T} \right)_P$. Since H and s are two independent functions involving T , P , and v , they also serve to define the thermodynamic state of a system. The above relations are essentially thermodynamic ones, since they presuppose that the system has attained thermodynamic equilibrium. At very high flow velocities, this is not necessarily the case.

Many thermodynamic calculations can be considerably simplified if it is assumed that the heat capacities c_p and c_v remain constant as the temperature varies, which would be so if all the internal energy of the gas existed in the form of translational energy of the molecules. In combustion processes, however, temperatures are high enough for the internal energy to exist in the rotational and vibrational forms. The variation of $\gamma (= c_p/c_v)$ with temperature is therefore of some importance, and kinetic theory shows that γ should be given by

$$\gamma = 1 + \frac{2}{x} ,$$

where x is the number of degrees of freedom of the gas molecule - 3 for monatomic gases, 5 for diatomic gases, and 6 for polyatomic gases. The corresponding theoretical values of γ are thus 1.67, 1.40 and 1.33. For the case of air, the value of 1.40 is very nearly correct at low temperatures and pressures, the value for O_2 being slightly lower and that for N_2 slightly greater. (The value for combustion products differs somewhat.) The effect of pressure on the value of γ , particularly within the relatively low pressure range at which the ramjet engine operates, i.e., less than about 200 psia, is small. Figure 2 shows the variation of γ with temperature and pressure (Ref. 1).¹ The value of 1.40 is a convenient one, in that its use results in

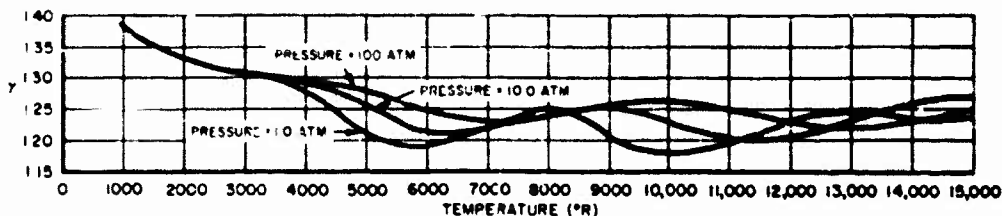


Fig. 2 Variation of γ (c_p , c_v) with Temperature and Pressure

the exponents common in various Mach number functions referred to below having whole number values, for example,

$$\frac{2\gamma}{\gamma - 1} = 7, \quad \frac{2}{\gamma - 1} = 5, \quad \text{and} \quad \frac{\gamma + 1}{2(\gamma - 1)} = 3.$$

$\gamma = 1.40$ has therefore also been incorporated as a basic parameter into the International Standard Atmosphere. Although for the sake of simplifying analyses many relatively simple empirical equations have been proposed to express c_p and c_v as functions of temperature, these equations can at best yield only average values over certain ranges of temperature. It is therefore preferable to use actual data, particularly as the burden of handling this material can be alleviated to a large

¹References may be found on page 173.

extent by the use of computers with large storage capacities. (In practice, a computer would store all the equilibrium constants, vibrational properties, and moments of inertia, and then utilize a program to calculate the thermodynamic constants as needed.)

2.2 The Speed of Sound

This is a parameter of major significance in defining the nature of high speed fluid flow. A derivation is accordingly presented here, the starting points being Newton's Second Law and the Law of Conservation of Matter. Consider first a moving coordinate system which has the same velocity as a weak shock or sound wave (a small pressure discontinuity moving at the speed of sound) so that the wave becomes stationary with respect to the moving coordinates. If the wave is taken as being propagated from right to left with respect to the gas at rest, then in the moving coordinate system there is a flow of gas from left to right through the wave. Since this wave is considered one-dimensional, i.e., planar, it extends theoretically to infinity in a direction normal to that of propagation. Under these conditions there is thus no change along the wave normal to the flow direction; furthermore, a stream tube entering from the left must retain the same cross section and the mass rate of flow through it remains constant, even though velocity, density, temperature, and pressure may change as the tube passes through the wave front, as in Fig. 3.

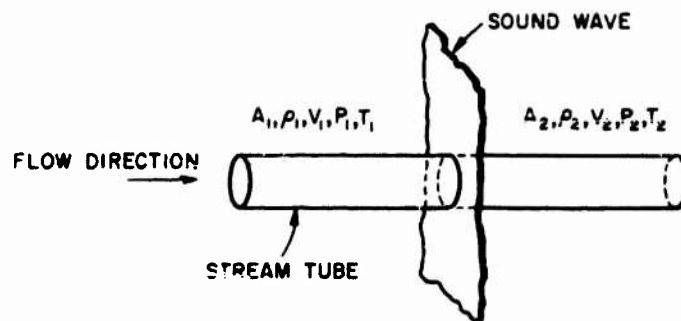


Fig. 3 Definitions for Gas Flow through Weak Shock Wave

By Newton's Third Law, the forces acting from the left on the sound wave must balance those acting from the right. The reactions on the two sides are therefore respectively the sums of the pressure forces and the rates of change of momentum:

$$A_1 P_1 + \frac{d}{dt} (m_1 V_1) = A_2 P_2 + \frac{d}{dt} (m_2 V_2)$$

for steady flow.

V_1 and V_2 are constant with time at fixed locations and their derivatives are thus zero.

$$\therefore A_1 P_1 + V_1 \frac{dm_1}{dt} = A_2 P_2 + V_2 \frac{dm_2}{dt}.$$

The mass rates of flow, dm/dt , are given by the Equation of Continuity, or of Conservation of Matter:

$$\frac{dm_1}{dt} = A_1 \rho_1 V_1 \quad \text{and} \quad \frac{dm_2}{dt} = A_2 \rho_2 V_2.$$

$$\therefore A_1 P_1 + V_1 (A_1 \rho_1 V_1) = A_2 P_2 + V_2 (A_2 \rho_2 V_2)$$

$$\text{or } A(P + \rho V^2) = \text{constant.}$$

This latter will be referred to as the momentum equation. The quantity $A(P + \rho V^2)$ is constant along any stream tube, in the absence of wall forces, and can be differentiated to determine how P , ρ , and V vary as the flow passes through the sound wave. For a constant area stream tube,

$$A(dP + 2 V \rho dV + V^2 d\rho) = 0, \tag{5}$$

but

$$A \rho V = \text{constant.}$$

Differentiating the last expression,

$$A(\rho dV + V d\rho) = 0 \quad (6)$$

Inserting Eq. (6) into Eq (5),

$$A(dP - 2 V^2 d\rho + V^2 d\rho) = 0 ,$$

and solving for V^2 ,

$$V^2 = \frac{dP}{d\rho} . \quad (7)$$

If the flow velocity is high enough for there to be negligible heat conduction from the wave front, the flow will be adiabatic, for which

$$\frac{P}{\rho^\gamma} = \text{constant},$$

or

$$dP = \gamma \frac{P}{\rho} d\rho ,$$

so that

$$V = \sqrt{\gamma \frac{P}{\rho}} ,$$

which for ideal gases gives

$$V = \sqrt{\gamma R T}$$

$$= a, \text{ the speed of sound.} \quad (8)$$

γ is here the 'instantaneous' value corresponding to the temperature T . Also,

$$a^2 = \frac{dP}{d\rho} .$$

This equation defines the speed at which a small amplitude disturbance will propagate itself through the medium. This sonic velocity will be found to be a convenient quantity for simplifying analyses since the Mach number M is defined in terms thereof. It may again be emphasized that the equation $a = \sqrt{\gamma R T}$ is only valid for a condition of thermodynamic equilibrium, which may not always be a realistic assumption when combustion gases are being considered. If a chemical lag occurs, a as given above must be regarded as a lower limiting value. A higher limiting value, a_{frozen} , may be determined on the assumption that flow is 'frozen', i.e., its chemical composition is unable to react to changing state parameters. This distinction may be important if the flow velocity is changing rapidly, as in a nozzle.

Sound waves are very weak types of shock waves, the theory of which is dealt with in greater detail below. The speed of sound is thus the rate at which only the smallest pressure disturbances travel. True shock waves, in which the pressure ratio across the discontinuity may be much greater than unity, may on the other hand travel at speeds of several times that of sound. In this category fall explosion waves and certain types of detonation waves in combustion chambers.

In view of the definition of M in terms of a , it is of interest to consider how the value of a is affected by a variation in temperature, as both γ and R are temperature-dependent. In the case of R , where $R = (c_p - c_v)$, this difference is almost constant with T up to temperatures of several thousand degrees Fahrenheit. γ is therefore the parameter most affected by the variation of T , and in the atmosphere, since the temperature varies in a complicated way with altitude, so also does the speed of sound, the latter ranging in value from somewhat less than 1000 fps in the stratosphere to over 1400 fps at 400,000 feet.

2.3 The Mach Number

The nature of the wave system representing small disturbances traveling with the speed of sound is dependent on the absolute (free-

stream) velocity of the source of the disturbances in relation to the speed at which the disturbances travel, or, more succinctly, on its Mach number M , a parameter which has already been referred to. In Fig. 4(a), let successive positions of the source of a disturbance

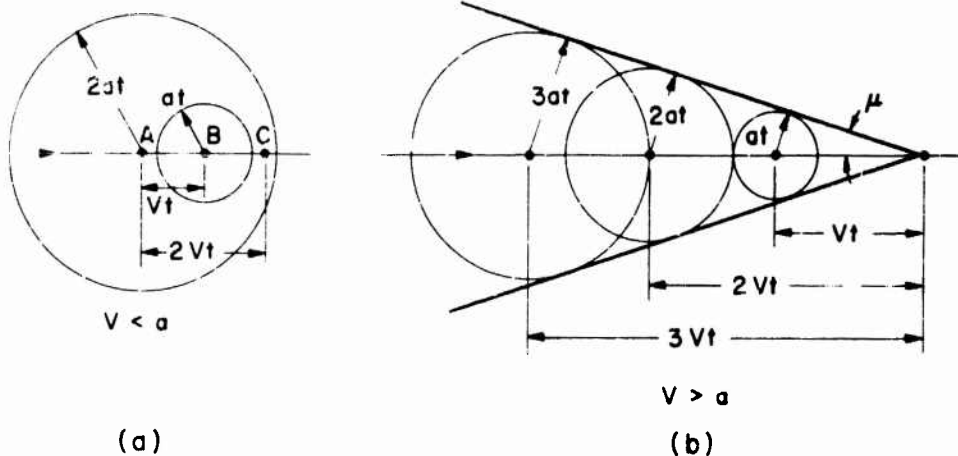


Fig. 4 Mach Patterns Set Up by Small Pressure Disturbances Moving at Subsonic and Supersonic Velocities

(traveling at velocity $V < a$) be A, B, and C. When the point C has been reached after a time $2t$, the front of the wave emitted when the source was at A will have traveled a distance $2at$; that emitted from position B will only have traveled a distance at , i.e., the source can never overtake the wave representing the 'advance warning'. In Fig. 4(b), however, when $V > a$, it is seen that there exists a conical envelope to the wave fronts (which in three-dimensional flow are spherical). Supersonic flow is thus characterized by the existence of a 'zone of silence' external to the envelope, in which disturbances representing pressure signals cannot be received. If, for example, the source of disturbances is stationary and the fluid is moving in the opposite direction, i.e., from right to left, supersonic flow will continue in the zone of silence undisturbed by the source whose presence is only felt downstream of the 'Mach cone'. The envelope shown

is known as a Mach wave (in either two- or three-dimensional flow), and it is clear that

$$\sin \mu = \frac{a t}{V t} = \frac{1}{M}.$$

μ is here the Mach angle. If the source of a disturbance moves at the speed of sound, $\mu = \pi/2$.

The wave configuration shown in Fig. 4(b) will remain similar even when the pressure disturbance is large, except that the velocity of propagation will now be greater than a , and the half-cone angle will thus be larger than $\sin^{-1} 1/M$. Such a wave is known as an oblique shock wave. Since it is traveling faster, a stronger shock wave will thus overtake a weaker one, and by a similar process, a series of weak waves will coalesce to form a stronger one, as will be the case if the boundary has a continuous concave curvature.

It is convenient to express many of the common thermodynamic flow relations in the form of functions of the Mach number, and various relations involving M are therefore derived in a subsequent section, and plotted in the Appendix.

When $M < 1$, the flow is said to be subsonic,

when $M \approx 1$, it is transonic, and

when $M > 1$, it is said to be supersonic,

hypersonic flow referring to the case when $M > 5$ approximately. This latter definition is merely one of convenience, since the ranges in which supersonic and hypersonic flow relations are valid will of necessity overlap (Ref. 2). The Mach number may also be regarded as an indication of the ratio of the ordered kinetic energy of flow of a fluid to the random kinetic energy of molecular motion.

2.4 Isentropic Compressible Flow

The simplest type of flow to consider is steady flow without transfer of heat or work across the boundaries of a duct. The conditions at any two Stations (1) and (2) may be related by noting the equality of the energy states; the energy conserved is partly thermal (internal) energy, partly pressure (potential) energy, and partly kinetic energy. Writing expressions for these terms, one has for unit mass, neglecting gravitational effects,

$$c_p T + \frac{v^2}{2} = c_v T + \frac{p}{\rho} + \frac{v^2}{2} = \text{constant.} \quad (9)$$

For stagnation conditions (reduction of kinetic energy to zero),

$$c_v T_t + \frac{p_t}{\rho_t} = c_v T + \frac{p}{\rho} + \frac{v^2}{2}. \quad (10)$$

From the isentropic law, using the perfect gas relationship,

$$\frac{T_t}{T} = \left(\frac{p_t}{p}\right)^{\frac{\gamma-1}{\gamma}}$$

Let this ratio be K .

Then

$$\frac{\rho_t}{\rho} = \left(\frac{p_t}{p}\right)^{\frac{1}{\gamma}} = K^{\frac{1}{\gamma-1}},$$

and

$$v = \sqrt{\frac{2 R \gamma T_t}{\gamma - 1} \left[1 - \left(\frac{p}{p_t}\right)^{\frac{\gamma-1}{\gamma}}\right]} = \sqrt{\frac{2 R \gamma T_t}{\gamma - 1} \left[1 - \frac{1}{K}\right]}. \quad (11)$$

Stage V $M \sqrt{\gamma R T}$ for the flow of a compressible medium,

$$M^2 = \frac{V^2}{\gamma R T} = \frac{2 R \gamma T_t}{(\gamma - 1) \gamma R T} \left[1 - \frac{1}{K} \right]$$

$$= \frac{2}{\gamma - 1} (K - 1).$$

$$\therefore K = 1 + \frac{\gamma - 1}{2} M^2. \quad (12)$$

From Eq. (11), the mass flow per unit area is given by

$$\frac{\dot{m}}{A} = \rho V = \sqrt{\frac{2\gamma}{\gamma - 1} P_t \rho_t \left[\left(\frac{P}{P_t} \right)^{\frac{2}{\gamma}} - \left(\frac{P}{P_t} \right)^{\frac{\gamma+1}{\gamma}} \right]}. \quad (13)$$

The mass flow cannot, however, be made to increase indefinitely with increasing P_t , for the flow velocity cannot be accelerated beyond the sonic value by a simple contracting section.

For a maximum, therefore,

$$d \left[\left(\frac{P}{P_t} \right)^{\frac{2}{\gamma}} - \left(\frac{P}{P_t} \right)^{\frac{\gamma+1}{\gamma}} \right] = 0,$$

i.e.,

$$\left(\frac{P}{P_t} \right) = \left(\frac{2}{\gamma + 1} \right)^{\frac{\gamma}{\gamma - 1}}. \quad (14)$$

For air ($\gamma = 1.40$) this ratio has the value of 0.528, and for combustion bases it is about 0.548. The critical velocity corresponding to this pressure ratio may be found by substitution of Eq. (14) in Eq. (11):

$$V_c = \sqrt{\frac{2\gamma}{\gamma + 1} R T_t} = \sqrt{\gamma R T} = a. \quad (15)$$

Thus a maximum discharge occurs when P_t reaches a value $(1/0.528)P$ for air, the Mach number being then equal to unity. This is known as the 'choking' condition, i.e., an increase of upstream pressure will not further increase the velocity beyond the local speed of sound [although the mass flow can still increase, because of the presence of the density term in Eq. (13)]. The location where this occurs is known as a 'throat,' from which small pressure disturbances cannot travel upstream, as previously demonstrated for the case of the zone of silence.

Summarizing, the pressure, density, and temperature ratios may be written as

$$\frac{P}{P_t} = K^{-\frac{\gamma}{\gamma-1}}, \quad (16)$$

$$\frac{\rho}{\rho_t} = K^{-\frac{1}{\gamma-1}}, \quad \text{and} \quad (17)$$

$$\frac{T}{T_t} = K^{-1}. \quad (18)$$

It is interesting to note that the total or stagnation temperature T_t is independent of the method by which the gas is brought to rest, provided no external work is done and no heat is transferred across the boundary. The relationship in Eq. (18) is therefore true whether or not the flow is isentropic.

These relations are of great value in determining the nature of the flow in a variable area duct. From Bernoulli's equation in differential form,

$$V dV + \frac{dP}{\rho} = 0.$$

Substituting from $a^2 = \frac{dP}{d\rho}$,

$$a^2 \frac{d\rho}{\rho} = -V dV,$$

or $\frac{d\rho}{\rho} = -M^2 \frac{dV}{V}$ since $M^2 = \frac{V^2}{a^2}$.

When, therefore, $M < 1$, the velocity will increase faster than the density can decrease, so that the area must decrease for the flow to continue to fill the passage. When $M > 1$, the density will decrease faster than the velocity will increase, so that the area must increase. Nozzles to produce supersonic flow are constructed so as to make use of this principle, and are thus convergent-divergent. To find the area relationship in terms of M for isentropic flow, one has

$$\rho A V = \rho^* A^* V^*,$$

where the asterisk refers to the throat condition (at which $M = 1$), so that

$$\frac{A}{A^*} = \frac{\rho^* V^*}{\rho V} = \frac{\rho^* a^*}{\rho a M}.$$

Now $\frac{\rho^*}{\rho} = \frac{\rho^*}{\rho_t} \frac{\rho_t}{\rho} = \left[\frac{K}{K^*} \right]^{\frac{1}{\gamma-1}}$,

where $K^* = 1 + \frac{\gamma-1}{2} = \frac{1+\gamma}{2}$.

Furthermore $\frac{a^{*2}}{a^2} = \frac{\gamma P^* \rho}{\gamma P \rho^*} = \frac{K}{K^*}$.

Also $\frac{a^{*2}}{a_t^2} = \frac{1}{K^*}$, since $M_t = 0$.

Hence

$$\frac{A}{A^*} = \frac{1}{M} \left(\frac{K}{K^*} \right)^{\frac{\gamma+1}{2(\gamma-1)}} \quad (19)$$

The corresponding (isentropic) pressure may be derived from Eqs. (16) and (19):

$$\left(\frac{A}{A^*} \right)^2 = \frac{\gamma-1}{2} \left\{ \frac{\left(\frac{2}{\gamma+1} \right)^{\frac{\gamma+1}{\gamma-1}}}{\left(\frac{P}{P_t} \right)^\gamma \left[1 - \left(\frac{P}{P_t} \right)^\gamma \right]} \right\} \quad (20)$$

The relationship between area, pressure and Mach number may likewise be obtained from Bernoulli's equation and the continuity relation in differential form:

$$v \, dV + \frac{dP}{\rho} = 0 \quad \text{and} \quad \frac{d\rho}{\rho} + \frac{dV}{V} + \frac{dA}{A} = 0.$$

Now

$$\begin{aligned} \frac{dA}{A} &= -\frac{d\rho}{\rho} - \frac{dV}{V} = -\frac{d\rho}{\rho} + \frac{dP}{\rho V^2}, \quad \text{since } dV = -\frac{dP}{\rho V} \\ &= \frac{dP}{\rho} \left(\frac{1}{V^2} - \frac{1}{a^2} \right), \quad \text{since } d\rho = \frac{dP}{a^2} \\ &= \frac{dP}{P} \left(\frac{1 - M^2}{\gamma M^2} \right), \end{aligned} \quad (21)$$

since

$$\rho V^2 = \rho M^2 \gamma R T = P \gamma M^2.$$

Since matter is conserved in a flow process,

$$\dot{m} = \rho_1 V_1 A_1 = \rho_2 V_2 A_2, \quad \text{and}$$

Setting $\rho = P E T$ and $V = Ma$,

$$\frac{P_1}{R T_1} M_1 a_1 A_1 = \frac{P_2}{R T_2} M_2 a_2 A_2 .$$

Since $a = \sqrt{\gamma R T}$,

$$A_1 P_1 M_1 \sqrt{\frac{\gamma}{R T_1}} = A_2 P_2 M_2 \sqrt{\frac{\gamma}{R T_2}} . \quad (22)$$

Equation (22) is in an inconvenient form since the temperatures are 'static' values, as would be determined by an 'observer' moving with the stream. In attempting to measure temperature, a sensing device would normally bring the flow to rest and would thus sense the 'total,' or stagnation, value. Combining Eqs. (18) and (22), therefore, to get over this difficulty,

$$\dot{m} = \frac{A_1 P_1 M_1}{\sqrt{T_t}} \left[\frac{\gamma K_1}{R} \right]^{\frac{1}{2}} = \frac{A_2 P_2 M_2}{\sqrt{T_t}} \left[\frac{\gamma K_2}{R} \right]^{\frac{1}{2}} . \quad (23)$$

Suffixes for T_t are unnecessary here since T_t remains constant in adiabatic flow.

Thus far, flow quantities have been considered on a mass basis. For flow on a weight basis,

$$\dot{w} = g\dot{m} = \frac{A_1 P_1 g M_1}{\sqrt{T_t}} \left[\frac{\gamma K_1}{R} \right]^{\frac{1}{2}} = \frac{A_2 P_2 g M_2}{\sqrt{T_t}} \left[\frac{\gamma K_2}{R} \right]^{\frac{1}{2}} . \quad (24)$$

The quantity

$$g M \left[\frac{\gamma K}{R} \right]^{\frac{1}{2}}$$

is defined by the symbol \dot{w} and is read 'w circle'.² Weight flow may thus be expressed by

$$\dot{w} = \frac{AP\dot{w}}{\sqrt{T_t}} \quad (25)$$

Replacing the static pressure P in Eq. (25) by the total pressure P_t , one has

$$\dot{w} = \frac{A P_t}{\sqrt{T_t}} \left[(P/P_t)^{\dot{w}} \right] \quad (26)$$

Equation (26) may be used to relate constant weight flow between any two points (1) and (2) for two values P_{t1} and P_{t2} of total pressure which may be dissimilar. Thus,

$$\dot{w}_1 = \dot{w}_2 = \frac{A_1 P_{t1}}{\sqrt{T_t}} \left[(P/P_t)^{\dot{w}} \right]_1 = \frac{A_2 P_{t2}}{\sqrt{T_t}} \left[(P/P_t)^{\dot{w}} \right]_2 \quad (27)$$

For constancy of entropy and enthalpy, the total pressure as well as the total temperature will be the same at Station 2 as at Station 1. Thus,

$$A_1 \left[(P/P_t)^{\dot{w}} \right]_1 = A_2 \left[(P/P_t)^{\dot{w}} \right]_2 \quad (28)$$

The function $\left[(P/P_t)^{\dot{w}} \right]$ may also be expressed in terms of the Mach number:

²The symbol \dot{w} here replaces the symbol \dot{m} , erroneously listed as a mass flow function in Ref. 22.

$$\frac{A_1}{A_2} = \frac{M_2}{M_1} \left[\frac{K_1}{K_2} \right]^{\frac{\gamma+1}{2(\gamma-1)}} \quad (29)$$

If A_2 be replaced by A^* , as at the throat of a supersonic nozzle,

$$\frac{A}{A^*} = \frac{1}{M} \left[\frac{K}{K^*} \right]^{\frac{\gamma+1}{2(\gamma-1)}} \quad (30)$$

It follows that

$$\frac{A}{A^*} = \frac{[(P/P_t)^{\frac{\gamma}{\gamma-1}}] M}{[(P/P_t)^{\frac{\gamma}{\gamma-1}}]^*}$$

and it is also obvious that

$$\frac{A_1}{(A/A^*)_1} = \frac{A_2}{(A/A^*)_2} \quad (31)$$

Several of the above relations are plotted (for two representative values of γ) in terms of M in the Appendix. These area relations may be used to find the areas corresponding to different values of M , both sub- and supersonic. When flow is assumed to be isentropic, no change of total pressure through the system is considered. [Static pressures may be computed at any point by using Eq. (16).] Since $P_{t_2} = P_{t_1}$,

$$\frac{P_2}{(P/P_t)_2} = \frac{P_1}{(P/P_t)_1} \quad (32)$$

so that (P/P_t) at both M_1 and M_2 may be found from tables or curves

and substituted into Eq. (32). For example, if a flow accelerates from $M = 0.1$ to $M = 1.0$, the value of (P/P_t) changes from 0.993 to 0.528. Hence

$$P \Big|_{M=1} = \left[\frac{0.528}{0.993} \right] P \Big|_{M=0.1}$$

(P/P_t) is a continuously decreasing and single-valued function of Mach number.

When the flow is adiabatic but nonisentropic, Eqs. (16) and (31) no longer apply, but Eq. (27) may be used. The amount of energy degradation (entropy increase) can be specified by means of the total pressure ratio (P_{t_2}/P_{t_1}) . Using Eq. (27), an exit Mach number and area may be related to an initial Mach number and area as follows:

$$A_2 \left[(P/P_t)^{\frac{\gamma}{\gamma-1}} \right]_2 = \frac{A_1 \left[(P/P_t)^{\frac{\gamma}{\gamma-1}} \right]_1}{P_{t_2}/P_{t_1}} \quad (33)$$

This relationship may be solved for either the unknown area or Mach number function as required, and it is useful for the calculation of ramjet inlet capture area ratios for imperfect diffusers—where the total pressure recovery ratio, exit Mach number, and freestream Mach number are known. In this case, the equation is set up for Stations 0 and 2 (see Fig. 1), and is expressed in terms of area ratios:

$$\frac{A_0}{A_1} P_{t_0} \left[(P/P_t)^{\frac{\gamma}{\gamma-1}} \right]_0 = \frac{A_2}{A_1} P_{t_2} \left[(P/P_t)^{\frac{\gamma}{\gamma-1}} \right]_2$$

Solving for (A_0/A_1) ,

$$\frac{A_0}{A_1} = \left(\frac{P_{t_2}}{P_{t_0}} \right) \left(\frac{A_2}{A_1} \right) \frac{\left[(P/P_t)^{\frac{\gamma}{\gamma-1}} \right]_2}{\left[(P/P_t)^{\frac{\gamma}{\gamma-1}} \right]_0} \quad (34)$$

All the terms on the right hand side are known. Alternatively, if all the terms except (P_{t2}/P_{t0}) are measurable quantities, this relation may be used to determine the total pressure recovery.

2.5 The Normal Shock

One-dimensional gas dynamics is adequate to describe a case of nonisentropic flow represented by a discontinuous rise of pressure, density, temperature, and entropy known as the normal shock wave. This rise of pressure is of particular importance in the design of a ramjet diffuser which is designed to produce compression of the entering air without the use of moving parts.

Now from Euler's equation

$$v \, dv + \frac{dP}{\rho} = 0,$$

and the isentropic equation

$$P = \rho^\gamma k,$$

which can be differentiated to

$$dP = k \gamma \rho^{\gamma-1} d\rho,$$

there results

$$\frac{v^2}{2} + \int k \gamma \rho^{\gamma-2} d\rho = \frac{v^2}{2} + \frac{P}{\rho} \frac{\gamma}{\gamma-1} = \frac{\gamma}{\gamma-1} \frac{P_t}{\rho_t},$$

the stagnation value. This is the energy equation in compressible flow and may be applied to either side of a shock wave.

Hence

$$\frac{\gamma}{\gamma - 1} \frac{p_t}{\rho_t} = \frac{\gamma}{\gamma - 1} R T_t = \frac{a_t^2}{\gamma - 1} = \frac{\gamma + 1}{2(\gamma - 1)} a^*{}^2 .$$

Consider now the flow in a duct through a normal shock front, using subscripts 1 and 2 for the immediate upstream and downstream locations (Fig. 5).

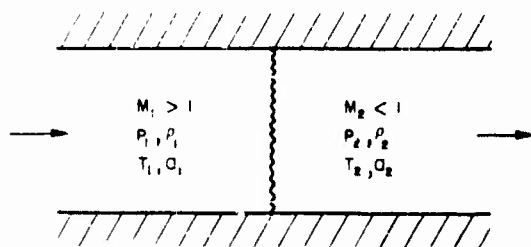


Fig. 5 Definition of Normal Shock Wave Relations

Then for the two sides of the shock--which may be considered infinitely thin--using the continuity and momentum relations,

$$\begin{aligned} \overbrace{\frac{\gamma}{\gamma - 1} \frac{p_1}{\rho_1} + \frac{v_1^2}{2}}^1 &= \overbrace{\frac{\gamma}{\gamma - 1} \frac{p_2}{\rho_2} + \frac{v_2^2}{2}}^2 \\ &= \frac{\gamma}{\gamma - 1} \frac{p_2}{\rho_2} \frac{v_2}{v_1} \left(p_1 + \rho_1 v_1^2 - \rho_1 v_1 v_2 \right) + \frac{v_2^2}{2} \\ &= \overbrace{\frac{1}{2} \frac{\gamma + 1}{\gamma - 1} a^*{}^2}^3 . \quad (35) \end{aligned}$$

From the first two parts of Eq. (35),

$$\frac{\gamma}{\gamma - 1} \frac{p_1}{\rho_1} \left(\frac{v_1 - v_2}{v_1} \right) + \frac{v_1^2 - v_2^2}{2} = \frac{\gamma}{\gamma - 1} v_2 (v_1 - v_2) .$$

Since $V_1 \approx V_2$, division by $(V_1 - V_2)$ gives

$$\frac{\gamma}{\gamma - 1} \frac{P_1}{\rho_1 V_1} + \frac{V_1 + V_2}{2} = \frac{\gamma}{\gamma - 1} V_2$$

or

$$\frac{\gamma}{\gamma - 1} \frac{P_1}{\rho_1} + \frac{V_1^2}{2} = \left(\frac{\gamma}{\gamma - 1} - \frac{1}{2} \right) V_1 V_2 = \frac{\gamma + 1}{2(\gamma - 1)} V_1 V_2$$

Combining this result with the third part,

$$\frac{\gamma + 1}{2(\gamma - 1)} V_1 V_2 = \frac{\gamma + 1}{2(\gamma - 1)} a^{*2} \quad \text{or} \quad V_1 V_2 = a^{*2} \quad (36)$$

This relation, according to Prandtl, shows that for a normal shock V_2 is subsonic.

Now
$$\left(\frac{a}{a^*} \right)^2 = \frac{T}{T^*} = \frac{K^*}{K}, \quad \text{and}$$

$$\left(\frac{V}{a^*} \right)^2 = M^2 \left(\frac{a}{a^*} \right)^2 = M^2 \frac{K^*}{K}$$

$$\therefore \left(\frac{V_1}{a^*} \right)^2 = M_1^2 \left(\frac{a_1}{a^*} \right)^2 = M_1^2 \frac{K^*}{K_1}, \quad \text{and}$$

$$\left(\frac{V_2}{a^*} \right)^2 = M_2^2 \left(\frac{a_2}{a^*} \right)^2 = M_2^2 \frac{K^*}{K_2}$$

Multiplying,

$$\left(\frac{v_1}{a^*}\right)^2 \left(\frac{v_2}{a^*}\right)^2 = 1 = M_1^2 M_2^2 \left(\frac{K^*}{K_1}\right) \left(\frac{K^*}{K_2}\right)$$

$$\frac{K^* M_1^2}{K_1} = \frac{K_2}{K^* M_2^2}$$

Solving for M_2^2 by substituting for K_1 , K_2 , and K^* ,

$$M_2^2 = \frac{2 K_1}{2\gamma M_1^2 - \gamma + 1} = \frac{1 + \frac{\gamma - 1}{2} M_1^2}{\gamma M_1^2 - \frac{\gamma - 1}{2}} \quad (37)$$

Also

$$\frac{v_2}{v_1} = \frac{v_1 v_2}{v_1^2} = \frac{a^{*2}}{v_1^2} = \frac{1}{M_1^2} \frac{a^{*2}}{a_1^2} = \frac{1}{M_1^2} \frac{K_1}{K^*} \quad (38)$$

The variation of (v_2/v_1) and (M_2/M_1) with M_1 is shown in Fig. 6. Pressure, density, and temperature relations across a normal shock wave may be found as follows:

$$\frac{\rho_2}{\rho_1} = \frac{v_1}{v_2} = M_1^2 \frac{K^*}{K_1} \quad (39)$$

From the momentum relationship

$$P_2 - P_1 = \rho_1 v_1^2 - \rho_2 v_2^2,$$

and since

$$a^2 = \gamma \frac{P}{\rho},$$

$$\begin{aligned} \frac{P_2}{P_1} &= 1 + \frac{\rho_1}{\rho_2} \frac{V_1^2}{V_2^2} - \frac{\rho_1}{\rho_2} \frac{V_1}{V_2} \frac{V_2}{V_1} \\ &= \gamma M_1^2 - \frac{\gamma a^*}{a_1^2} = \gamma M_1^2 - \gamma \left(\frac{2}{\gamma + 1} + \frac{\gamma - 1}{\gamma + 1} M_1^2 \right) \\ &= \frac{2\gamma}{\gamma + 1} (M_1^2 - 1) = \frac{\gamma}{K^*} (M_1^2 - 1) . \end{aligned}$$

Hence

$$\frac{P_2}{P_1} = 1 + \frac{\gamma}{K^*} (M_1^2 - 1) = \frac{K^* + \gamma(M_1^2 - 1)}{K^*} = \frac{2\gamma M_1^2 - (\gamma - 1)}{\gamma + 1} . \tag{40}$$

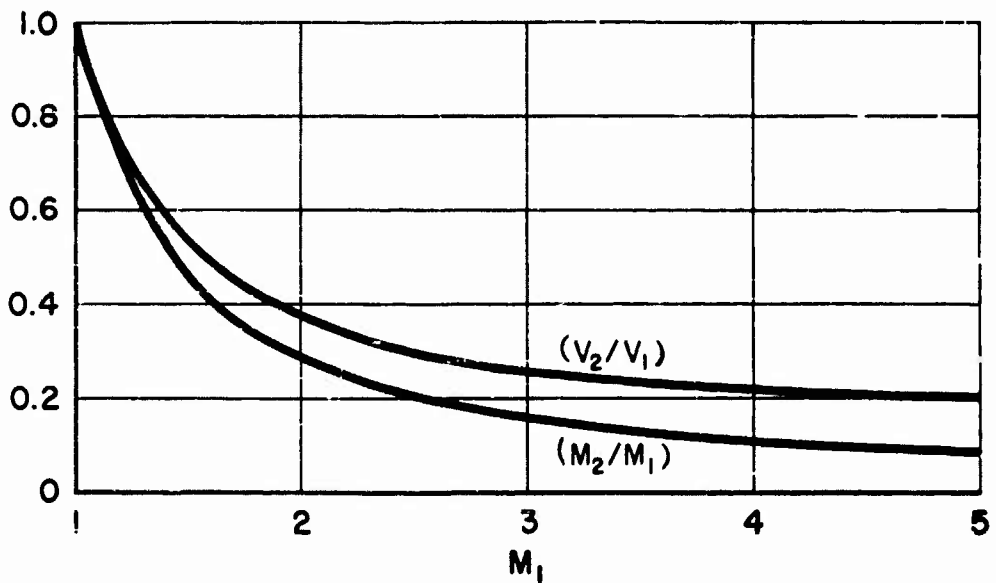


Fig. 6 Normal Shock Functions \$(V_2/V_1)\$ and \$(M_2/M_1)\$, \$\gamma = 1.4\$

Note that as $M_1 \rightarrow \infty$, $(P_2/P_1) \rightarrow 0$, but $(\rho_2/\rho_1) \rightarrow \frac{\gamma+1}{\gamma-1}$ (which has the value 6 for $\gamma = 1.4$).

Since $P = \rho R T$,

$$\frac{T_2}{T_1} = \frac{\rho_2/P_1}{\rho_1/P_2} = \left[\frac{K^* + \gamma(M_1^2 - 1)}{K^*} \right] \frac{K_1}{K^* M_1^2} \quad (41)$$

These relations are shown in Figs. 7 and 8. Figure 9 shows a comparison between the curve relating pressure and density ratios for isentropic flow, and that for flow across a normal shock wave

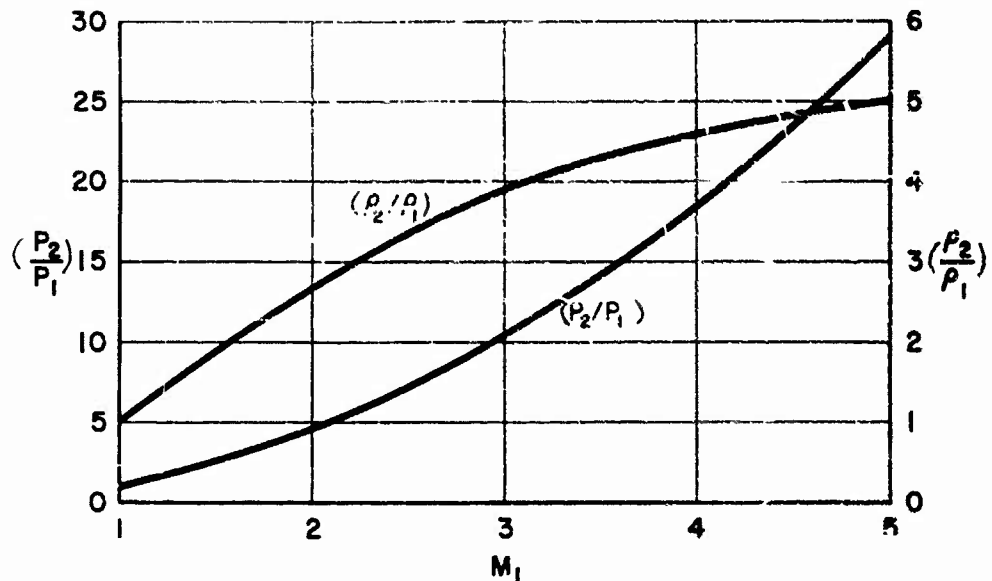


Fig. 7 Normal Shock Functions (P_2/P_1) and (ρ_2/ρ_1) , $\gamma = 1.4$

At very high Mach numbers, the static temperature rise of the gas passing through a shock wave may give rise to considerable ionization, which may be felt ahead of the wave if the ionized particles are

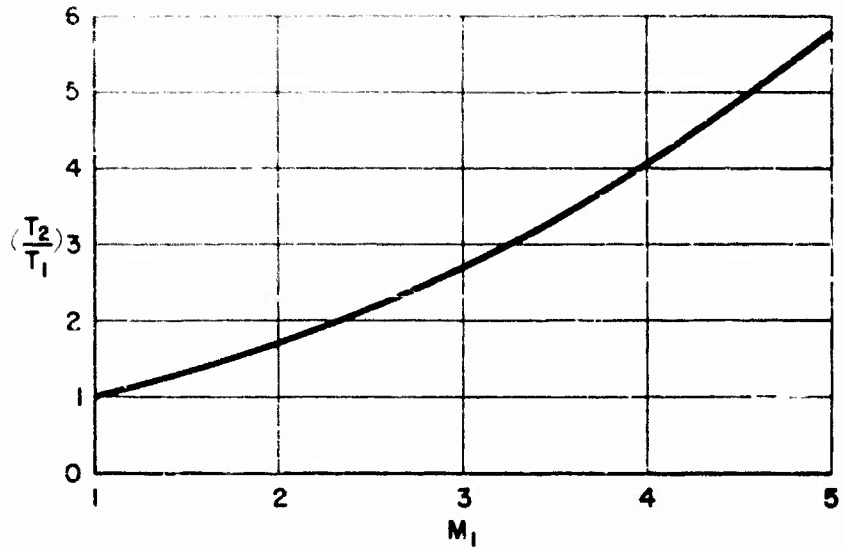


Fig. 8 Normal Shock Function (T_2/T_1) , $\gamma = 1.4$

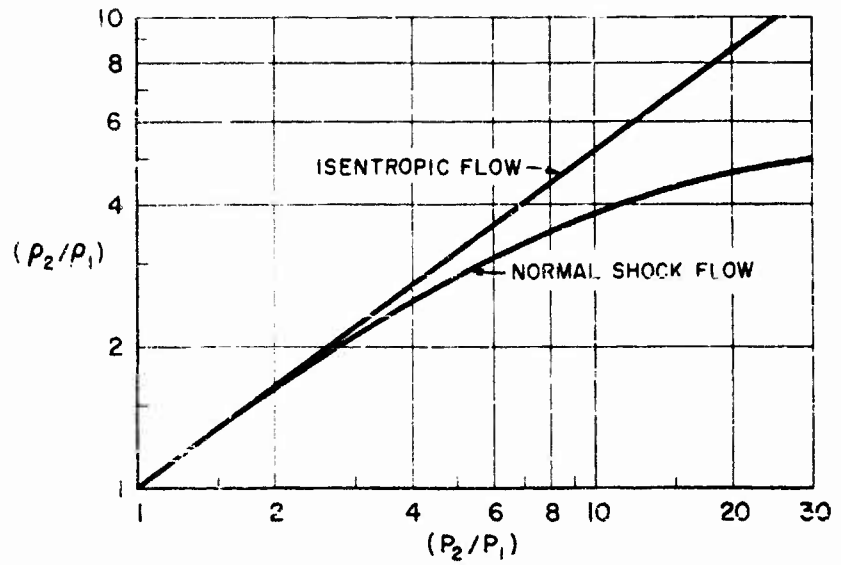


Fig. 9 Normal Shock Function and Isentropic Flow Function of (P_2/P_1) versus (ρ_2/ρ_1) , $\gamma = 1.4$

is given by the following Mach number relation-

Therefore, the Mach number upstream of a shock is measured by the stagnation pressure ratio across the shock wave.

$$\frac{P_{t2}}{P_2} = K_2^{\frac{\gamma}{\gamma-1}} \left(1 + \frac{\gamma-1}{2} M_2^2 \right)^{\frac{\gamma}{\gamma-1}}$$

Substituting the relation for M_1 and M_2 across a normal shock wave

$$\frac{P_{t2}}{P_2} = \left[1 + \frac{\gamma-1}{2} \frac{2 + (\gamma-1)M_1^2}{2\gamma M_1^2 - (\gamma-1)} \right]^{\frac{\gamma}{\gamma-1}}$$

$$\left[\frac{(\gamma+1)^2 M_1^2}{2(2\gamma M_1^2 - (\gamma-1))} \right]^{\frac{\gamma}{\gamma-1}} \tag{42}$$

It is also a simple matter to determine the ratio of the stagnation pressure downstream of a shock to the upstream static pressure. These quantities represent readings conveniently available from the use of an impact probe or pitot tube inserted into a supersonic stream. As shown in Fig. 10, the detached bow wave has the form of a normal shock immediately ahead of the probe.

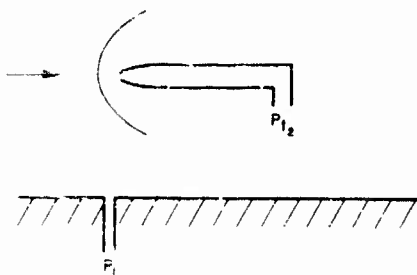


Fig. 10 Pitot Tube in Supersonic Stream

$$\begin{aligned}
\frac{P_{t2}}{P_1} &= \frac{P_{t2}}{P_2} \frac{P_2}{P_1} = \left[\frac{(\gamma + 1)^2 M_1^2}{2[2\gamma M_1^2 - (\gamma - 1)]} \right]^{\frac{\gamma}{\gamma-1}} \left[\frac{2\gamma M_1^2 - (\gamma - 1)}{\gamma + 1} \right] \\
&= \frac{\gamma + 1}{2} M_1^2 \left[\frac{(\gamma + 1)^2 M_1^2}{2(2\gamma M_1^2 - \gamma + 1)} \right]^{\frac{1}{\gamma-1}} = K^* M_1^2 \left[\frac{2 K^* M_1^2}{2\gamma M_1^2 - \gamma + 1} \right]^{\frac{1}{\gamma-1}}
\end{aligned}
\tag{43}$$

This relation is known as the Rayleigh pitot tube formula and is plotted in Fig. A-12 in the Appendix.

It may be noted that a velocity transition from subsonic to supersonic through a normal shock wave--though permitted by the above consideration--is not possible, as this would involve a contradiction of the Second Law of Thermodynamics. The total pressure relationship shows that a loss occurs during deceleration (as actually observed), whereas flow in the reverse direction would imply an increase in total pressure and thereby a reduction of entropy.

2.6 Steady Diabatic Flow

The foregoing adiabatic analysis obviously cannot refer to the case in which flow takes place with a change in enthalpy, such as occurs through the combustion chamber of a ramjet, or in a duct where friction effects are not inappreciable. This may conveniently be handled by one of the methods relating to diabatic processes, i.e., those in which heat is added to the system either from within or across the walls, as developed by Shapiro et al. (Ref. 3) and others.

From the momentum equation, taking subscripts (1) and (2) before and after the point of heat addition,

$$P_1 + \rho_1 v_1^2 = P_2 + \rho_2 v_2^2,$$

and from the perfect gas law, $P = \rho R T$, and $M^2 = \frac{v^2}{\gamma R T} = \frac{v^2 \rho}{\gamma P}$,

$$P_2 - P_1 = M_1^2 \gamma P_1 - M_2^2 \gamma P_2,$$

or

$$1 - \frac{P_1}{P_2} = \gamma (M_1^2 \frac{P_1}{P_2} - M_2^2).$$

$$\therefore \frac{P_1}{P_2} = \frac{1 + \gamma M_2^2}{1 + \gamma M_1^2}. \quad (44)$$

Since

$$P_t = P K^{\frac{\gamma}{\gamma-1}},$$

$$\frac{P_{t1}}{P_{t2}} = \frac{1 + \gamma M_2^2}{1 + \gamma M_1^2} \left(\frac{K_1}{K_2} \right)^{\frac{\gamma}{\gamma-1}} \quad (45)$$

From the perfect gas law,

$$\frac{T_1}{T_2} = \frac{P_1 \rho_2}{P_2 \rho_1} \quad \text{and} \quad \frac{\rho_1}{\rho_2} = \frac{v_2}{v_1} = \frac{M_2}{M_1} \sqrt{\frac{T_2}{T_1}}.$$

$$\therefore \frac{T_1}{T_2} = \frac{(1 + \gamma M_2^2) M_1^2}{(1 + \gamma M_1^2) M_2^2}. \quad (46)$$

One also has $T_t = T K$.

$$\frac{T_{t1}}{T_{t2}} = \frac{T_1 K_1}{T_2 K_2} = \frac{M_1^2 (1 + \gamma M_2^2)^2 K_1}{M_2^2 (1 + \gamma M_1^2)^2 K_2} \quad (47)$$

Likewise

$$\frac{\rho_1}{\rho_2} = \frac{V_2}{V_1} = \frac{M_2^2 (1 + \gamma M_1^2)}{M_1^2 (1 + \gamma M_2^2)} \quad (48)$$

Since $\rho = \rho_t K^{-\frac{1}{\gamma-1}}$ (where the density assumes its stagnation value ρ_t if the flow is brought adiabatically to rest),

$$\frac{\rho_1}{\rho_2} = \frac{\rho_{t1} \left(\frac{K_1}{K_2}\right)^{-\frac{1}{\gamma-1}}}{\rho_{t2}} = \frac{M_2^2 (1 + \gamma M_1^2)}{M_1^2 (1 + \gamma M_2^2)} \quad (49)$$

and

$$\frac{\rho_{t1}}{\rho_{t2}} = \frac{M_2^2 (1 + \gamma M_1^2)}{M_1^2 (1 + \gamma M_2^2)} \left(\frac{K_1}{K_2}\right)^{\frac{\gamma}{\gamma-1}} \quad (50)$$

Since the stagnation temperature changes with heat addition, a more convenient reference condition is one associated with a particular value of the mass flow. This is the condition at which 'thermal choking' ($M = 1$) occurs. There is thus but one value of T^* , P^* and ρ^* for any particular flow.

$$\text{Thus, } \left(\frac{T}{T^*}\right)_1 = \left(\frac{T_1}{T^*}\right)$$

The corresponding pressure, temperature and density equations are thus found by substitution of $M = 1$ into Eqs. (44) to (50):

$$\frac{P}{P^*} = \frac{1 + \gamma}{1 + \gamma M^2} \quad (51)$$

and

$$\frac{P_t}{P_t^*} = \frac{1 + \gamma}{1 + \gamma M^2} \left[\frac{K}{K^*} \right]^{\frac{\gamma}{\gamma-1}} \quad (52)$$

Also,

$$\frac{T}{T^*} = \frac{(1 + \gamma)^2 M^2}{(1 + \gamma M^2)^2} \quad (53)$$

and

$$\frac{T_t}{T_t^*} = \frac{M^2 (1 + \gamma)^2 K}{(1 + \gamma M^2)^2 K^*} = \frac{2 M^2 (1 + \gamma) K}{(1 + \gamma M^2)^2} \quad (54)$$

From Eq. (48),

$$\frac{\rho}{\rho^*} = \frac{V}{V^*} = \frac{M^2 (1 + \gamma)}{1 + \gamma M^2} \quad (55)$$

and

$$\frac{\rho_t}{\rho_t^*} = \frac{M^2 (1 + \gamma)}{(1 + \gamma M^2)} \left(\frac{K}{K^*} \right)^{\frac{\gamma}{\gamma-1}} \quad (56)$$

These functions are plotted in Figs. A-16 and A-17 in the Appendix for two values of γ and they are also tabulated in various texts listed in the Bibliography (Cambel and Jennings, Zucrow, and Shapiro) and in Ref. 22. For initially subsonic conditions, addition of heat to the flow causes P , ρ_t , ρ and P_t to fall, and V , T_t and T to rise.

flow is that ρ , ρ_1 , ρ_1^* and V fall, while T_1 , T , ρ_1^* , P and P_1^* rise. Heat addition thus causes the Mach number to be driven toward unity, for flow initially either subsonic or supersonic. The reverse effects occur when heat is withdrawn from the fluid. This principle has been applied in the 'aerothermopressor' developed by Shapiro (Ref. 4), liquid being injected into a subsonic gas stream flowing in a duct in order to increase the stagnation pressure. It will have been noticed that an anomaly occurs in the curves for (T/T^*) and (ρ^*/ρ) in that these ratios reach a maximum at a value somewhat less than unity. It is easily seen from differentiating Eq. (53) that this maximum occurs at $M = 1/\sqrt{\gamma}$, i.e., at $M = 0.845$ for $\gamma = 7/5$, and at $M = 0.882$ for $\gamma = 9/7$. For $1/\sqrt{\gamma} < M < 1$, therefore, where $1.029 > (T/T^*) > 1$, further addition of heat to the fluid brings about an increase in kinetic energy to compensate for the drop in the value of (T/T^*) . The behavior of (ρ^*/ρ) is similar.

Since with flow initially subsonic, it is clear from the thermal choking effect that the addition of more heat to the fluid cannot then result in a further increase of velocity, the assumed mass flow condition at the entrance to the heat transfer region becomes incompatible with that at the thermal throat, and the mass flow must then decrease. This reduction in mass flow is analogous to the pressure choking effect resulting from a progressive reduction in the size of a geometric throat. The situation in initially supersonic flow may be illustrated by a comparison with the case of flow through a duct with multiple (geometric) throats, as shown in Fig. 11, which is an extension of the nozzle condition discussed later with reference to Fig. 18. The adjustment to sonic conditions at the thermal throat is accomplished by the flow first becoming subsonic through a normal shock; it may then accelerate again if further heating occurs (as by friction) up to the sonic point, finally decelerating through a normal shock. At least in theory, shock-free deceleration of supersonic flow to Mach 1 by heat addition is possible, but if friction effects are present, it is clear that the length of a duct is an important variable, since the effect of friction is to bring about a progressive addition of heat to the fluid, with consequent change of Mach number

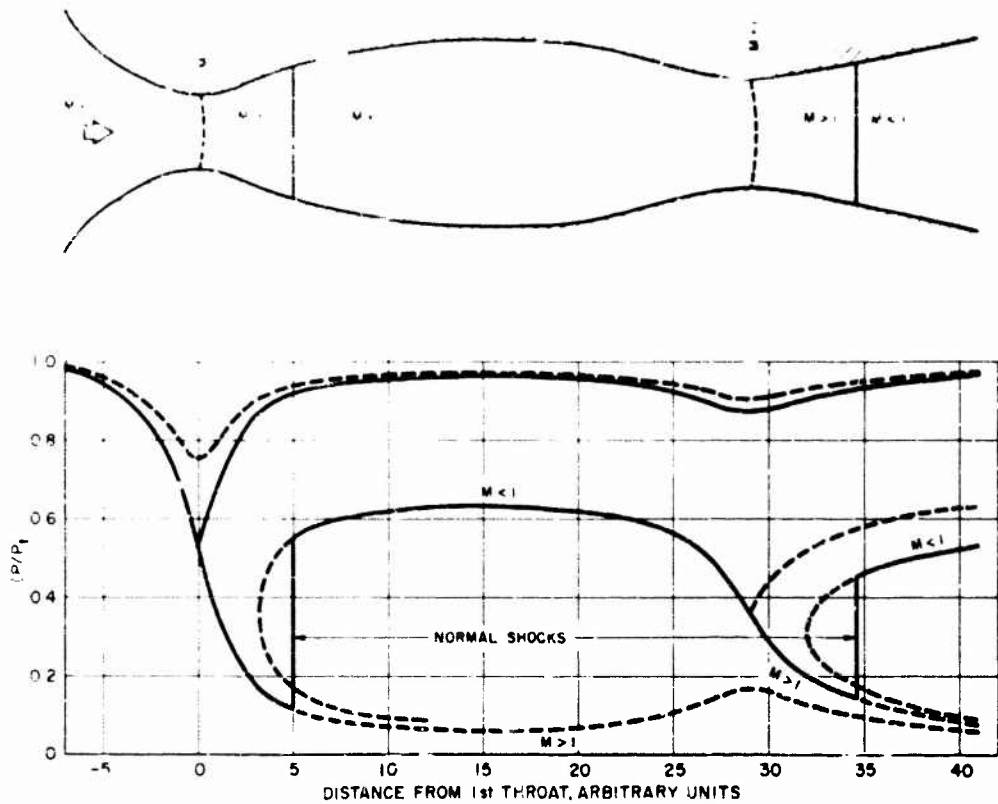


Fig. 11 Analogy of Diabatic Flow of Air with that in a Duct Having Multiple (Leametric) Throats, Showing Unstable Nature of Decelerating Flow

It may be noted that the creation of a thermal throat is not normally aimed at in the design of ramjet combustion chambers, since the function of accelerating the flow to sonic velocity is reserved to the propulsion nozzle.

For no output of shaft work, the energy equation (per unit mass) is as follows:

$$dQ = c_p dT + V dV.$$

Integrating,

$$Q_{1 \rightarrow 2} = c_p(T_2 - T_1) + \frac{v_2^2 - v_1^2}{2} = H_2 - H_1 + \frac{v_2^2 - v_1^2}{2},$$

or, in terms of stagnation enthalpy,

$$Q_{1 \rightarrow 2} = H_{t_2} - H_{t_1} = c_p(T_{t_2} - T_{t_1}),$$

where

$$T_{t_2} \approx T_{t_1}.$$

When the continuity and momentum equations apply, then for a constant area duct the mass velocity G is given by

$$G = \rho v,$$

and therefore

$$P + G^2/\rho = \text{constant.} \quad (57)$$

Likewise, for constant stagnation temperature, the energy equation may be written

$$H + \frac{v^2}{2} = \text{constant.} \quad (58)$$

The effects are shown graphically on a diagram plotted to ordinates of temperature (or enthalpy) and entropy, such as Fig. 12. The lines on the diagram which represent Eqs. (57) and (58) are known as Rayleigh and Fanno lines respectively. The points A and B of maximum entropy for the two curves correspond to the choking condition, which can thus be approached along either the subsonic (upper) or supersonic (lower) branches. A process of thermal choking brought about by heat addition to initially subsonic flow is shown by following along the line DB; heat addition to supersonic flow with deceleration through a shock wave (with corresponding increase of entropy) and

subsequent acceleration to the choking condition is illustrated by the curve CDB. The point of maximum enthalpy on the Rayleigh line corresponds to the value $M = 1/\sqrt{2}$.

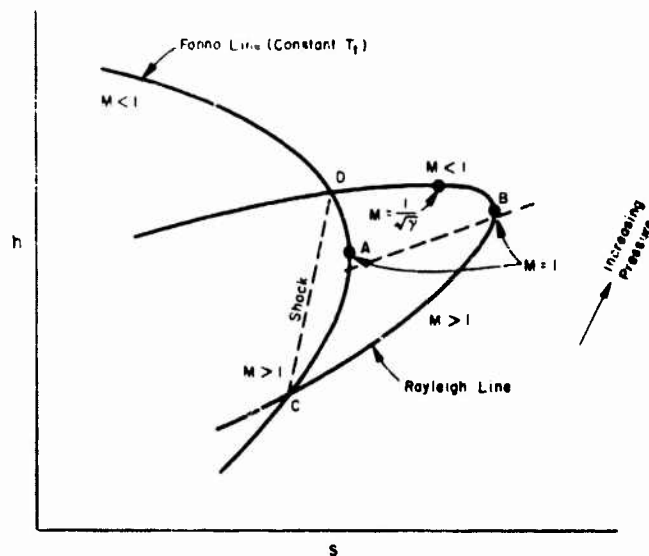


Fig. 12 Fanno and Rayleigh Lines

Some practical outcomes of these considerations as related to supersonic combustion are referred to later.

2.7 Thrust and Drag

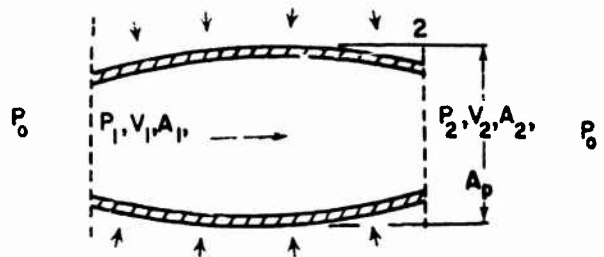
Further use will now be made of the momentum equation as derived initially in the section on the speed of sound. In the form given,

$$P + \rho V^2 = \text{constant},$$

a constant area duct was assumed. The momentum changes that the internal flow through a ramjet undergoes due to both area variation and heat

addition are made use of in the generation of thrust. Consider first how internal thrust is set up by fluid flow in a duct of variable area (Fig. 13).

Fig. 13 Duct Flow Variables



On any cross-sectional area A , the force acting is composed of the static pressure over the area plus the rate of transport of momentum, i.e.,

$$f = P A + V \frac{dm}{dt} ,$$

or, using the mass flow relation $\dot{m} = \rho V A$,

$$\begin{aligned} f &= A(P + \rho V^2) \\ &= AP(1 + \gamma M^2) \text{ for a perfect gas.} \end{aligned}$$

A function f is also defined by

$$f = P(1 + \gamma M^2) . \tag{59}$$

This function is shown plotted in the Appendix. f is here known as the stream thrust (or impulse function). It is clear that the stream thrust remains constant in a duct of constant area (such as, for example, certain types of ramjet combustion chambers) and thus corresponds to the Rayleigh line previously referred to. In a variable

area duct, the reaction force exerted by the fluid on the duct is known as the internal thrust F_{int} , and between Stations (1) and (2) is given by

$$F_{int} = \dot{m}(V_2 - V_1) + P_2 A_2 - P_1 A_1$$

$$= \dot{m} V_2 - \dot{m} V_1$$

This force acts in an opposite direction to that of the flow. The internal thrust is thus equal to the difference of the stream functions. It may be noted that the relative values of V_2 and V_1 will reflect not only the difference of cross-sectional area, but also the difference in enthalpy of the gas at the two stations. Considering the ramjet engine as a whole, the entering fluid will be air, while that leaving will represent the result of mixing air and fuel. An additional internal thrust term due to the injection and acceleration of fuel is therefore given by $\dot{m}_f V_2$. The magnitude of the external thrust (or drag) is given by the resolution in the direction of flow of the forces acting on the projected area A_p :

$$F_{ext} = P_0(A_p - A_2) - P_0(A_p - A_1) = P_0(A_1 - A_2).$$

The sum of the internal and external thrusts is known as the gross thrust of the ramjet engine:

$$F_g = \dot{m}_e V_e + A_e(P_e - P_0) - \dot{m}_0 V_0$$

$$= \dot{m}_e V_e - \dot{m}_0 V_0 - P_0(A_e - A_0)$$

$$= A_e P_e (1 + \gamma M_e^2) - P_0 A_e (1 + \frac{A}{A_c} \gamma M_0^2),$$

if the pressure at the exit from the nozzle differs from the free-stream value. The increase of momentum due to fuel addition may be taken account of by introducing the factor $(1 + y)$, where y is the fuel-air ratio:

$$F_g = (1 + y) \dot{m}_0 V_e + A_e (P_e - P_0) - \dot{m}_0 V_0 . \quad (60)$$

The net thrust is less than this by the amount of the external friction drag force D_{ext} , if the internal friction drag is considered to be small:

$$F_{net} = F_g - D_{ext} .$$

Under steady flight conditions,

$$F_g = D_{ext} .$$

F_{net} is observed to depend strongly on the ambient pressure and the freestream Mach number for a fixed engine geometry. A more constant parameter is the dimensionless coefficient obtained by dividing F_{net} by the product of the engine reference area (nominal cross section) A_n and the freestream dynamic pressure q_0 .

$$C_F = \frac{F_{net}}{A_n q_0} . \quad (61)$$

This quantity varies only slowly with Mach number and ambient pressure level. Since it is independent of engine size, it is a useful measure of comparison between engines of different size under different flight conditions. The expression for the thrust coefficient may be transformed by the introduction of the mass flow equation and the perfect gas law. Since

$$F_g = \rho_0 V_0^2 A_0 \left((1 + y) \frac{V_e}{V_0} - 1 \right),$$

then, referred to the capture area A_C in the freestream,

$$C_{F_0} = 2 \left((1 + \gamma) \frac{v_c}{v_0} - 1 \right),$$

or, since for any arbitrary area A_n ,

$$C_{F_n} = C_{F_0} \frac{A_0}{A_n}.$$

$$C_{F_n} = 2 \frac{A_0}{A_n} \left((1 + \gamma) \frac{v_e}{v_0} - 1 \right).$$

A different comparison of engine performance that may be mentioned here is given by the quotient of the net thrust and the fuel weight flow:

$$I_f = \frac{F_{\text{net}}}{\dot{w}_f}. \quad (62)$$

This quantity is known as the fuel specific impulse. High values for I_f signify efficient engines, and values of from 1000 to 2000 seconds are obtainable. The reciprocal of I_f is clearly the specific fuel consumption; this latter is often stated in units of reciprocal hours.

It is also useful to express stream thrust in terms of other flow properties:

$$f = \dot{w} \sqrt{T_t} \frac{(1 + \gamma M^2)}{\bar{w}_0}.$$

Substituting for \bar{w}_0 ,

$$f = \dot{w} \sqrt{T_t} \frac{(1 + \gamma M^2)}{M g} \sqrt{\frac{R}{\gamma K}}. \quad (63)$$

This relation will serve as a measure of jet reaction if the total temperature and Mach number are known as well as the rate of flow. Since, however, it is difficult to measure elevated stagnation temperatures in flowing gases, it is therefore customary to evade this by measuring instead the sonic jet reaction \mathcal{F}^* which would be that felt at a choked nozzle. The quotient of the jet reaction \mathcal{F}^* into the weight rate of air flow \dot{w}_a is then defined as the air specific impulse S_a :

$$S_a = \frac{\mathcal{F}^*}{\dot{w}_a} .$$

S_a is a parameter widely used to compare the performance of a ramjet engine under different conditions. Substituting for \mathcal{F}^* the expression in Eq. (63), for $M = 1$, gives

$$S_a = \frac{\dot{w} \sqrt{T_t} (1 + \gamma)}{\dot{w}_a g \sqrt{1 + \frac{\gamma - 1}{2}}} \sqrt{\frac{R}{\gamma}} . \quad (64)$$

Since $\dot{w} = \dot{w}_a (1 + y)$, then from Eq. (64),

$$S_a = (1 + y) \sqrt{\frac{T_t}{g}} \sqrt{\frac{2R (1 + \gamma)}{\gamma}} . \quad (65)$$

Combining Eqs. (63) and (64),

$$\mathcal{F} = \dot{w}_a S_a \frac{1 + \gamma M^2}{M \sqrt{2(1 + \gamma) K}} \quad (66)$$

$$= \dot{w}_a S_a \vartheta(M) . \quad (67)$$

This Mach number function $\vartheta(M)$, according to Rudnick (Ref. 5), thus relates the stream thrust of a jet of Mach number M to the sonic

value, $w_a S_a$, of the thrust (at the same total temperature). By definition, therefore,

$$\theta(M) = \frac{y}{y^*} \quad (68)$$

This function is also shown plotted in the Appendix.

It may be noted that both deceleration of supersonic flow through a normal shock and heat addition to flow in a combustion chamber of constant area are cases that illustrate constant stream thrust. Between Stations (1) and (2), Eq. (67) gives

$$y_1 = y_2 ;$$

for constant stagnation temperature.

$$w_a S_a \theta(M)_1 = w_a S_a \theta(M)_2 ,$$

whence

$$\theta(M)_1 = \theta(M)_2 \quad (69)$$

In flow with heat addition, different values of S_a must be used corresponding to the appropriate inlet and exit stagnation temperatures. Using subscript (2) to denote conditions at the combustion chamber entrance, and (b) for conditions after combustion, then for $y = 0$ and $\gamma = 7/5$, and using Eq. (65), then for T_t in $^{\circ}\text{R}$, and w_a in Lb/sec,

$$\theta(M)_b = 2.382 \frac{\theta(M)_2}{S_{ab}} \sqrt{T_{t2}} \quad (70)$$

The ratio of the Mach functions is thus inversely proportional to $(S_{ab} / \sqrt{T_{t2}})$, a parameter which will frequently be referred to below. In practice, the above relationship needs to be modified by the inclusion of a flameholder drag term to enable it to apply to a real

combustion chamber if combustion is stabilized on such a device. The drag force acts in an opposite direction to that of the flow through the combustion chamber and is hence to be deducted from the inlet stream thrust when the exit value is being determined:

$$F_b = F_2 - D_b .$$

Such a drag term is generally computed in the form of a coefficient C_{D_b} , obtained as before by dividing D_b by the product of the combustion chamber area A_2 into the combustion chamber inlet stream dynamic pressure q_2 :

$$C_{D_b} = \frac{D_b}{A_2 q_2} = \frac{D_b}{A_2 \frac{\gamma}{2} P_2 M_2^2} . \quad (71)$$

This drag coefficient is not strictly constant except for flows at very low speeds which may be treated as incompressible.

Then

$$\dot{w}_a S_{a_b} \theta(M)_b = 2.382 \sqrt{T_{t_2}} \dot{w}_a \theta(M)_2 - \frac{A_2 C_{D_b} \gamma P_2 M_2^2}{2} . \quad (72)$$

\dot{w}_a may be expressed in terms of P_2 , M_2 , and T_{t_2} in order to eliminate it from the preceding equation:

$$\frac{P_2 A_2 \dot{w}_2^0}{\sqrt{T_{t_2}}} S_{a_b} \theta(M)_b = 2.382 \dot{w}_2^0 A_2 P_2 \theta(M)_2 - \frac{A_2 C_{D_b} \gamma P_2 M_2^2}{2} ,$$

whence

$$\left[S_{a_b} / \sqrt{T_{t_2}} \right] \theta(M)_b = 2.382 \theta(M)_2 - \frac{C_{D_b} \gamma M_2^2}{2 \dot{w}_2^0} . \quad (73)$$

Alternatively, using Eq. (72)

$$\left[S_{a_b} / \sqrt{T_{t_2}} \right] \vartheta(M)_b = \frac{1 - (C_{D_b} - 2) \gamma \frac{M_2^2}{2}}{\frac{\rho_2}{w_2}} \quad (74)$$

This equation for combustor flow cannot be further simplified unless C_{D_b} takes on such values as 0, 1, or 2. If $C_{D_b} = 0$, Eq. (70) results. If $C_{D_b} = 1$, the numerator of the right hand side of Eq. (74) reduces to $(1 + \gamma M_2^2/2)$, which is approximately equal to (P_{t_2}/P_2) , if higher powers of M_2^2 are neglected, so that

$$\left[S_{a_b} / \sqrt{T_{t_2}} \right] \vartheta(M)_b \approx \frac{1}{\left[(P/P_t) \frac{\rho}{w} \right]_2} \quad (75)$$

If $C_{D_b} = 2$, the numerator of the right hand side becomes unity, and

$$\left[S_{a_b} / \sqrt{T_{t_2}} \right] \vartheta(M)_b = \frac{1}{\frac{\rho_2}{w_2}} \quad (76)$$

For each of these three cases one may select any two of the parameters $(S_{a_b} / \sqrt{T_{t_2}})$, M_b , and M_2 , in order to solve for the third quantity directly.

The total pressure after combustion may thus be related to the inlet total pressure by means of the continuity of either mass flow or stream thrust. It is therefore possible to write an expression for stream thrust in terms of Mach number and total pressure across the region of combustion. Since

$$(f/P_t)_2 = (f/P)_2 \cdot (P/P_t)_2,$$

then for constancy of stream thrust,

$$\frac{A_2}{A_1} = \frac{P_{t1}}{P_{t2}} \left(\frac{P_{t1}}{P_{t2}} \right)^{\frac{\gamma-1}{\gamma}}$$

$$P_{t1} = P_{t2} \left(\frac{P_{t1}}{P_{t2}} \right)^{\frac{\gamma}{\gamma-1}} \quad (77)$$

Static pressure and temperature after combustion may be obtained if desired from total pressure and temperature in a manner similar to that used to obtain the value of the flow after a normal shock, but such quantities are seldom of interest. The flow after combustion is completely defined by a knowledge of the parameters of Mach number, total temperature (or S_a), and mass flow (or total pressure), and the pressure, Mach number, and area of the exhaust stream at exit from a nozzle may be calculated from these parameters as previously indicated.

III TWO-DIMENSIONAL SUPERSONIC WAVE SYSTEMS

At supersonic flight velocities, a ramjet is accompanied by a traveling, fore-and-aft shock wave system, as indicated in Fig. 1. Such waves can no longer be discussed under the heading of one-dimensional flow; for example, flow through the oblique bow wave set up by the conical center body of an actual ramjet diffuser is a complicated three-dimensional case that is described by a nonlinear differential equation. Sufficient analysis will, however, be presented to illustrate what is implied by oblique shock waves and by Prandtl-Meyer expansions, since some of these are fundamental to the internal aerodynamics of the ramjet engine, and to the case of 'external' combustion as discussed briefly below.

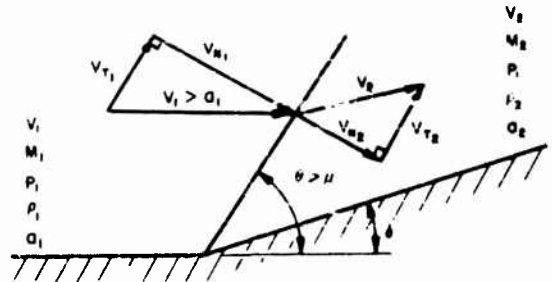
3.1 Oblique Shock Waves

The simpler case of oblique shock waves generated, e.g., by a wedge in a supersonic stream, is here considered to illustrate the principles involved. As before, the first assumption made is that the wave is infinitely thin. It is also necessary that the wave be 'attached' to the point of change of section of the boundary and hence that it is plane. This is because a rigorous theory for detached flows does not exist. A conical case gives rise to curved waves, and this is also true of a detached wave which results, for example, when the angle δ in Fig. 14 is large at low Mach numbers. In general, flow downstream of an oblique wave is supersonic, but it is possible to obtain subsonic flow just before δ becomes large enough to cause detachment.

It is convenient to commence by considering how the flow is turned by the action of a wedge of angle δ projecting into the stream. The inclination θ of the oblique wave set up by a wedge is greater

than the Mach angle μ . (Figure 4 should be consulted here, since it illustrates in effect the relationship between the fluid velocity and the propagation velocity of a disturbance.) The propagation velocity

Fig 14 Definition of Velocity Vectors across Two-Dimensional Oblique Shock Wave



of a shock wave is greater than that of a Mach wave. The flow vectors V_1 and V_2 , representing the flow on entering and leaving the shock wave, are shown resolved into normal and tangential components along the wave. V_2 is actually obtained by vectorial addition of a tangential component V_{T2} ($= V_{T1}$) to the normal velocity V_{N2} . The relation between V_{N1} and V_{N2} is that for flow passing through a normal shock so that V_{N2} is subsonic. These quantities may also be related by means of the continuity equation normal to the wave front,

$$\rho_1 V_{N1} = \rho_2 V_{N2} = (V_{N1} + dV_N)(\rho_1 + d\rho) ,$$

whence

$$V_{N1} d\rho = -\rho_1 dV_N, \text{ so that } dV_N = -V_{N1} \frac{d\rho}{\rho_1} .$$

Application of the momentum equation parallel to the wave front gives

$$(\rho_1 V_{N1}) V_{T1} = (\rho_1 + d\rho)(V_{N1} + dV_N)(V_{T1} + dV_T) ,$$

across the shock

$$\rho_1 v_{N1} v_T = 0 \quad \text{or} \quad v_{T1} = v_{T2}$$

The energy equation for compressible flow across the shock

$$\frac{v_{N1}^2 + v_{T1}^2}{2} + \frac{\gamma}{\gamma - 1} \frac{p_1}{\rho_1} = \frac{v_{N2}^2 + v_{T2}^2}{2} + \frac{\gamma}{\gamma - 1} \frac{p_2}{\rho_2}$$

simplifies to

$$\frac{v_{N1}^2 - v_{N2}^2}{2} = \frac{\gamma}{\gamma - 1} \left(\frac{p_2}{\rho_2} - \frac{p_1}{\rho_1} \right) \quad (78)$$

From the momentum equation, for the normal component of the shock,

$$p_1 + \rho_1 v_{N1}^2 = p_2 + \rho_2 v_{N2}^2$$

so that

$$v_{N1}^2 - v_{N2}^2 = (p_2 - p_1) \left(\frac{1}{\rho_1} + \frac{1}{\rho_2} \right) \quad (79)$$

Combining Eqs. (78) and (79), one has

$$\frac{p_2}{p_1} = \frac{\frac{\gamma + 1}{\gamma - 1} \frac{p_2}{\rho_1} - 1}{\frac{\gamma + 1}{\gamma - 1} - \frac{\rho_2}{\rho_1}} \quad \text{or} \quad \frac{\rho_2}{\rho_1} = \frac{\frac{\gamma + 1}{\gamma - 1} \frac{p_2}{p_1} + 1}{\frac{\gamma + 1}{\gamma - 1} + \frac{p_2}{p_1}} \quad (80)$$

These are well-known Rankine-Hugoniot relations.

It can be seen that

$$\frac{\tan \theta}{\tan(\theta - \delta)} = \frac{V_{N_1} V_{T_2}}{V_{T_1} V_{N_2}} = \frac{V_{N_1}}{V_{N_2}} = \frac{\rho_2}{\rho_1}$$

and

$$V_{T_1} = V_{T_2}$$

Hence

$$1 - \frac{\rho_1}{\rho_2} = \frac{\tan \theta - \tan(\theta - \delta)}{\tan \theta} = \frac{\sin \delta}{\sin \theta \cos(\theta - \delta)} \quad (31)$$

and

$$\frac{\rho_2}{\rho_1} - 1 = \frac{\tan \theta - \tan(\theta - \delta)}{\tan(\theta - \delta)} = \frac{\sin \delta}{\cos \theta \sin(\theta - \delta)} \quad (32)$$

Introducing the Mach numbers on the two sides of the wave,

$$V_{N_1} = V_1 \sin \theta = a_1 M_1 \sin \theta \quad (33)$$

and

$$V_{N_2} = V_2 \sin(\theta - \delta) = a_2 M_2 \sin(\theta - \delta) \quad (34)$$

From the momentum and continuity equations,

$$P_2 - P_1 = \rho_1 V_{N_1}^2 \left(1 - \frac{\rho_1}{\rho_2}\right) = \rho_2 V_{N_2}^2 \left(\frac{\rho_2}{\rho_1} - 1\right),$$

so that

$$V_{N_1}^2 = \frac{P_2 - P_1}{\rho_1 \left(1 - \frac{\rho_1}{\rho_2}\right)} = \frac{(\gamma + 1) P_2 + (\gamma - 1) P_1}{2\rho_1},$$

and

$$V_{N_2}^2 = \frac{(\gamma + 1) P_1 + (\gamma - 1) P_2}{2\rho_2}$$

by substitution from Eq. (80).

From Eqs. (83) and (84),

$$M_1^2 \sin^2 \theta = \frac{V_{N_1}^2}{a_1^2} = \frac{\gamma + 1}{2\gamma} \frac{P_2}{P_1} + \frac{\gamma - 1}{2\gamma}, \quad (85)$$

and

$$M_2^2 \sin(\theta - \delta) = \frac{V_{N_2}^2}{a_2^2} = \frac{\gamma + 1}{2\gamma} \frac{P_1}{P_2} + \frac{\gamma - 1}{2\gamma}. \quad (86)$$

Standard relationships thus exist between M_1 , M_2 , δ , θ , (P_2/P_1) and (ρ_2/ρ_1) . Some of the most important are shown in Fig. 15, in which it will be seen that for given values of M_1 and δ , two solutions of θ are possible; experimentally, however, it is observed that only the lower or weaker wave solution occurs. Above the line marked $\theta = \theta_{\max}$ the shock wave detaches. Although the constant value of 1.40 has been used for γ in plotting this figure, for Mach numbers higher than about 3 the temperature rise through the shock wave will necessitate account being taken of variable specific heat. Similar effects occur in the case of flow through a three-dimensional oblique shock set up by a cone facing into a supersonic stream. In this case stream properties are constant along radii from the vertex. The compression effect of a cone is weaker than a wedge, however, and the oblique shock becomes detached at a lower Mach number.

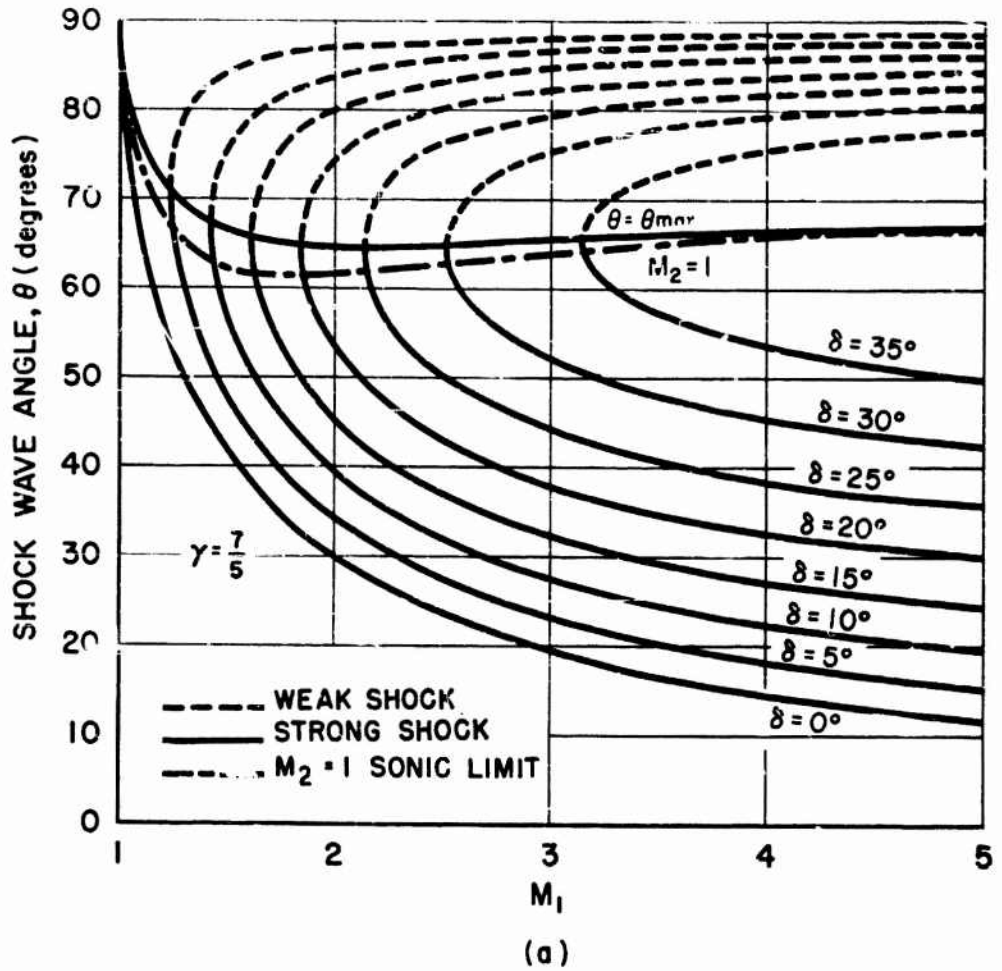
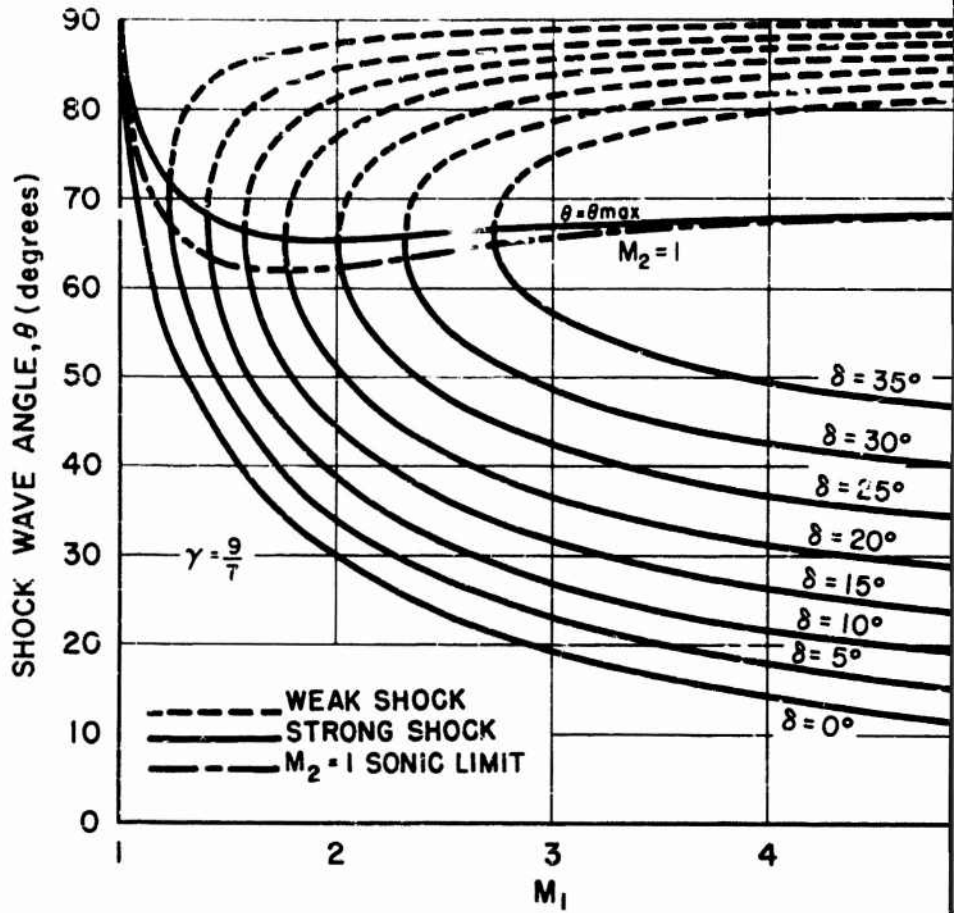


Fig. 15(a) Variation of Shock Wave Angle with Upstream Mach Number for Various Flow Deflection Angles



(b)

Fig. 15(b) Variation of Shock Wave Angle with Upstream Mach Number for Various Flow Deflection Angles

It is of interest at this stage to consider briefly the reflection and intersection of oblique shock waves. Figure 16(a) shows the simple case of ideal reflection of a shock wave at a solid boundary whereby the downstream flow is turned parallel to the boundary. A similar case is shown in Fig. 16(b) for the intersection of shock waves of equal strength. In Fig. 16(c) the effect of the intersection of shock waves of unequal strength is shown: pressure, temperature, density and entropy discontinuities occur while the two flow velocity vectors remain parallel. If the wedge angle δ is fixed and M_1 is decreased, a point is reached when it is no longer possible to deflect the M_2 stream through the angle δ parallel to the wall. This case, shown in Fig. 16(d), is known as a 'Mach reflection.' A similar surface of discontinuity is set up. The corresponding situation brought about by the Mach reflection of two shocks of equal strength is shown in Fig. 16(e). The above case, Fig. 16(a), of 'positive' reflection at a solid boundary, may be compared to the case of 'negative' reflection at the free boundary of a jet, as shown in Fig. 19, which is the Prandtl-Meyer expansion case dealt with in the next section.

3.2 Prandtl-Meyer Expansions

In contradistinction to subsonic flow, supersonic flow may expand around a sharp corner without loss, and unlike the shock phenomena described above, the expansion wave is an isentropic flow case, and can be considered to be a succession of Mach waves. The two-dimensional case shown in Fig. 17 will now be referred to. A turning angle $d\psi$ is shown.

The equation of continuity may be written down as for the oblique shock case, giving

$$dV_N = -V_{N1} \frac{d\rho}{\rho_1} \quad (87)$$

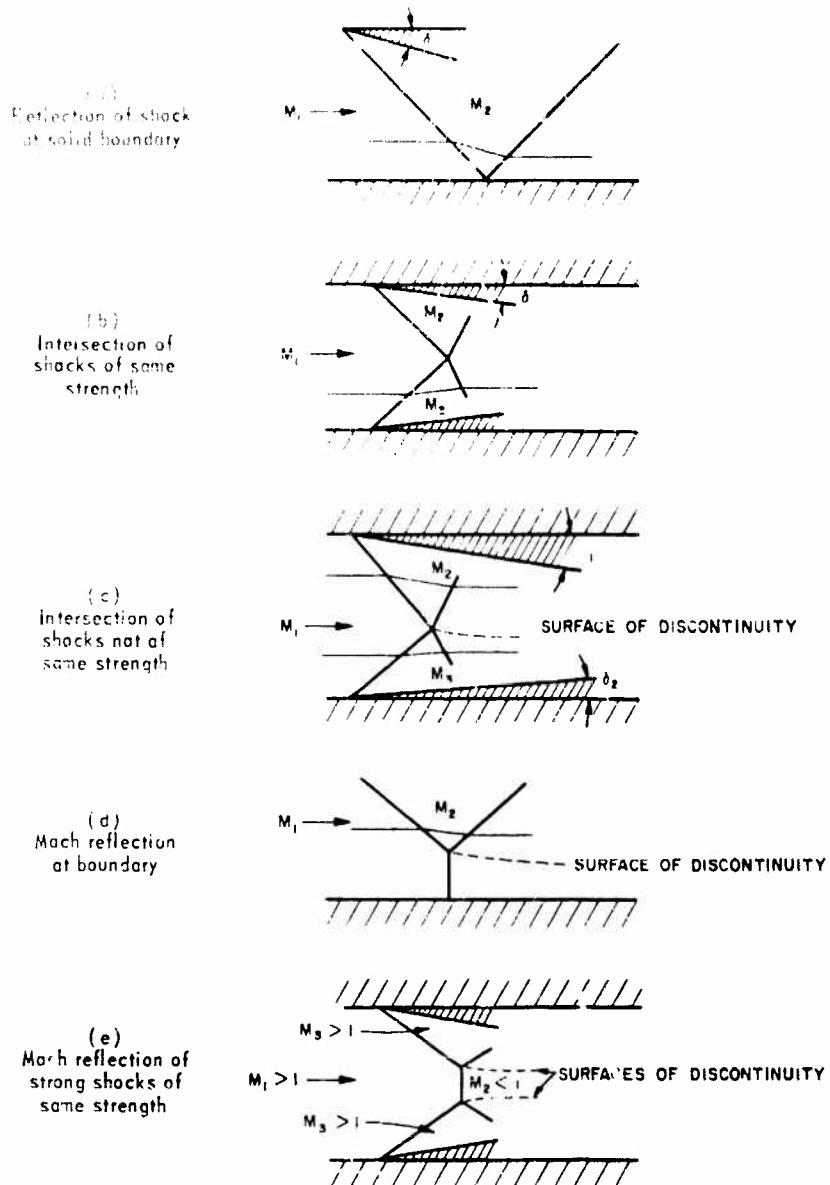
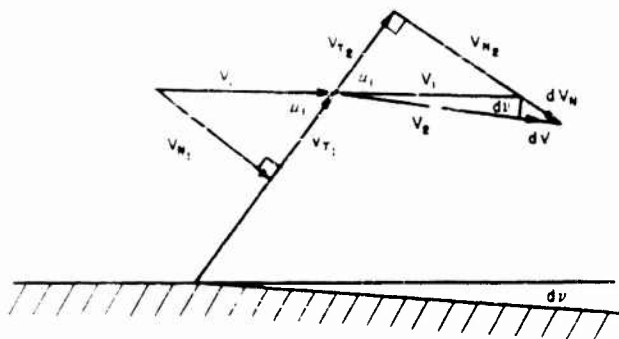


Fig. 16 Reflection and Intersection of Oblique Shock Waves

Fig. 17 Prandtl-Meyer Expansion around Two-Dimensional Corner.



and from the momentum equation applied parallel to the shock front,

$$V_{T1} = V_{T2}, \quad (88)$$

as before.

From the equation of momentum normal to the wave front,

$$dP = P_2 - P_1 = (\rho_1 V_{N1}) V_{N1} - (\rho_1 + d\rho)(V_{N1} + dV_N)(V_{N1} - dV_N), \quad (89)$$

whence

$$\frac{dP}{\rho_1} = -V_{N1} dV_N.$$

Eliminating dV_N between Eqs. (87) and (89), $V_N^2 = \frac{dP}{d\rho} = a^2$, which emphasizes that this is an isentropic process.

From the Mach triangle,

$$V_2 - V_1 = dV = dV_N \sin \mu_1,$$

$$\text{where } \mu_1 = \sin^{-1} \frac{V_{N1}}{V_1} = \sin^{-1} \frac{1}{M_1}$$

$$\tan^{-1} \frac{1}{\sqrt{M_1^2 - 1}}$$

The turning angle d ,
$$\frac{dV \cos \mu_1}{V_1} = \frac{dV \cos \mu_1}{V_1 \sin \mu_1},$$

from which

$$\frac{dV}{V_1} = \frac{dv}{\sqrt{M_1^2 - 1}}$$

Now from the energy equation

$$\frac{V_1^2}{2} + \frac{a_1^2}{\gamma - 1} = \frac{\gamma + 1}{2(\gamma - 1)} a^{*2},$$

$$\left(\frac{V_1}{a^*}\right)^2 = \frac{\gamma + 1}{\gamma - 1 + \frac{2}{M_1^2}}, \quad \text{since } M_1^2 = \frac{V_1}{a_1},$$

$$= V_1^2.$$

$$\therefore M_1^2 = \frac{2V_1^2}{(\gamma + 1) - (\gamma - 1)V_1^2}, \quad (90)$$

and

$$dv = \sqrt{\frac{V_1^2 - 1}{1 - \frac{(\gamma - 1)V_1^2}{\gamma + 1}}} \frac{dV}{V_1}. \quad (91)$$

As the flow expands, it is said to accelerate the flow from $M_1 = 1$ to $M_1 = \infty$. For $M_1 = 1$, it follows that $\theta = 0$, and $\bar{V}_1 = 1$.

Therefore,

$$\int_0^{\theta} d\theta = \int_1^{\bar{V}_1} \frac{\bar{V}_1^2 - 1}{\left[1 - \left(\frac{\gamma-1}{\gamma+1}\right)\bar{V}_1^2\right] \bar{V}_1} \frac{d\bar{V}_1}{\bar{V}_1} .$$

$$\theta = \frac{1}{2} \sqrt{\frac{\gamma+1}{\gamma-1}} \left[2 - \sin^{-1} \left(\gamma - \{\gamma-1\} \bar{V}_1'^2 \right) \right] - \left[\frac{\pi}{2} + \sin^{-1} \left(\gamma - \{\gamma-1\} \frac{1}{\bar{V}_1'^2} \right) \right] . \quad (92)$$

Since M_1 and \bar{V}_1 are related by Eq. (90), Eq. (92) may be transformed into the following form:

$$\theta = \sqrt{\frac{\gamma+1}{\gamma-1}} \tan^{-1} \left(\sqrt{\frac{\gamma-1}{\gamma+1}} \sqrt{M_1'^2 - 1} \right) - \tan^{-1} \sqrt{M_1'^2 - 1} . \quad (93)$$

A maximum value of θ occurs when $M_1' = \infty$ (assuming that the flow is still gaseous), i.e.,

$$\theta_{\max} = \frac{\pi}{2} \left(\sqrt{\frac{\gamma+1}{\gamma-1}} - 1 \right) = 130.5^\circ \text{ for } \gamma = 1.4 .$$

In practice, flow will not expand around a sharp corner to anything like this value, and boundary layer separation limits θ to about 30° .

3.3 Nozzle Flow and Jet Structure

The isentropic equations for variable area duct flow, together with the shock wave equations derived above, are also useful for illustrating various phenomena occurring in nozzles. For example, it was shown in Eq. (21) that

$$\frac{dA}{A} = \frac{dP}{P} \frac{1 - M^2}{\gamma M^2}$$

i. e., the change of pressure with area depends on the Mach number of the flow. When $M < 1$, dP has the same sign as dA , but when $M > 1$, dP has the opposite sign, the change occurring at a throat where $M = 1$. A nozzle attached to a reservoir may thus consist of a subsonic portion (converging) and a diverging portion which will run partially or wholly supersonic if the reservoir pressure is sufficient to cause choking at the throat. As may be seen in the two-dimensional diagram, Fig. 18, if the pressure P as obtained at the throat during flow is initially such that $(P/P_t) > 0.528$, the critical pressure ratio for air, the nozzle corresponds to a subsonic venturi, and the pressure variation follows a line above ABC. The pressure downstream of the nozzle then corresponds to a certain exit pressure ratio (P_e/P_t) . When the pressure ratio $(P/P_t) = 0.528$, two flow solutions are theoretically possible, the pressure variation lying along either ABC or ABD, for flow in the diverging portion to be either completely subsonic or supersonic. Which one is followed depends on the value of the downstream pressure ratio (P_e/P_t) , and acceleration of the flow beyond the subsonic condition may only be brought about by reduction of (P_e/P_t) below the value at C, by varying either component of this ratio. (If P_t remains constant, the mass flow through the throat cannot then be increased.)

It may be noted that the surface in the flow at the throat where M becomes unity is not plane, but is slightly convex down-

sition. This is due to the fact that one-dimensional flow is an oversimplification. The smooth nozzle contour shown in Fig. 18 is not the only possible arrangement for accelerating the flow to supersonic velocity, but is a simple case chosen to illustrate the various flow conditions. Such nozzles are designed on the principle of avoidance of shock losses by successive cancellation of compression and expansion waves, and by good design nearly one-dimensional flow can be obtained at the parallel exit section of the nozzle shown.

For supersonic flow to occur downstream of the sonic throat, the pressure and Mach number reached are now fixed by the expansion ratio (A/A^*). Since for supersonic flow to occur throughout the nozzle, the exit ratio must correspond to the point ν ; for all values of $P_C > P_e > P_D$, the solution will be represented by supersonic followed by subsonic flow in the diverging portion of the nozzle. In the absence of a converging section to act as an isentropic diffuser to bring about this transition, the change must occur nonisentropically through a shock wave, its position being completely determined by the pressure ratio across the shock with the downstream subsonic pressure rise following one of the paths BEFG, in order that $P_e = P_G$, say. If $P_e = P_H$, the shock in its simplest form will be a normal shock positioned at the nozzle exit. As (P_e/P_t) is reduced further, reexpansion of the flow will occur through oblique shocks, either by Mach reflection (P_e near P_H) or simple reflection (P_e near P_D). These are represented by the overexpanded cases shown in Figs. 19(a) and 19(b) in somewhat idealized form. The supersonic core of the whole jet gradually diminishes in cross section as the subsonic jet boundary extends due to entrainment of the surrounding atmosphere, when present. As P_e is reduced to P_D , the external shocks become weaker, but never entirely disappear, even with a parallel jet emerging from the exit when $P_e = P_D$. Since P_D is fixed by the reservoir pressure, further reduction of P_e will result in the formation of expansion waves at the exit, as shown in Fig. 19(c). This is the underexpanded case.

So far no mention has been made of viscous effects, but in actual flow the pressure rise through the shock wave may give rise to

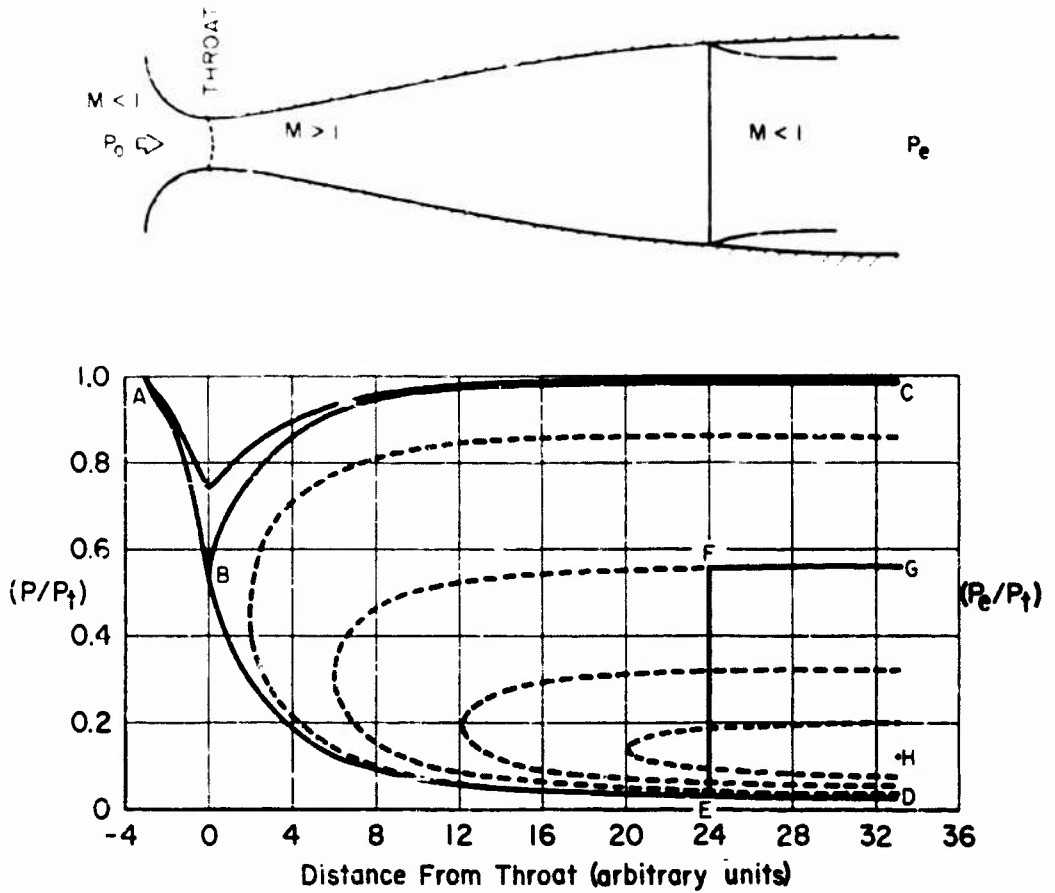


Fig. 18 Flow with Normal Shock In Air, $M = 3$ de Laval Nozzle

boundary layer separation on the walls of the nozzle, with resulting flow downstream as shown in the upper diagram of Fig. 18. As an example of this, it may be noted that in the rocket (straight-sided) type of nozzle referred to below, separation of the boundary layer will occur when the nozzle exit pressure is approximately 0.45 of the ambient pressure, whatever the divergence angle may be. More complicated shock wave-boundary layer interactions are also possible but need not be considered in detail in this treatment. A typical case is the bifurcation of the shock at the nozzle wall (Mach reflection).

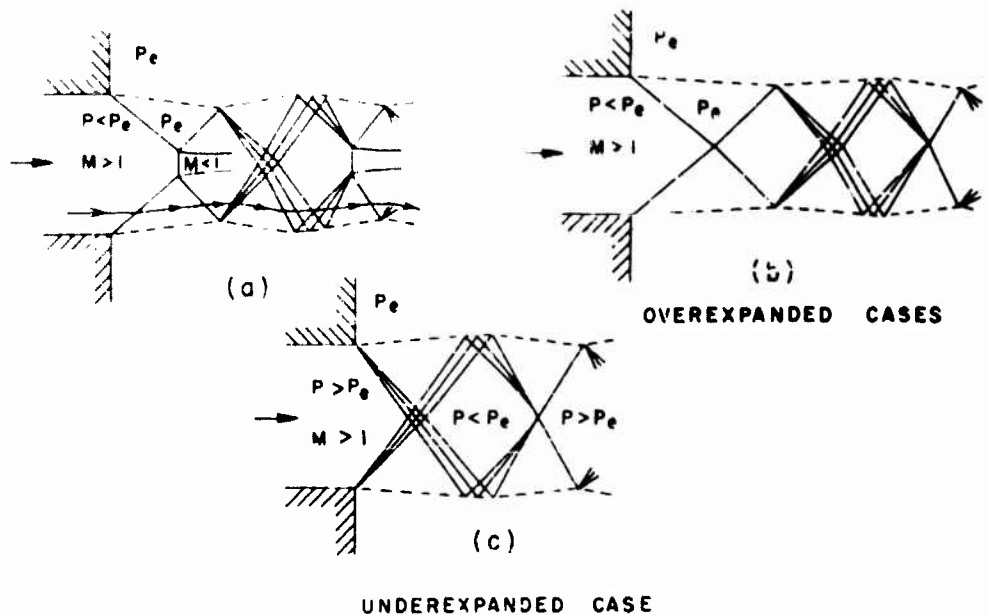


Fig. 19 Two-Dimensional Supersonic Jet Structure

An actual supersonic jet emerging from a nozzle may show considerable fine structure, but it consists basically of a number of 'cells' representing cyclic flow transitions which persist until they are damped out by viscous interaction with the surrounding atmosphere. The jet, after it leaves the nozzle, exhibits successive negative, or opposite, reflections of shocks or expansion waves as required to turn the flow at a free (constant pressure) boundary, as shown in Fig. 19. The successive subsonic cores behind the Mach reflections in the overexpanded case, Fig. 19(a), are gradually energized by turbulent mixing, so that the surfaces of discontinuity die out rapidly.

It is convenient to illustrate such phenomena with reference to two-dimensional nozzles and jets, since the flow patterns are thereby simplified; for example, the jet boundaries are initially straight lines. In the more common axisymmetrical arrangement, these boundaries become curved. Such a convergent nozzle operating under high reservoir pressure gives rise to a heavily underexpanded type of jet, as shown in

the three-dimensional case of Fig. 20, and such a jet becomes subsonic after one cell. The form taken by the jet under various pressure conditions has been discussed by Wilcox *et al.*, (Ref. 6), among others. All these relations refer, as indicated previously, to equilibrium flow conditions.

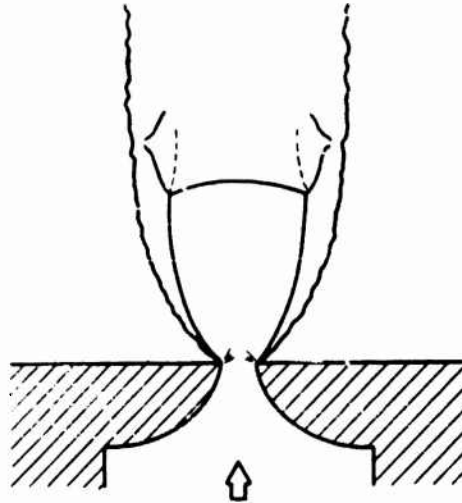


Fig. 20 Heavily Underexpanded Nozzle Flow Case

Up to now only completely expanded nozzle profiles have been considered, i.e., those in which the flow emerges parallel to the axis if the nozzle is operated under the correct pressure conditions. Exit nozzles used with many ramjet engines are customarily constructed with a conical diverging section, on the pattern of rocket nozzles, the shortening representing a compromise between reduction of weight and supersonic friction loss on the one hand, and increased divergence loss on the other. The most suitable expansion angle will thus be somewhat greater than that at which the thrust is a maximum. This simplified contour is clearly an advantage if the engine is designed for a limited life. The jet emerging from a conical nozzle is different from that previously considered in that divergence imparts a radial

component of velocity to the jet, which will then continue to expand and so on until the point where recompression sets in.

3.4 "Supersonic" Combustion

In view of the above, it is of interest to refer briefly to the modifying effect of heat addition (by burning) to a supersonic stream within a nozzle or free jet. (This case is of some importance in advanced ramjet design, since supersonic flow in the diffuser and combustion chamber could be a desirable mode of operation.) A theoretical analysis of such a concept of burning in a supersonic stream in ramjet engines has been published by Weber and Mackay (Ref. 7). It has been previously shown that one of the immediate effects of such heat addition is the reduction of the Mach number, either through a shock system or otherwise. Three recent demonstrations of combustion in a supersonic stream are shown in Figs. 21 to 23 (Refs. 8 through 10).

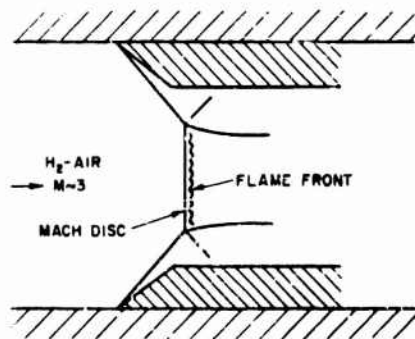


Fig. 21 Strong Standing Detonation Wave
(Two-Dimensional Mach
Reflected Shock)
(Taken from Ref. 8.)

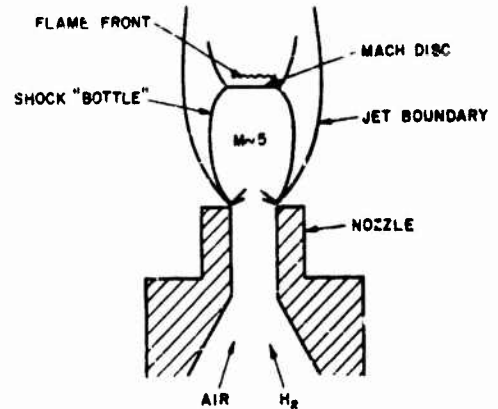


Fig. 22 Combustion in Open Jet from
Underexpanded Axisymmetric
Nozzle
(Taken from Ref. 9.)

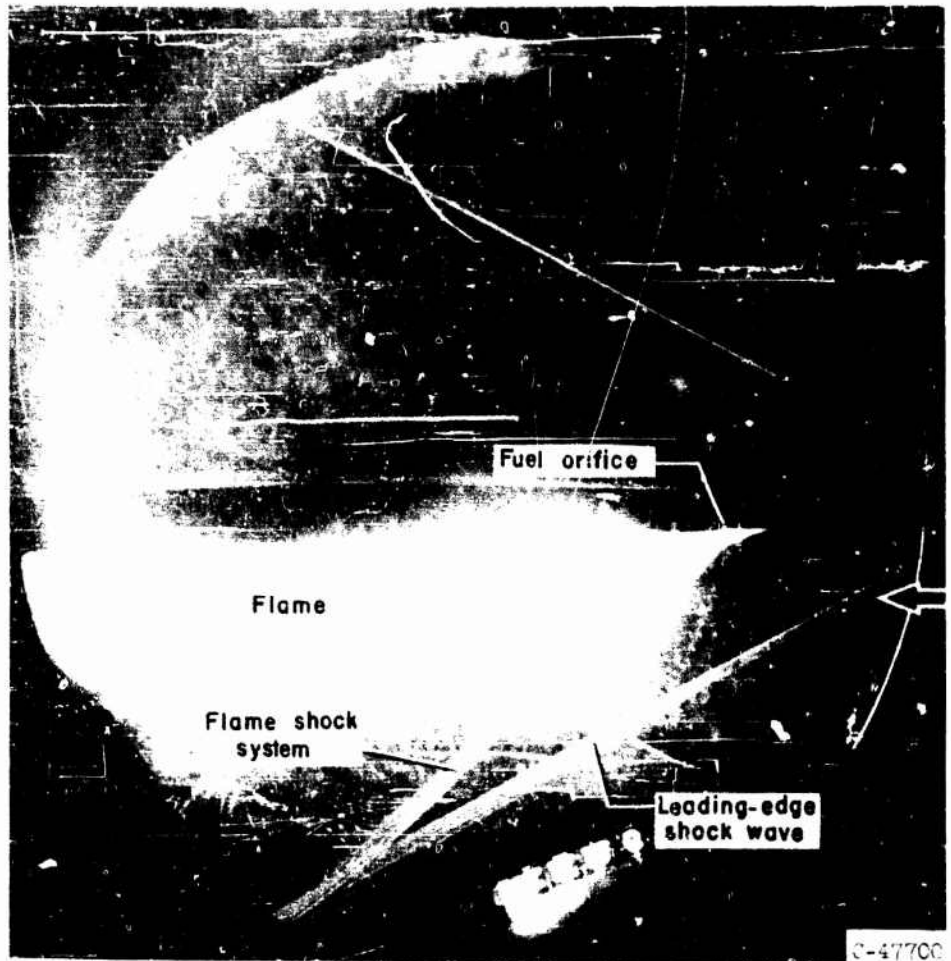


Fig 23 Combination Open-Shutter and Schlieren Flash Photograph of Flame and Associated Shock-Wave System in Stream below Surface of Wing, Mach Number, 2.47, Angle of Attack, 2° (Taken from Ref. 10.)

In the first of these cases a Mach-reflected normal shock wave was set up by inserting wedges in a wind tunnel. The rise of static pressure and temperature downstream of the normal part of the shock system ignited the combustible gas mixture (H_2 - air) at this point. The on-

set of combustion was observed to displace the normal shock upstream (Fig. 21). In the second instance, Fig. 22, a similar situation was set up downstream of the first Mach disc occurring in an underexpanded open jet, and it was considered that the axial distance between the flame front and the Mach disc corresponded to that expected from ignition delay. Interaction between the combustion region and the wave system was also observed in some cases, resulting in the wave system moving upstream, corresponding to a reduction in Mach number. Neither of these two cases, however, illustrates true supersonic burning, but they are considered to represent strong standing detonation waves.

To obtain combustion of a liquid fuel in a supersonic stream without the formation of normal shock waves, it might at first sight seem desirable to inject the fuel into a supersonic air stream with a component in the air flow direction equal to that of the air, but this is clearly out of the question because of the enormous pressures necessary to effect this. In fact, demonstrations to date have taken the form of simple injection at right angles to the flow, and Fig. 23 typifies a case of external burning of a liquid fuel beneath a wing section. Here combustion would appear to be fairly generalized in the supersonic region downstream of the oblique shock formed at the point of injection. These and other studies indicate that this application of external supersonic burning may be important in ramjet propulsion at high Mach numbers. A recent report by Woolard (Ref. 11) lists further useful references to published work in this field.

IV. RAMJET COMPONENT PERFORMANCE

The above gas dynamic considerations now need to be applied--with emphasis on component performance--in order to illustrate the functioning of a ramjet as a heat engine. Mention will be made of the design and the detailed functioning of the diffuser, combustor, and exit nozzle and how these are affected by flight environmental conditions and the requirements of thrust and power output.

4.1 The Ramjet Thermodynamic Cycle

The ideal thermodynamic operating cycle of the ramjet is shown in Pv form in Fig. 24. Strictly speaking, such a diagram, which here represents a continuous flow process, should not close, although it is conveniently represented in this form for purposes of analysis. This cycle, the Brayton or Joule cycle, consists of four parts, three of which are associated with the engine proper, while the fourth is assumed to be completed in the external atmosphere. The first part of the theoretical cycle consists of adiabatic compression of air which enters at high velocity and low pressure, as shown by $a \rightarrow b$. Heat is then added under conditions of constant pressure P , and constant momentum ($P + \rho V^2 = \text{constant}$). This operation increases the entropy of the gas, and there is an increase of velocity as the gas density is reduced. This is shown by $b \rightarrow c$. The heated gases are then further expanded, transforming a part of the added thermal energy into mechanical energy. This portion of the cycle is shown by $c \rightarrow d$. This exhaust jet, even if expanded to the freestream value, emerges with a much higher temperature and velocity than the entering air flow. The force required to accelerate the expanding exhaust gases thus reacts against the interior surfaces of the ramjet and thereby propels the engine forward. In the final phase of the heat engine cycle, assumed to occur in the

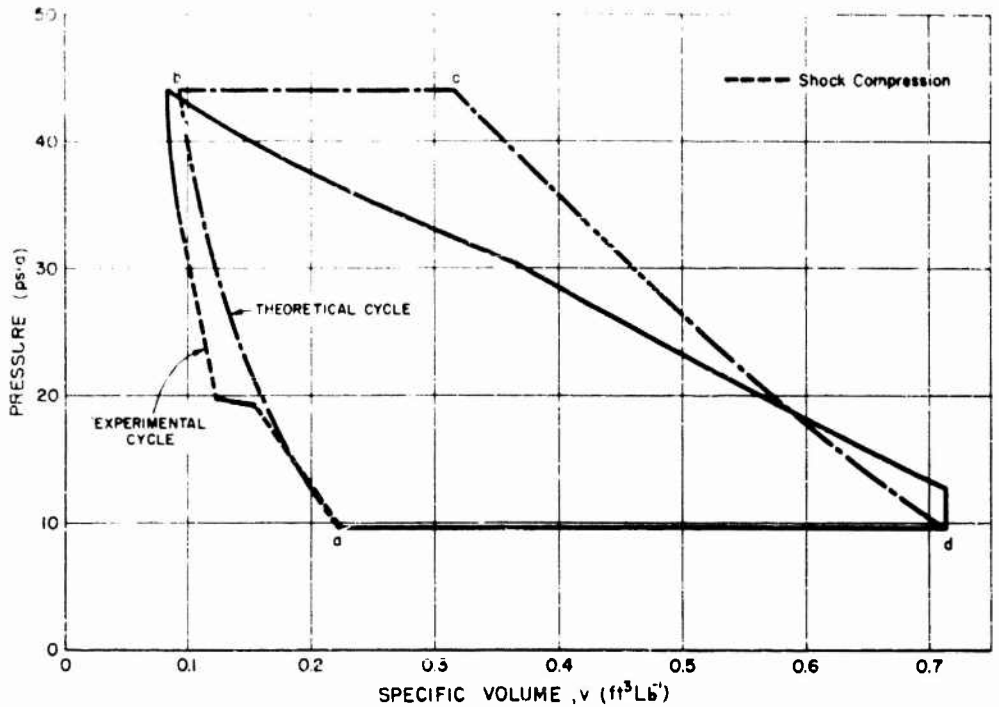


Fig. 24 Thermodynamic Cycle of a Ramjet Engine

free atmosphere, the hot exhaust gases are cooled by contact with this relatively infinite reservoir, with consequent increase in density at constant pressure, as shown by $d \rightarrow a$.

Since the ramjet engine is a continuous flow device, the functions of compression of the inlet gas, addition of heat, and expansion of the hot gas need to be performed by separate components; the devices which carry out these functions, the diffuser, combustion chamber, and exit nozzle, were shown in Fig. 1. The changes in gas state from Station 0 (located in the free air stream) to Station 2 are accomplished by the diffuser and are characterized by partial conversion of the kinetic energy of the gas into pressure energy, usually through both oblique and normal shocks followed by diffusion in the internal

tion. An oblique shock is set up by the apex of the center body and propagates forward of the inlet; this feature is characteristic of all designs operating at supersonic Mach numbers in excess of about 1.8. Various losses reduce the pressure obtainable at the end of diffusion, and the diffuser total pressure recovery, which reflects the efficiency of the compression process, decreases as the flight Mach number is increased. Although on the actual Pv diagram (Fig. 24) the compression process may seem to conform closely to the ideal adiabatic case, a Ts diagram would show that the process of shock compression of air is attended by some considerable increase of entropy due to the shock transitions and the diffusion losses mentioned.

Addition of thermal energy to the air in the combustion chamber between Stations 2 and b is generally brought about by the oxidation of a fuel (although it could equally well be effected by other chemical reactions or by a physical heat source such as a nuclear reactor). As previously shown, the addition of heat to a moving air stream increases the velocity of the stream and thereby produces an effect analogous in some ways to that which occurs when the stream passes through a shock wave: an increase of entropy together with a fall in total pressure. In the representation of the combustion process on the Ts diagram, if this actually followed a line of constant pressure, it could be represented on such a line, as shown in Fig. 12. In practice, flameholder drag will contribute to a drop in pressure during the combustion process. However, it seems plausible that a Rayleigh line for constant mass flow would be a faithful reproduction of the heat transfer process; Fig. 25, which is an amplification of the previous case, shows Rayleigh lines for different duct areas which thus enable the whole diffusion process to be represented. Referring to Fig. 25, the thermodynamic efficiency η_t is thus given by

$$\eta_t = \frac{\text{Heat received} - \text{heat rejected}}{\text{heat received}}$$

$$= \frac{\text{areas C} - (\text{E} + \text{B})}{\text{areas C} + \text{D}}$$

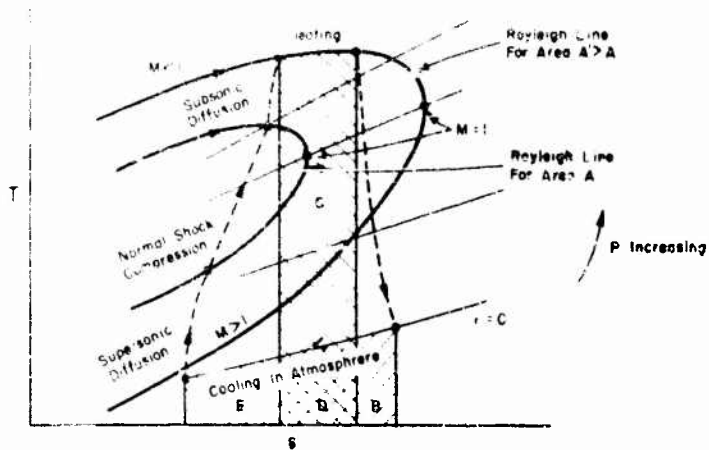


Fig. 25 Ramjet Cycle on Ts Diagram

The Fanno lines are omitted for clarity.
(Taken from Ref. 7.)

If the propulsion coefficient η_p accounts for the ratio of useful engine work to theoretical cycle work, then the over-all efficiency η_o is given by

$$\eta_o = \eta_t \eta_p$$

Since acceleration of the exhaust gases to sonic or supersonic velocity is a function of the exhaust nozzle, the formation of a thermal throat at the exit to the combustion chamber is avoided. The complete pressure drop in the nozzle will not be realized, however, owing to losses due to friction and cooling. Typical average gas states at different points of the system are shown in Fig. 26. These diagrams are reasonably representative for an engine operating at a flight Mach number of about 2.

The functioning of the various engine components will now be discussed in somewhat greater detail. For convenience, flows will be discussed with reference to a system of axes chosen to move with the vehicle, i.e., the engine is assumed to be stationary with the gases in motion.

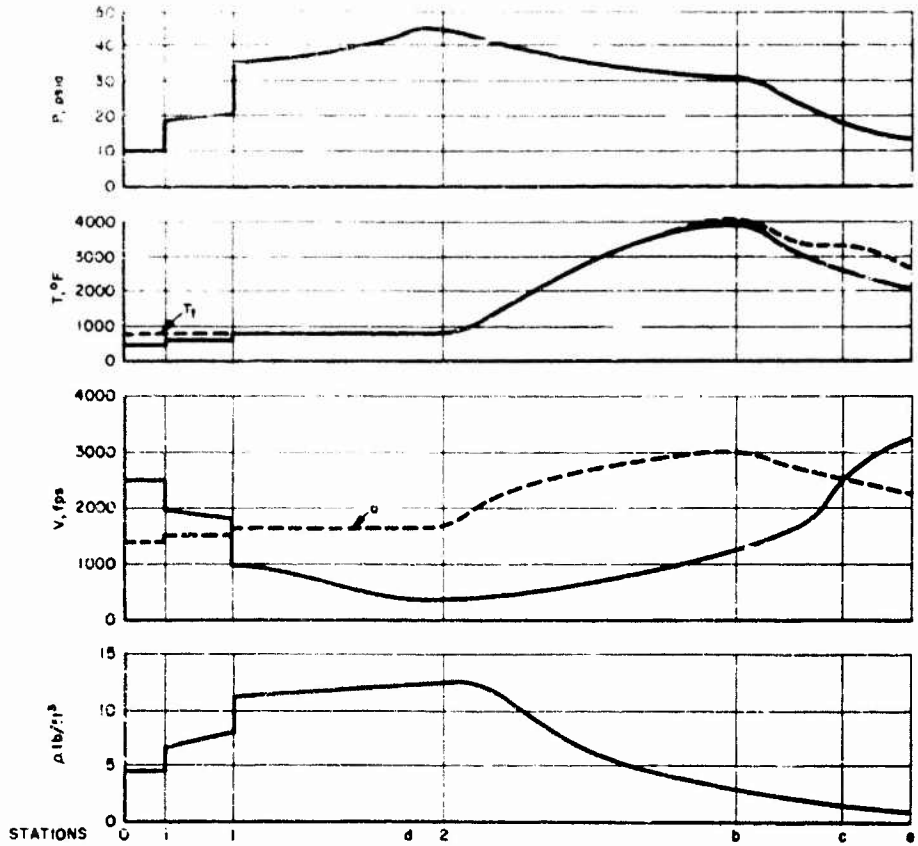


Fig. 26 Pressure, Temperature, Velocity, and Density at Various Stations in a Ramjet Engine

(Taken from Zucrow, Aircraft and Missile Propulsion, Vol. 1, p. 98.)

3.2 The Diffuser

This is generally the forwardmost component of the ramjet engine and serves to convert the high velocity, low pressure energy of the free air stream into low velocity, high pressure energy to meet the requirements of the downstream combustion chamber. Since no heat is

transferred at this stage, the compression from 0 to 2 is adiabatic, but the flow is not isentropic³ because of shock, skin friction, and other losses due to turbulence in the flow. Static pressure and static temperature are also increased between Stations 0 and 2 by compression, while the velocity is reduced. Flow within the diffuser duct from Stations 1 to 2 may be either partly subsonic and partly supersonic, or else wholly subsonic, depending on the location of the normal shock wave attached to the center body. If this is upstream of the inlet 1, the diffuser is said to be operating 'subcritically' or 'with spill-over,' whereas if it is downstream of the inlet 1, the diffuser is said to be operating 'supercritically' or 'with shock swallowed'. If the normal shock is located at 1, the condition is then said to be that with 'shock on the rim' or 'critical.' These definitions, illustrated in Fig. 27, do not imply that the diffuser performance is satisfactory or otherwise, but merely indicate the relationship between actual and design operating conditions. Diffuser total pressure recovery generally tends to a maximum at the critical condition although this is by no means always true.

The diffuser exit Mach number is determined by the combustor impedance since all the air flowing through the diffuser (except that diverted to power auxiliaries) continues on into the combustion chamber at the subsonic speed determined by downstream drag, heat addition, and exit nozzle throat area. The independent operational variables determining diffuser performance are thus the fixed values of free-stream and exit Mach numbers. These variables, together with that of the diffuser total pressure recovery ratio, fix the two diffuser-dependent flow variables, inlet area capture ratio, and inlet drag force coefficient.

Diffusers which utilize either multiple shock or continuous (isentropic) supersonic compression experience smaller total pressure losses in decelerating supersonic streams to subsonic velocities than

³It may be noted that it is also possible to make use of a center body of gradually increasing curvature ('isentropic diffuser') which does not give rise to a strong oblique shock in the air inflow region.

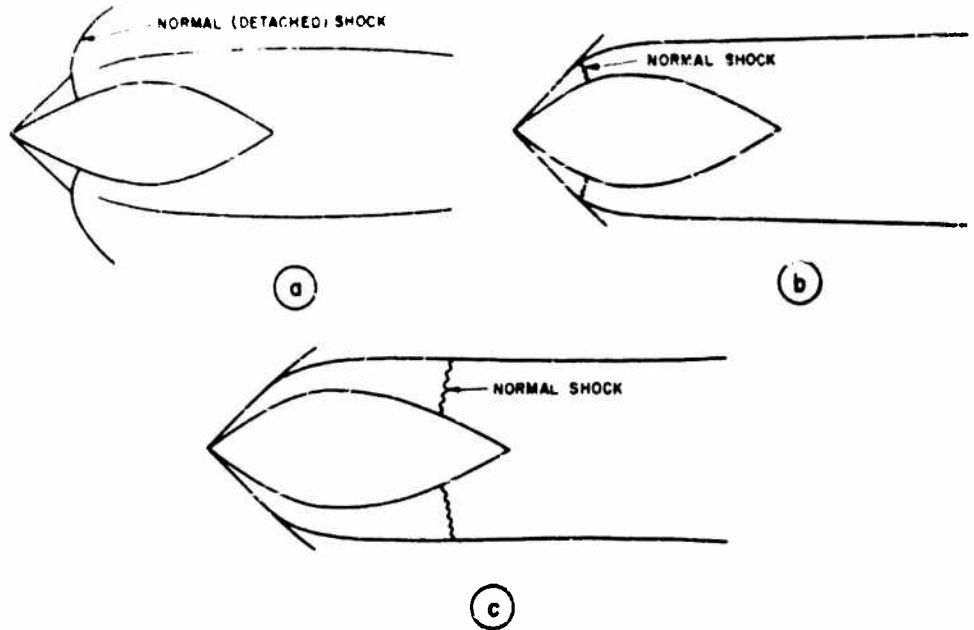


Fig. 27 Subcritical (a), Critical (b), and Supercritical (c) Diffuser Operation

do those which effect compression by means of a single normal shock. The superiority of the former type over normal shock inlets is small in the freestream Mach number region from 1.0 to 1.6, but this superiority increases rapidly thereafter, and makes such diffusers essential at Mach numbers above 2.0. There are also appreciable total pressure losses in the diffusion process from a high subsonic Mach number downstream of the last diffuser shock down to the low subsonic Mach number required at the combustion chamber inlet. The picture is further complicated by the possibility of the diffuser operating out of alignment with the oncoming airstream. The presence of yaw or pitch gives rise to an asymmetric shift of the shock wave pattern generally resulting in a reduction of the total pressure recovery and air capture, particularly if flow separation also occurs. Normal shock diffusers experience a small (and nearly predictable) loss in mass flow and pressure

of the inlet flow, the angle of yaw, which may more completely but not necessarily, be controlled. Diffusers suffer greater and less predictable behavior under different circumstances. At times diffusers exhibit behavior which causes the air flow capture and pressure recovery oscillating continuously or stepwise when the diffuser is operated at less than its design value of inlet flow. This phenomenon is known as "flow instability," an example of which is shown in Fig. 28. In most diffuser designs, the amplitude of this phenomenon is small and the disturbance does not impair engine operation significantly; in some cases, however, it is liable to interfere with the combustion process and reduce the engine power output.

Some general considerations relating to instability have been presented by Pearce (Ref. 12), and the subject is also covered in greater detail in TG 370-4 of this series. Pearce's stability criterion is simply that the slope of the curve of diffuser pressure recovery versus mass flow is less than the slope of the curve of combustion chamber inlet pressure versus mass flow. If this requirement is met, the system is self-compensating, since any fall in diffuser air flow then brings about a greater fall in the combustion chamber pressure than that which occurs in the available diffuser pressure so that the flow immediately comes to a condition of stable equilibrium. On this basis, surge cannot occur in a diffuser which provides for increasing pressure recovery with increased spillover in the working range. Accordingly, a safe criterion for stability is that the slope of the curve of diffuser pressure versus flow at the maximum thrust output point for the engine shall be negative, since the slope of the curve of combustor pressure versus flow is then always positive. The diffuser pressure recovery is likely to fall during subcritical operation as a result of disturbance of the inlet shock pattern arising both from boundary layer separation as a result of increased inlet pressure, and from forward motion of the normal shock which divides the regions of supersonic and subsonic flow. This boundary layer separation phenomenon can, by changing the boundary layer thickness, alter the effective shape of the inlet and thus lead to a change in the shock wave pattern, thereby reducing recovery. This effect is

BEST AVAILABLE COPY

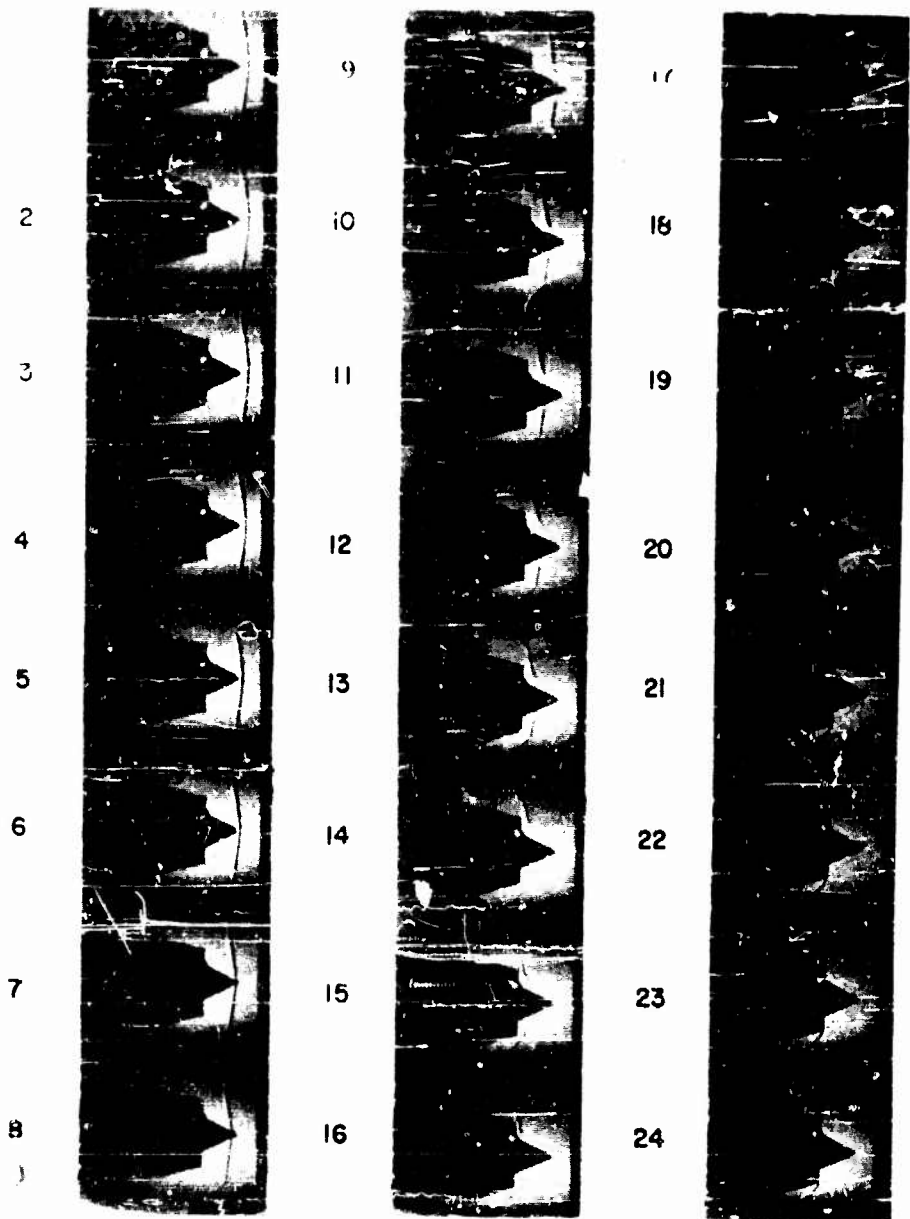


Fig. 28 Fast Motion Picture Sequence of Flow Instability at Intake of 1/7-Scale Model Ramjet, Showing One-Half Cycle of the Oscillation

The timing light is flashing at 1/120 second intervals; framing rate of 2880 per second at $M = 2.72$.

generally dependent on the flow Reynolds number and can be minimized or avoided by suitable boundary layer control. The adverse effect of the second phenomenon, i.e., forward motion of the normal shock, can generally be avoided by positioning the oblique shock wave slightly ahead of the diffuser cowl inlet so that the normal shock can be expelled slightly without disturbing the oblique shock. In this way the small amount of supercritical spillover (which occasions a slight increase in inlet drag) permits stable operation of the diffuser at its most efficient point. The engine may be operated with the diffuser at the critical point, and operation is very likely to be stable in the presence of low level pressure transients arising from the combustion process for a limited amount of spillover. The measures mentioned above are applied to diffusers as required and are not a part of this discussion--which presupposes stable diffuser and combustor operation.

The mass flow passing through the area A_0 in the undisturbed freestream passes into the diffuser inlet, is decelerated by a combination of supersonic and subsonic compression, and flows out through the area A_d . This stream has done no work; consequently its enthalpy (considered as the sum of its kinetic, potential, and internal thermal energies) has not changed, and the stream remains at a constant total temperature T_{t0} throughout the flow. Since the compression of the high velocity, low density inlet flow to a high density, low velocity state is not perfectly efficient, the entropy will have increased; this increase is manifest in the reduction of diffuser exit total pressure to below the freestream total pressure. The condition of continuity of the mass flow enables one to relate the freestream capture area A_0 to the exit area by means of the freestream and exit Mach numbers. Corresponding to the continuity equation

$$\dot{m} = \rho_0 V_0 A_0 = \rho_d V_d A_d ,$$

there exists the following relationship between areas, pressures, Mach numbers, and temperatures:

$$\psi_a = A_0 \left[\frac{(P/P_t) \frac{\rho}{W}}{\sqrt{T}} \right]_0 \frac{P_{t0}}{\sqrt{T_{t0}}} = A_d \left[\frac{(P/P_t) \frac{\rho}{W}}{\sqrt{T}} \right]_d \frac{P_{td}}{\sqrt{T_{td}}} \quad (94)$$

whence

$$A_0 = A_d \left(\frac{P_{td}}{P_{t0}} \right) \frac{\left[\frac{(P/P_t) \frac{\rho}{W}}{\sqrt{T}} \right]_d}{\left[\frac{(P/P_t) \frac{\rho}{W}}{\sqrt{T}} \right]_0} \quad (95)$$

The capture area A_0 may now be expressed as a function of the ratios (A_0/A_1) and (A_d/A_1) :

$$\left(\frac{A_0}{A_1} \right) = \left(\frac{A_d}{A_1} \right) \left(\frac{P_{td}}{P_{t0}} \right) \frac{\left[\frac{(P/P_t) \frac{\rho}{W}}{\sqrt{T}} \right]_d}{\left[\frac{(P/P_t) \frac{\rho}{W}}{\sqrt{T}} \right]_0} \quad (96)$$

Here A_1 is the diffuser inlet area, and (A_0/A_1) is thus the effective inlet capture area ratio. Thus, if one fixes the diffuser exit and the freestream Mach numbers, the air flow capture ratio will be determined by the pressure recovery for subsonic flow within the diffuser. When the value of (A_0/A_1) attains its maximum (critical flow) value in Eq. (96), it is then no longer possible for the flow to increase further. If M_d is increased for a given M_0 at constant air flow, the pressure recovery ratio (P_{td}/P_{t0}) at this moment must become a function of M_d since it is the only free variable for a fixed value of (A_0/A_1) . Now the flow within what is normally the subsonic diffuser becomes partially supersonic and experiences a total pressure loss in returning to subsonic flow. This added diffuser total pressure loss serves to render (P_{td}/P_{t0}) variable and consistent with $(A_0/A_1)_{\max}$, and the exit to inlet diffuser area ratio (A_d/A_1) will show the same pressure recovery in this region of 'swallowed shock' flow regardless of geometrical design. The inlet drag (force over the diffuser inlet) is needed as well as the total pressure recovery for the performance of a diffuser.

to be determined. Both quantities are ordinarily determined by experiment for a given diffuser design, although they may be calculated exactly for inlet flow wholly supersonic, and approximately for mixed supersonic-subsonic flow.

In computing the total pressure recovery, losses attendant on flow passage through a shock may readily be calculated from the stream Mach number by supersonic flow theory. Subsonic losses are more difficult to calculate since flow properties are not simply related to local diffuser duct contours. Inlet drag may be calculated from the magnitude of the area intercepted by the cowl lip if the peripheral streamlines to the cowl lip is in the undisturbed free supersonic stream, since for this case there are constant momentum and pressure forces acting within the stream tube and the inlet stream thrust may be computed from the freestream flow state:

$$F_1 = P_0 A_1 + \rho_0 A_1 V_0^2 = P_0 A_1 (1 + \gamma M_0^2) \quad (\text{absolute basis}). \quad (97)$$

This may be converted to coefficient form by dividing by the product of the freestream dynamic pressure q_0 and a reference area A_n :

$$C_{D1} = \frac{A_1 (1 + \gamma M_0^2)}{A_n (q/P)_0} \quad (\text{absolute basis}), \quad (98)$$

or, as expressed on a gauge basis by subtracting the quotient of $(P_0 A_1)$ and $(q_0 A_n)$, and substituting $q/P = (1/2) \gamma M^2$,

$$C_{D1} = 2(A_1/A_n) \quad (\text{gauge basis}). \quad (99)$$

Alternatively, in terms of weight flow,

$$F_1 = 2.382 \sqrt{T_{t0}} w_a \theta(M)_0 = 2.382 P_0 A_0 \frac{w}{w_0} \theta(M)_0 \quad \text{Lb} \\ (\text{absolute basis}), \quad (100)$$

and

$$C_{D_1} = 2.382(A_0/A_n) \frac{W}{(\rho/P)_0} \theta(M)_0 \quad (\text{absolute basis}). \quad (101)$$

The stream thrust of the air entering the diffuser is altered if the diffuser inlet spills over and intercepts a stream tube of smaller cross-section A_0 than the inlet area A_1 . In this case the streamline leading up to the cowl lip is not parallel but is divergent by an amount that indicates the increase in stream area needed to diffuse the air to the Mach number then existing at the inlet. The inlet force is then the stream thrust originally associated with the flow in passing through area A_0 in its freestream state plus the added force applied over the projected area $(A_1 - A_0)$, i.e.,

$$F_1 = F_0 + \int_{A_0}^{A_1} P \, dA . \quad (102)$$

The diffusion process between Stations 0 and 1 may thus be either subsonic or supersonic depending on the manner in which the flow is deflected. If this is initiated by a center body protruding from the diffuser inlet, the flow deflection may be gentle enough for it to remain supersonic (or with supercritical spillover), whereas if the deflection is such as to correspond to a low subsonic flow Mach number at the diffuser inlet, flow deceleration takes place abruptly through a normal shock. Equation (102) applies in either instance, but the pressure relationship between 0 and 1 will of course be different in the two cases.

The inlet air flow capture and the inlet drag can be determined conveniently for the supersonic spillover cone flow case by a method presented by G. Sears (of the Marquardt Aircraft Corporation) and W. J. Orlin (of ARO, Inc.)⁴. The diffuser inlet air flow and the inlet drag may be obtained by integrating the flow and the force over the conical

⁴ Unpublished paper.

surface defined by the vertex of the cone and the inlet lip of the cowl. Using the angle ω (Fig. 29) subtended by this conical surface, the freestream Mach number and the cone angle, and making use of

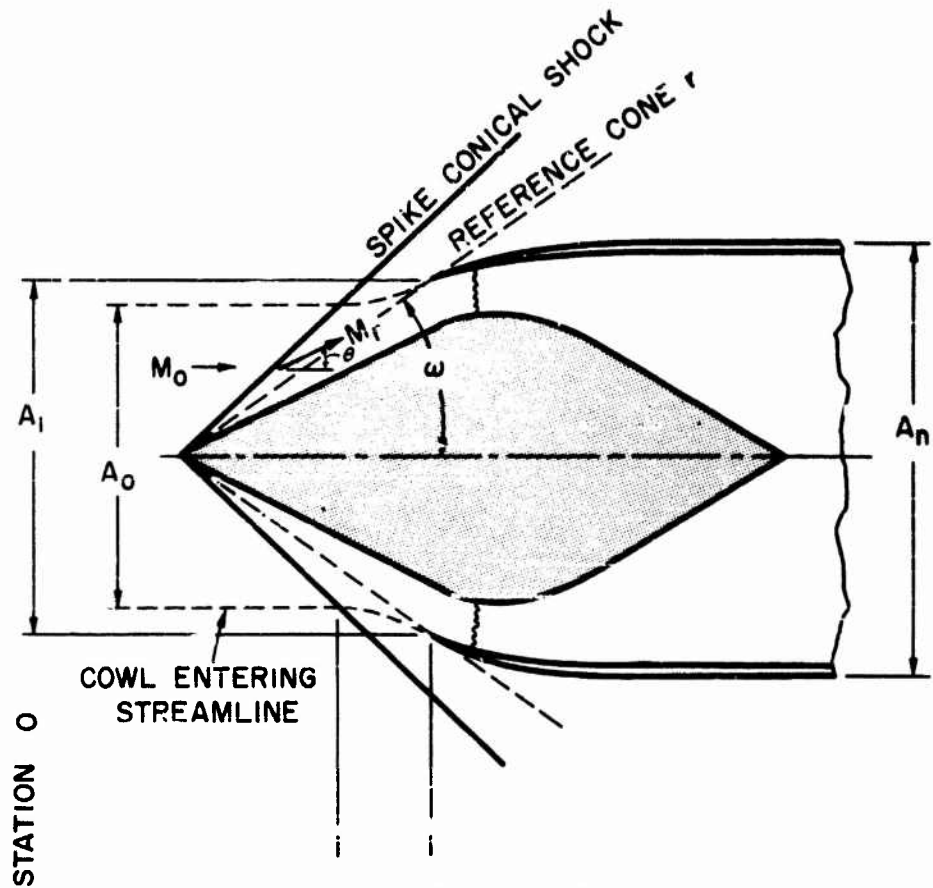


Fig. 29 Supercritical Spillover and Additive Drag

Zdenek's cone flow tables (Ref. 13), one may obtain the flow Mach number M_r and the flow angle θ at this surface. One may also determine the total pressure ratio (P_{t_r}/P_{t_0}) across the shock. Since flow properties are constant along the conical surfaces referred to, one may

simply multiply the total surface area by the normal component of the flow to obtain the mass flow. The momentum component of the inlet drag force is similarly obtained by multiplying the momentum per unit area of the incoming stream (which passes through the conical surface) by the surface area and the cosine of the angle between their respective directions, and then projecting this force in the direction of the diffuser axis. The total inlet drag force on an absolute basis consists of this force plus the product of the inlet area into the static pressure at the conical reference surface. The resulting equations are:

$$\dot{w}_a = A_1 \frac{P_{t_r} \left[\frac{(P/P_t)_r}{\sqrt{T_t}} \right] (\cos \theta) \left(1 - \frac{\tan \theta}{\tan \omega} \right)}{\sqrt{T_t}}, \quad (103)$$

and

$$D_i = A_1 P_{t_0} \left(\frac{P_{t_r}}{P_{t_0}} \right) \left(\frac{P}{P_t} \right)_r \left[1 + \gamma M_r^2 (\cos^2 \theta) \left(1 - \frac{\tan \theta}{\tan \omega} \right) \right]. \quad (104)$$

The equation for the inlet air flow may be equated to the corresponding relation in the undisturbed flow to obtain the value for (A_0/A_1) , namely,

$$A_0/A_1 = \left(\frac{P_{t_r}}{P_{t_0}} \right) \frac{\left[\frac{(P/P_t)_r}{\sqrt{T_t}} \right] (\cos \theta) \left(1 - \frac{\tan \theta}{\tan \omega} \right)}{\left[\frac{(P/P_t)_0}{\sqrt{T_t}} \right]}. \quad (105)$$

Equation (104) may be expressed as an inlet force coefficient on an absolute basis:

$$\begin{aligned} C_{D_i} &= \frac{D_i}{A_n q_0} \\ &= \frac{2(A_1/A_n)}{\gamma M_0^2} \left[\frac{(P/P_t)_r}{(P/P_t)_0} \left(\frac{P_{t_r}}{P_{t_0}} \right) \left\{ 1 + \gamma M_r^2 (\cos^2 \theta) \left(1 - \frac{\tan \theta}{\tan \omega} \right) \right\} \right] \end{aligned} \quad (106)$$

(absolute basis).

On a gauge basis,

$$C_{D_1} = \frac{2(A_1/A_0)}{\gamma M_0^2} \left[\frac{(P/P_t)_r (P_{t_r})}{(P/P_t)_0 (P_{t_0})} \right] \left\{ 1 + \gamma M_r^2 (\cos^2 \theta) \left(1 - \frac{\tan \theta}{\tan \omega} \right) - 1 \right\}$$

(gauge basis). (107)

The force exerted by the air stream upon the diffuser inlet may be looked upon as the total momentum (stream thrust) originally possessed by the freestream plus the forces exerted upon it by the surrounding air stream between Stations 0 and 1. Looked at in this fashion, the inlet drag consists of two terms, one of which is due to the initial momentum of the captured air, the other being the additive drag term; this latter reflects the drag caused by the increase in the momentum of the gas between its free state at Station 0 and its captured state at Station 1. This is due to the force exerted along the streamline from 0 to 1. The additive drag for the case of conical flow with supercritical spillover is obtained by subtracting $2(q_0 A_0)/(q_0 A_n)$ from the right-hand side of Eq. (107), yielding

$$C_{D_{add}} = \frac{2(A_1/A_n)}{\gamma M_0^2} \left[\frac{(P/P_t)_r (P_{t_r})}{(P/P_t)_0 (P_{t_0})} \right] \left\{ 1 + \gamma M_r^2 (\cos^2 \theta) \left(1 - \frac{\tan \theta}{\tan \omega} \right) - 1 \right\} - 2 \frac{A_0}{A_n}$$

(108)

Figures 30 through 35 present solutions of Eqs. (105) and (108) for cone half-angles of 20° , 25° , and 30° , and oblique shock-on-rim Mach numbers of about 1.9 through 3.0, for freestream Mach numbers ranging from low values (corresponding to sonic velocity on the cone surface) up to 3.0. Data are plotted in terms of $(C_{D_{add}})/(A_0/A_n)$, so that the drag is referred to the inlet area rather than to an arbitrary engine area.

The calculation of air flow capture and additive drag or an inlet force coefficient is much more complicated for mixed supersonic

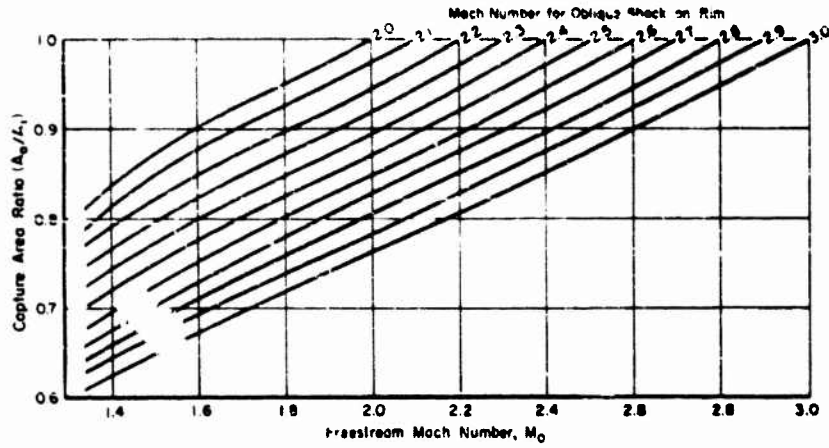


Fig. 30 Inlet Capture Area Ratio (A_0/A_1) for Supercritical Spillover, 20° Cone

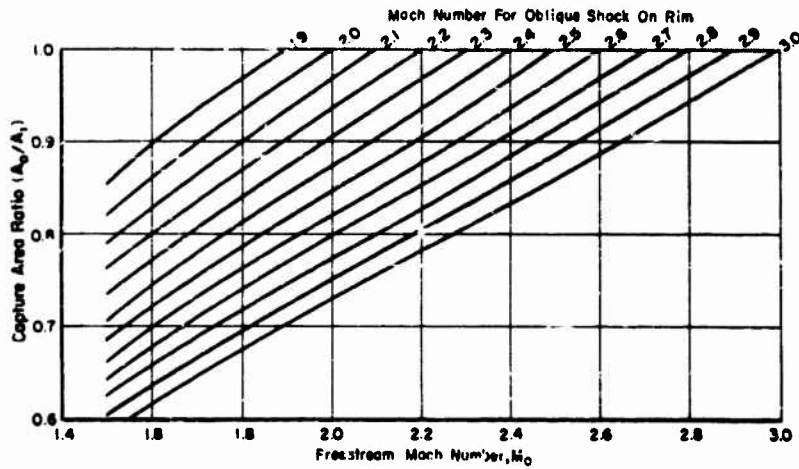


Fig. 31 Inlet Capture Area Ratio (A_0/A_1) for Supercritical Spillover, 25° Cone

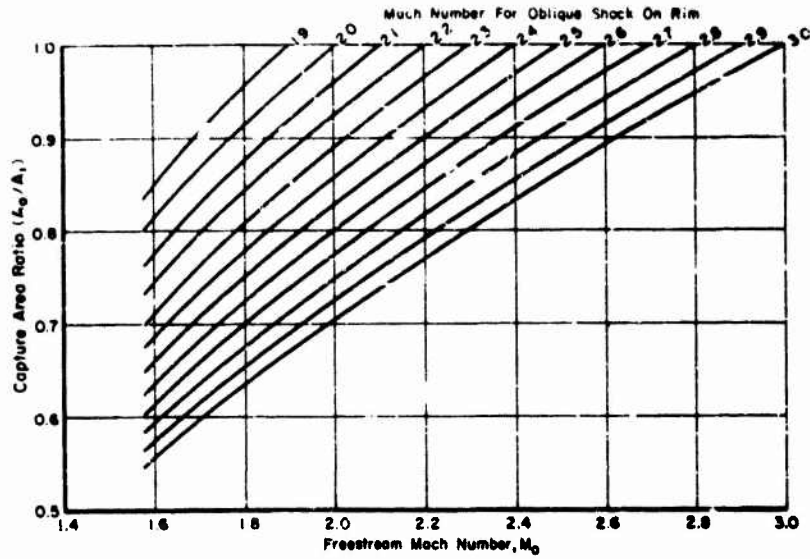


Fig. 32 Inlet Capture Area Ratio (A_0/A_1) for Supercritical Spillover, 30° Cone

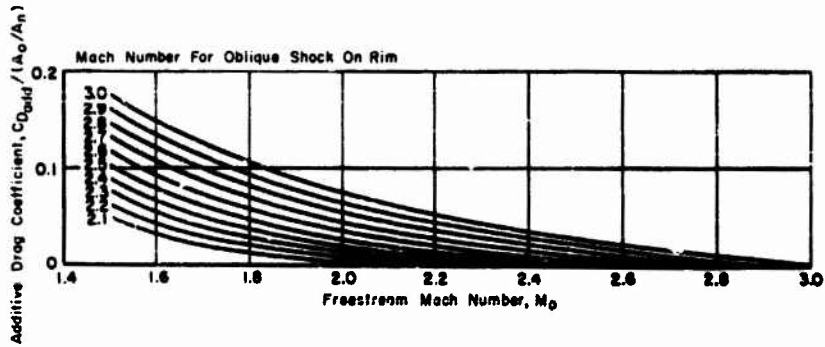


Fig. 33 Supercritical Additive Drag Coefficient for 20° Cone

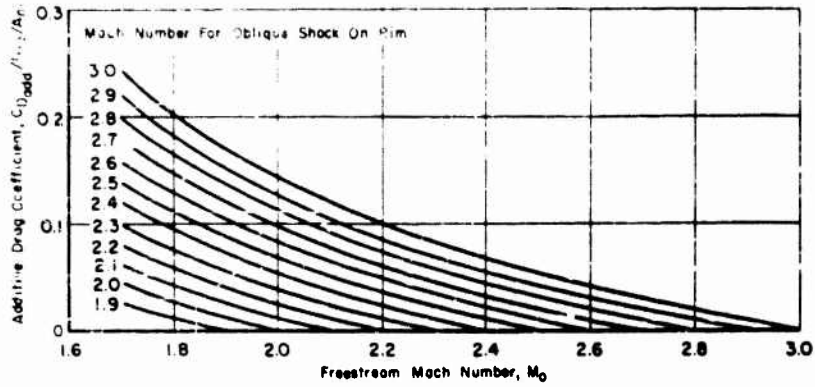


Fig. 34 Supercritical Additive Drag Coefficient for 25° Cone

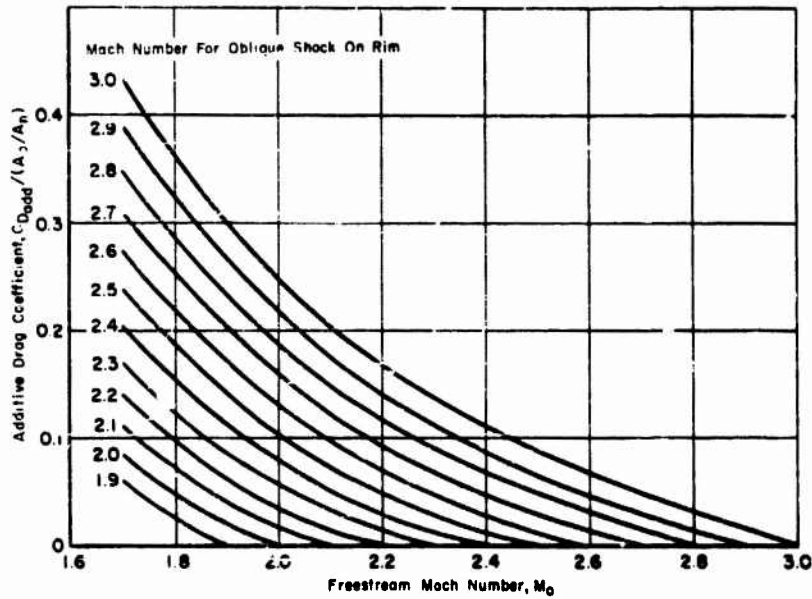


Fig. 35 Supercritical Additive Drag Coefficient for 30° Cone

and subsonic inlet flow. Approximate methods which are applicable to conical diffusers are presented in Ref. 14. In computing inlet additive drag for other cases, it is necessary to use an approximate value for the static pressure along streamlines between 0 to 1 and then to integrate this between corresponding areas. It is clear that if the freestream capture area A_0 is equal to the inlet area A_1 , the additive drag will be zero, and the inlet force coefficient may be computed simply from A_1 , A_n and the freestream Mach number. Data secured in experimental tests on a Ferri-type 25° half-angle conical diffuser are shown in Figs. 36, 37 and 38 as examples of typical diffuser operation. Figure 36 presents the relation between diffuser capture area ratio and total pressure recovery. The inlet force coefficient (on a gauge basis) is presented in Fig. 37 and a correlation of exit Mach number M_d with air flow capture is shown in Fig. 38. The inlet behavior can be evaluated at a fixed combustor heat release by matching values of M_d at the diffuser exit and at the combustion chamber inlet, and then reading off the air flow capture ratio from Fig. 38 at the desired flight Mach number. These values of air flow capture and flight Mach number may then be inserted in Fig. 37 to obtain the diffuser inlet force coefficient. The latter can then be used together with an exit coefficient obtained from combustor performance curves to determine the engine net thrust coefficient. Similar curves apply to more complex diffusers, bearing in mind that performance is then more sensitive to air flow capture ratio and freestream Mach number.

The use of such graphical correlations has an advantage over point-by-point algebraic calculation of performance if the diffusers are to be operated over a wide range of flight Mach numbers and air flow capture ratios. If the engine is to be operated at only one condition of flight Mach number and capture ratio, the algebraic calculation of inlet behavior will probably be more convenient than the former procedure.

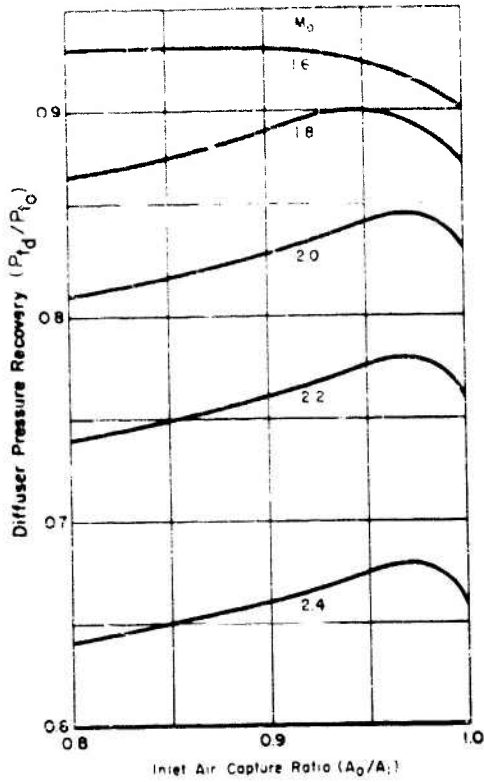
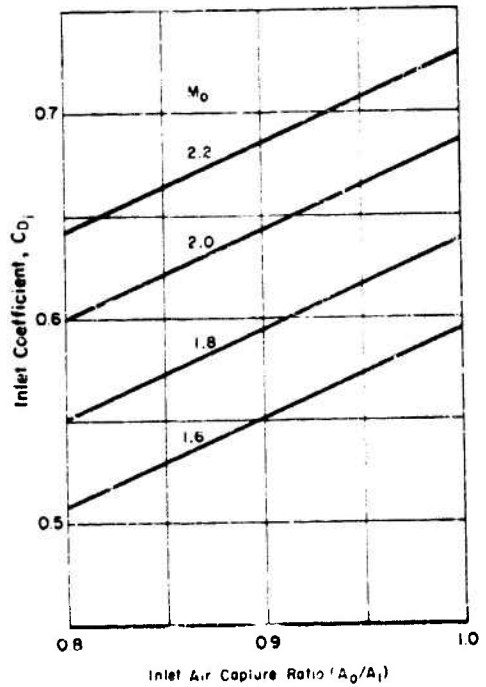


Fig. 36 Typical Diffuser Total Pressure Recovery for 25 Conical Diffuser

Fig. 37 Typical Inlet Force Coefficient for 25 Conical Diffuser, $(A_1/A_n) = 0.365$, $A_1 = 225$ Square Inches



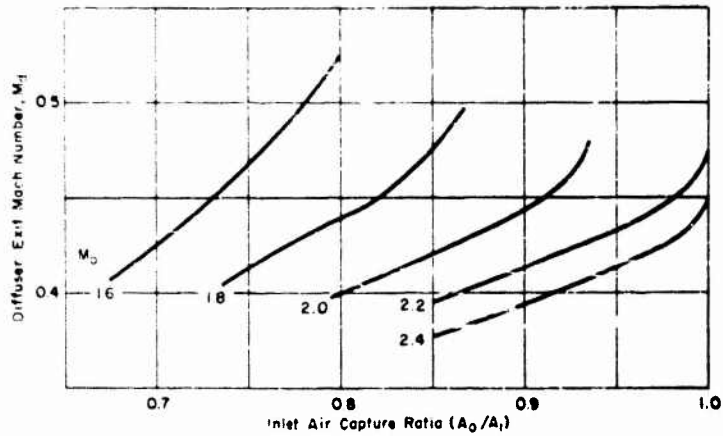


Fig. 38 Typical Correlation of Diffuser Exit Mach Number and Inlet Air Capture Ratio

4.3 The Combustor

A useful understanding of the combustion of fuel-air mixtures in a ramjet engine may be gained by breaking down the flow processes into the following steps:

1. The compressed air flow enters the combustion chamber from the diffuser at subsonic speed at a total temperature equal to the freestream value and at a rate of flow equal to that at the diffuser inlet less that diverted to power auxiliaries.
2. Fuel is added to the air stream, atomized, mixed with the air, and in part evaporated.
3. The stream velocity is further decreased to the low value suitable for the efficient combustion of the mixture.
4. The mixture is passed through a flame stabilization device to initiate combustion.

5. The mixture is burned in a cylindrical combustion chamber accompanied by the following phenomena:
 - a. Transformation of the chemical enthalpy of the fuel into thermal enthalpy of the gas, as marked by a rise in total temperature (or increase of S_a);
 - b. Reduction in gas density caused by the increase of temperature, with accompanying acceleration of the flow; and
 - c. Reduction in total pressure of the hot gas as a result of sudden acceleration on being heated.
6. The hot burned gas is passed into an exit nozzle to transform its thermal and pressure energy into kinetic energy, thereby developing thrust by jet reaction.

The processes listed under Steps 1, 2, 3, 4, 5b and 5c above are amenable to solution by the gas dynamic equations, provided the flow can be treated as one-dimensional. The amount of heat addition in Step 5a is a quantity which depends on the chemical reaction rate of fuel and air at the particular flow condition. It is convenient to compute the effect of the change from chemical to thermal enthalpy in terms of the temperature function ($S_a/\sqrt{T_t}$), since this latter expression includes such parameters of state as γ , R , and T_t .

Once the combustor flow conditions and the amount of heat release are set, consideration can be given to determining the space required to accomplish this heat release. Flow velocities in the combustor are within the range of one to several hundred feet per second, whereas normal flame velocities of the commoner fuels are only a few feet per second, so that it is not possible to effect significantly complete combustion of the fuel-air mixture by means of a flame spreading from a single point source within the length of a practical combustion chamber. An ignitor is therefore provided to initiate the combustion of the mixture at a sufficient number of points so that by

If the flame from these points the flame can consume the whole of the combustible mixture as it passes downstream. The usual recourse here is also to insert a complex-shaped grid into the fuel-air stream to produce a low velocity flow wake in which a flame can stabilize as a result of fresh mixture being ignited by recirculating combustion products. (It is possible to stabilize a flame aerodynamically by the use of opposing gas jets, but this procedure has not yet been used in full scale engines.) Such a stabilized flame ignites the combustible gases flowing around the baffle and rapidly effects combustion by virtue of the large value of the ratio of ignited stream perimeter to unburned flow area, in a manner analogous to that of a Meker burner. In a combustion chamber of insufficient length, the flame cannot thus consume all the mixture within the confines of the chamber and combustion will accordingly be incomplete. A second type of flame stabilizer commonly used, the can combustor, consists of a perforated tubular-shaped structure closed at the upstream end to provide a quiescent piloting region. The combustibles are ignited stagewise through the perforated holes. A correlation of some of the parameters affecting can combustor design has been made by Zelinski (Ref. 15). Since combustion chamber flow is everywhere subsonic, conditions downstream at the nozzle entrance may be propagated upstream to the diffuser after being modified by heat addition and drag. Combustion and flow phenomena are thus coupled, and under some circumstances such a system can become unstable, leading to burning under conditions of violent pressure and flow oscillation. One result of this interrelation is that the combustor inlet flow Mach number is dependent upon combustion efficiency and vice versa. For purposes of analysis, however, this coupling effect may be ignored, and analyses performed merely on the basis of an assumed enthalpy change in the combustion chamber; this enthalpy value may be estimated by considering the combustion of as much fuel as is required at a given combustion efficiency to obtain the required heat release. Combustion efficiency is thus introduced into engine performance calculations after the gas dynamic force balances across the engine have been completed.

Calculation of the flow conditions between the exit and the inlet of the combustion chamber now proceeds as outlined in Section 2.

Combustion is usually taken to occur at constant mass flow and cross-sectional area, in order to permit of the initial and final stream states being calculated on the basis of energy change at constant stream thrust. The energy change is described in terms of the increase of S_a from an initial value related to the inlet total temperature to a final value corresponding to the required heat release.

By Eq. (67) the burned gas stream thrust is

$$f_b = \dot{w}_a S_a \theta(M)_b, \quad (109)$$

the subscript (a) now being dropped.

But

$$\dot{w}_a = \frac{P_2 A_2 \dot{w}_2}{\sqrt{T_{t2}}},$$

whence

$$f_b = P_2 A_2 \dot{w}_2 \frac{S_a}{\sqrt{T_{t2}}} \theta(M)_b. \quad (110)$$

The exit stream thrust of a parallel-walled combustion chamber must equal the inlet stream thrust less the combustor drag, since wall forces (except friction) have no component in the direction of flow. The inlet stream thrust and the drag may be written respectively as

$$f_2 = P_2 A_2 (1 + \gamma M_2^2), \quad (111)$$

and

$$D_b = P_2 A_2 C_{D_b} \frac{\gamma M_2^2}{2} \quad (112)$$

whence

$$f_b = f_2 - D_b,$$

or

$$\frac{S_a}{\sqrt{T_{t_2}}} \theta(M)_b P_2 A_2 \dot{w}_2 = P_2 A_2 \left[1 - \frac{(C_{D_b} - 2) \gamma M_2^2}{2} \right]. \quad (113)$$

Collecting together the functions involving M_2 , and eliminating common terms, one has

$$\frac{1 - (C_{D_b} - 2) \gamma \frac{M_2^2}{2}}{\dot{w}_2} = \frac{S_a}{\sqrt{T_{t_2}}} \theta(M)_b. \quad (114)$$

Unfortunately it is not possible to solve this latter relation explicitly for either M_2 or M_b , even for a fixed value of the drag, so that it is generally necessary to fix M_b at a value corresponding to the selected exit nozzle area ratio, and then to use different values of M_2 in succession to find corresponding values of $(S_a/\sqrt{T_{t_2}})$ for a fixed geometry, variable flow engine. Otherwise M_2 may be fixed and various successive values of M_b chosen so that corresponding values of $(S_a/\sqrt{T_{t_2}})$ may be found for a fixed flow, variable geometry engine. In the case of a practical engine, it is more convenient to determine the relation between $(S_a/\sqrt{T_{t_2}})$, M_b and M_2 by experiment. At first sight it may appear that the correlation between M_2 , M_b , and $(S_a/\sqrt{T_{t_2}})$ is a variable one by virtue of the change of C_{D_b} with operating conditions. In many practical cases C_{D_b} will indeed be found to alter, but this change can be expressed as a function of M_2 , from which it may be seen that the left-hand side of Eq. (114) will still be solely a function of M_2 , whereas the right-hand side will remain a function of $(S_a/\sqrt{T_{t_2}})$ and M_b —which are already fixed by the engine exit nozzle geometry. Thus even where C_{D_b} is variable, and Eq. (114) is incapable of being solved explicitly, a unique experimental relation may be established between $(S_a/\sqrt{T_{t_2}})$ and M_2 for a given exit nozzle size.

If this relation is plotted, values may be taken from the curve for use in subsequent calculations, and the curve may also be adjusted for use with other sizes of exit nozzles. As the product of $(S_a/\sqrt{T_{t_2}})$ and $\theta(M)_b$ appears on the right-hand side of Eq. (114), a new value of $(S_a/\sqrt{T_{t_2}})$ may be found such that the new $\theta(M)_b$, corresponding to the new nozzle size times the new $(S_a/\sqrt{T_{t_2}})$, equals the old product of $(S_a/\sqrt{T_{t_2}})$ and $\theta(M)_b$, and therefore corresponds to the same M_2 . In this manner one may form a new correlation between values of $(S_a/\sqrt{T_{t_2}})$ and M_2 for a different exit nozzle area. Within the limits of experimental error, data currently available support such correlations.

The relations listed immediately above have now defined conditions upstream of the exit from Step 6 back to Step 4 (see page 93), but the flow at the entrance to the combustor still needs to be related to that at the diffuser exit, with some attention paid to the effect of fuel addition. If the latter is ignored, one may equate the flow at Station d to that of Station 2 on a basis corresponding to continuity at the same total temperature:

$$A_2 P_{t_2} \left[\frac{P}{P_t} \right]_2^{\circ} = A_d P_{t_d} \left[\frac{P}{P_t} \right]_d^{\circ} \quad (115)$$

M_d may be related to M_2 as soon as values are assigned to A_2 and A_d , and the relation of P_{t_2} to P_{t_d} known. This ratio, (P_{t_2}/P_{t_d}) , expresses the subsonic diffuser efficiency in the form of the total pressure recovery from Stations d to 2. If fuel is added either contra-stream or co-stream at less than stream velocity, the stream total pressure will be reduced slightly, as the force needed to accelerate the fuel must be balanced by a pressure gradient set up in the air stream. (The magnitude of this total pressure loss is small, amounting to only 0.7 per cent for a volatile fuel injected cross-stream at a fuel to air ratio of 0.06 into an air stream whose Mach number is 0.4.)

When the M_2 versus M_0 correlation is correlated with that of M_2 versus M_b and the temperature parameter $(S_a/\sqrt{T_{t_2}})$, a single relation will then exist between the combustion chamber inlet conditions and the exit conditions in terms of $(S_a/\sqrt{T_{t_2}})$. If required, the total pressure ratio across the combustor, (P_{t_b}/P_{t_d}) , may be obtained from M_d , M_b , and $(S_a/\sqrt{T_{t_2}})$. The exit stream thrust F_b may also be expressed either in terms of total pressure, a Mach number function $(f/P_t)_b$, and area, or as a product of mass flow, air specific impulse, and the Mach number function $\theta(M)$. The air flow is in turn expressible in terms of inlet total pressure, inlet total temperature, inlet area, and the Mach number function $[(P/P_t)^\theta]$, thus:

$$A_b P_{t_b} (f/P_t)_b = P_{t_d} (S_a/\sqrt{T_{t_2}}) [(P/P_t)^\theta]_d A_d \theta(M)_b, \quad (116)$$

whence

$$(P_{t_b}/P_{t_d}) = (A_d/A_b) [(P/P_t)^\theta]_d \frac{\theta(M)_b}{(f/P_t)_b} (S_a/\sqrt{T_{t_2}}). \quad (117)$$

Since

$$\frac{\theta(M)_b}{(f/P_t)_b} = \frac{1}{2.253} (A/A^*)_b,$$

$$(P_{t_b}/P_{t_d}) = \left[(S_a/\sqrt{T_{t_2}}) (A_d/A_b) [(P/P_t)^\theta]_d (A/A^*)_b \right] / (1.253). \quad (118)$$

Values of (P_{t_b}/P_{t_d}) may be plotted as parametric contours on curves of the earlier M_d , $(S_a/\sqrt{T_{t_2}})$ and M_b relations if the value of M_b is kept fixed.

Figures 39 through 41 show the characteristic curves of some typical can-type combustors. In Fig. 39, M_d is plotted against $(S_a/\sqrt{T_{t_2}})\phi(M)_b$; here M_d varies over a considerable range (0.45 to a mean value of about 0.7), corresponding to a change of $(S_a/\sqrt{T_{t_2}})$ from about 3.8 to 5.5, and of $\phi(M)_b$ from 1.269 to 1.347. These data are observed to correlate onto what is nearly a single curve, even though the nozzle throat area has been changed from 65 to 70 per cent of the combustion chamber area corresponding to the above change of $\phi(M)$, the combustion chamber temperature level has been more than doubled, and the engine pressure level has been varied by a factor of nearly ten.

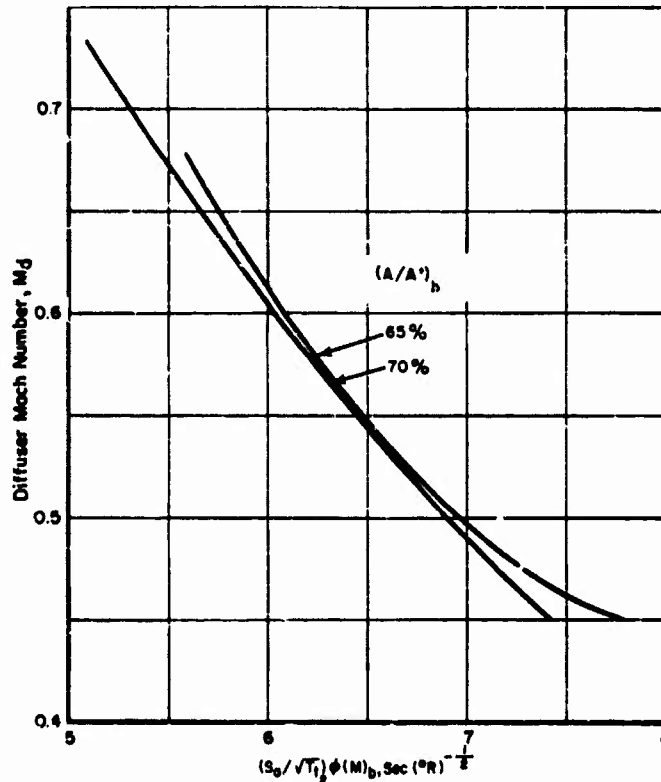


Fig. 39 Correlation of Combustor Inlet and Exit Mach Number for Can Combustor

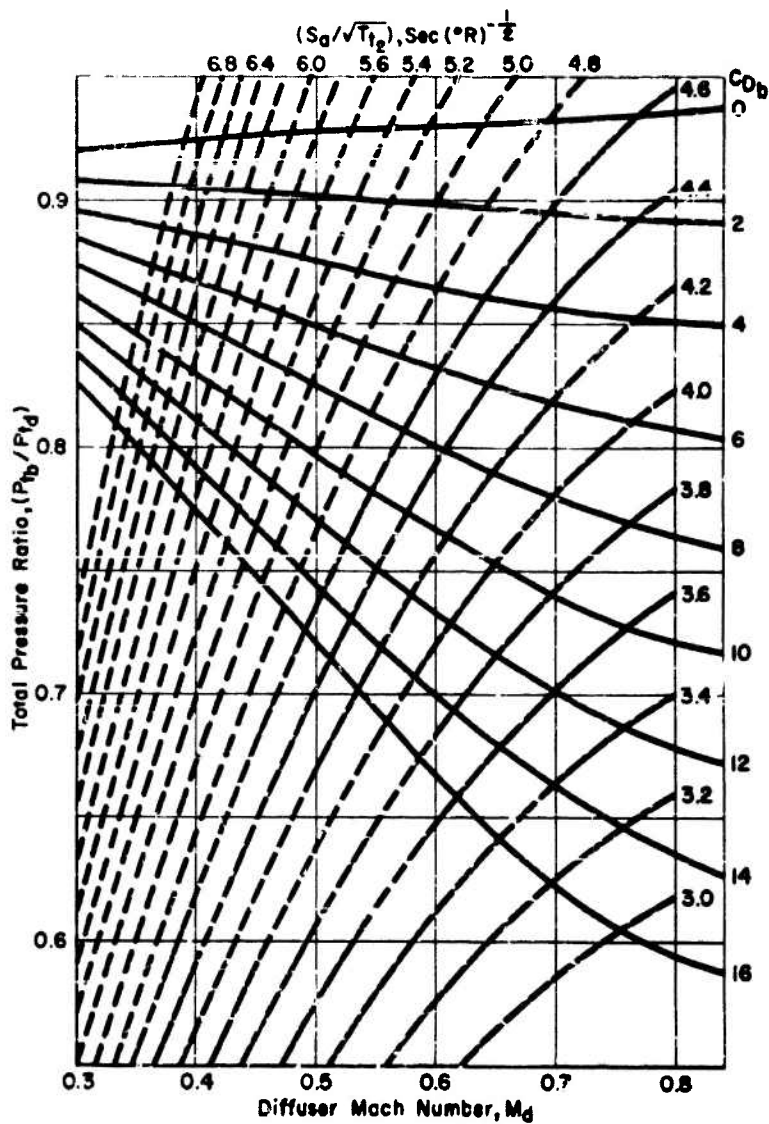


Fig. 40 Con Combustor Gas Dynamic Flow Correlation for Exit Nozzle Throat Area Equal to 65 Per Cent of Combustion Chamber Area

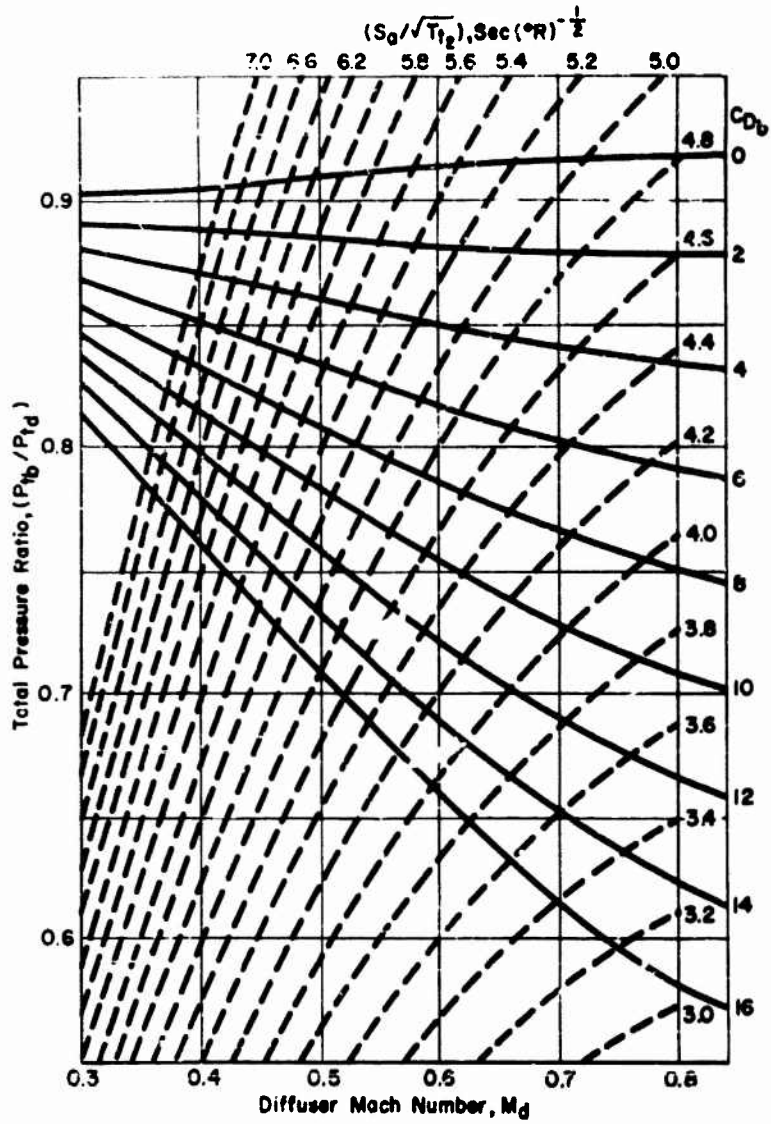


Fig. 41 Can Combustor Gas Dynamic Flow Correlation for Exit Nozzle Throat Area Equal to 70 Per Cent of Combustion Chamber Area

The accuracy of this correlation shows how well one-dimensional theory may be applied to describe the phenomena. For some purposes it is more convenient to set down the data so that the diffuser Mach number is plotted against the temperature parameter ($S_a / \sqrt{T_{t_2}}$), with nozzle area fixed, it is also possible to cross-plot values of the total pressure ratio across the combustor along lines of equivalent combustor drag. Figures 40 and 41 illustrate the behavior of the combustor, again with nozzle area ratios of 65 and 70 per cent. The smaller exit nozzle will be observed to be associated with lower diffuser exit Mach numbers for a given value of the temperature parameter, together with a lower total pressure loss during combustion. The total pressure losses indicated in these figures are made up of the following:

1. Friction and turbulence losses during subsonic diffusion between the plane where the combustion chamber joins the diffuser and that representing the full combustion chamber area,
2. Friction and drag losses caused by the presence of flameholders and fuel injectors, and
3. Momentum losses caused by heat addition.

In the cases illustrated, about 9 per cent of the available total pressure is considered to have been lost as a result of heat addition, and 2 or 3 per cent because of subsonic diffusion, the rest (about 12 per cent) resulting from flameholder drag. Combustion system total pressure losses are generally lower if the air stream is first diffused to a low Mach number and use is then made of a baffle combustor of low drag. The experimental correlation of diffuser exit Mach numbers and temperature parameters for a baffle combustor of average drag, with a nozzle area ratio of 70 per cent, indicates a minimum total pressure loss of only about 18 per cent, instead of the 20 per cent minimum for the earlier can burner results, with a burner drag corresponding to between 6 and 7 velocity heads, instead of to between 8 and 10. This lower pressure loss is of great significance in engines required to operate at low flight Mach numbers (subsonic values to about 1.7). and

of lesser significance up to a Mach number of about 2.5. At higher flight Mach numbers aerodynamic total pressure losses of 25 to 50 per cent in the diffuser so far exceed those in the combustor that only a minor improvement in performance is obtained by reducing the burner drag.

Consideration of combustor operation is here limited to the aspects affecting over-all engine design, as combustor operation is more fully covered in TG 370-9 and 10. Theoretical thermochemically-predicted combustion total temperatures and values of S_a are shown in Figs. 42 and 43. In the first figure, the effect of dissociation (which has not been taken into account) will be to bring about a smooth transition between the portions of the curves on either side of the stoichiometric fuel-to-air ratio. The only further aspect of combustion to be covered here is the utilization of either the results of a given test or of theoretical data on combustor operation in the prediction of over-all engine performance. Combustion performance enters into over-all calculations in two ways, (a) by setting the fuel flow needed to effect a desired value of combustion temperature as defined by S_a , and (b) by limiting the maximum temperature ratio obtainable from a power plant through a limited total heat release. The first limitation affects the efficiency at less than maximum engine power output; the second is equivalent to limiting the maximum available power (thrust), whatever the fuel consumption. Both theory and experiment show the combustion behavior to be a function of flow velocity, inlet temperature, combustion pressure, and equivalence ratio for a given fuel. This behavior varies for fuels of different types, but is relatively insensitive to minor variations within a given type. The paraffin hydrocarbons from propane through decane exhibit a very similar behavior for equivalent mixture states. It is possible by means of either the theory outlined in TG 370-9 and 10 or experiment to obtain a correlation between combustion heat release (as expressed in terms of a combustion specific impulse) and equivalence ratios for various inlet temperatures, velocities, and pressures. The flow velocity or Mach number has been shown to be dependent on both the area ratio between the combustion chamber and the exit nozzle, and on the

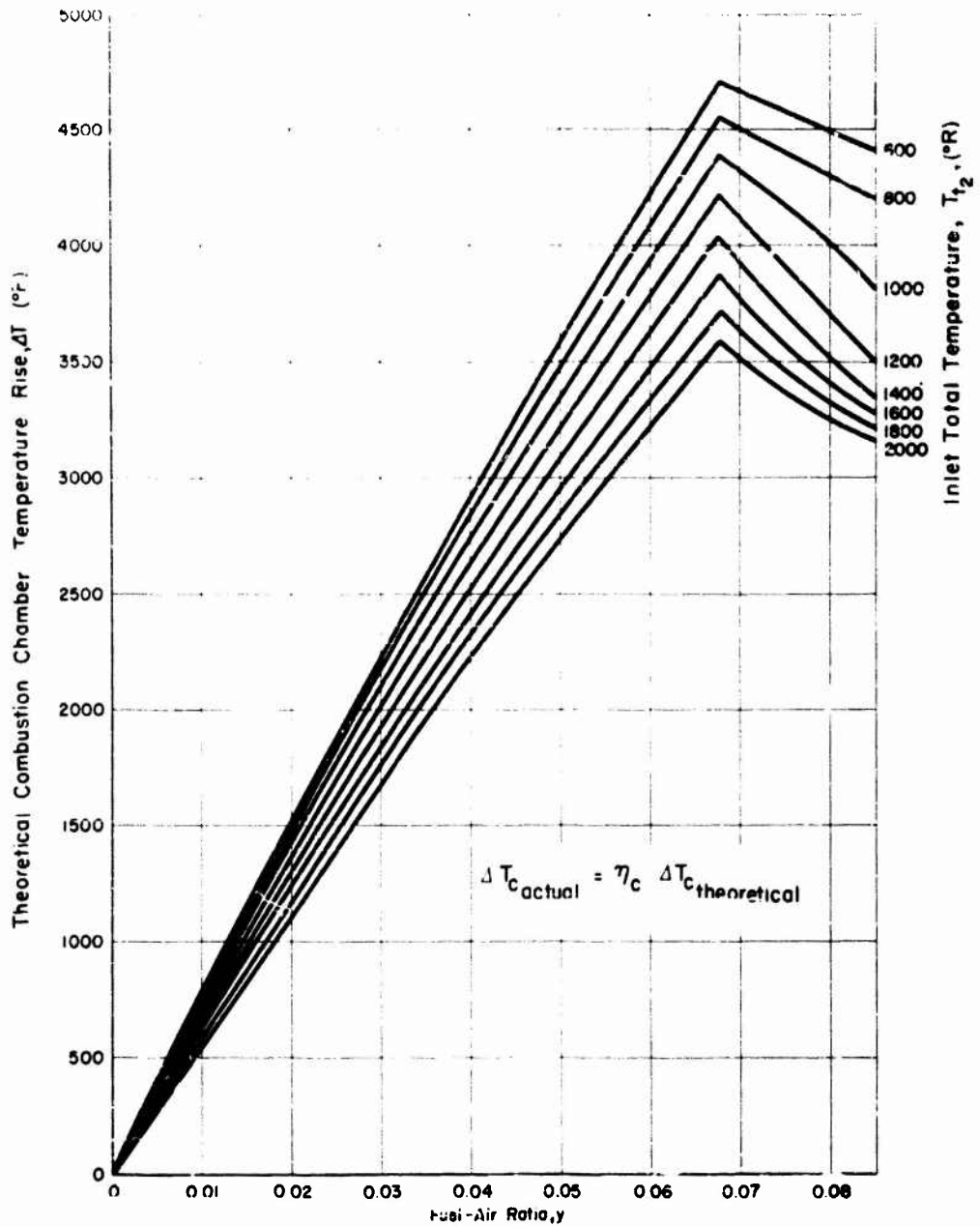


Fig. 42 Theoretical Effective Temperature Rise without Dissociation
Data taken from Ref. 17.

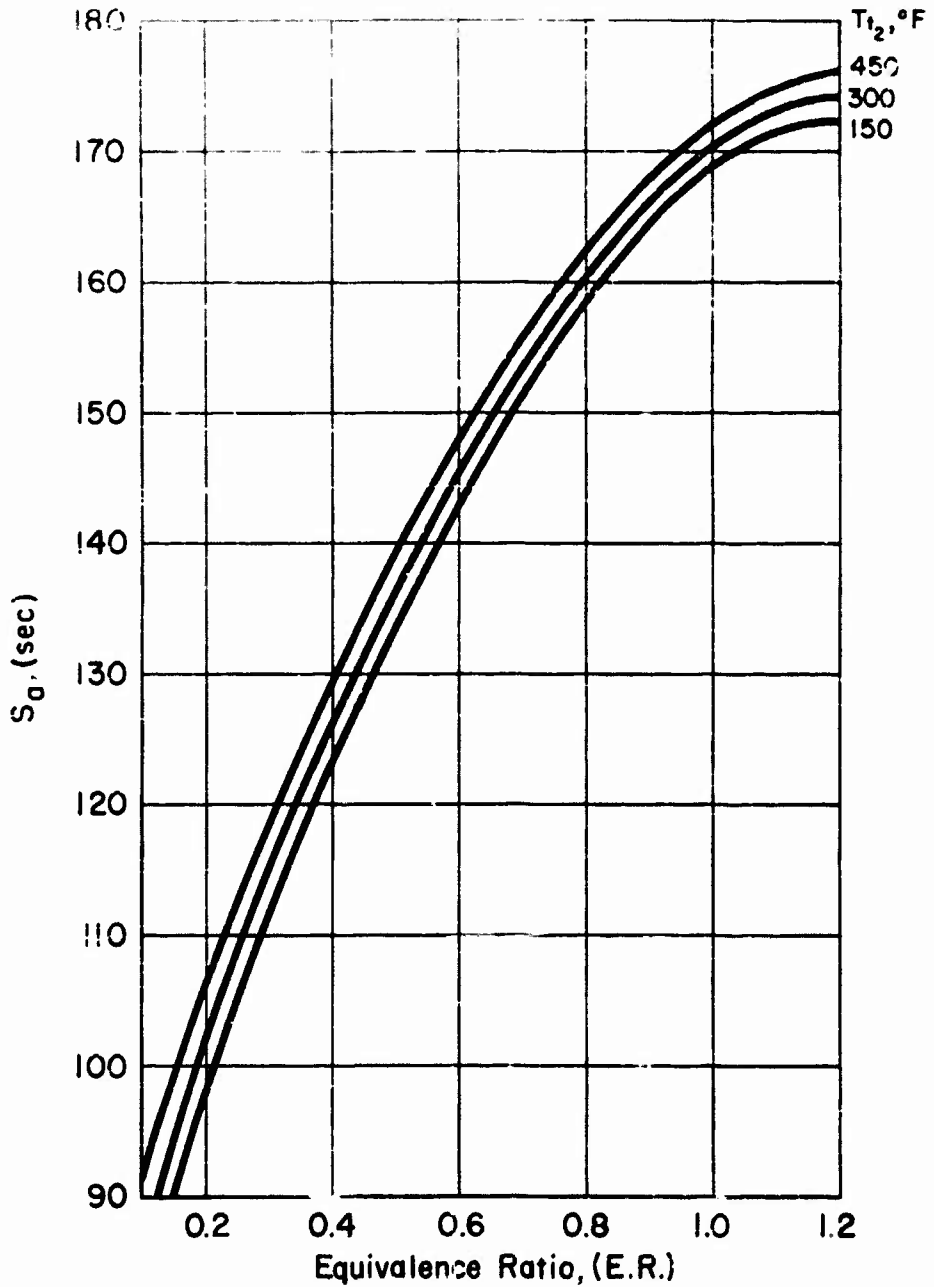


Fig. 43 Theoretical Air Specific Impulse, S_a , versus Equivalence Ratio, (E.R.) for Various Inlet Temperatures, T_2

ratio of final and initial gas temperature (or S_a) states. One can therefore eliminate the inlet flow velocity as a variable for an engine using a fixed area exit nozzle, because this velocity has a particular value for each operating point and only this value need be considered. The pressure and temperature of the stream of given velocity are uniquely determined by the quantities of mass flow and total temperature which are more easily observed and controlled. The final (and most convenient) correlations are then effected; these are based on a fixed combustion chamber exit area, and relate combustion efficiency to equivalence ratio at a fixed value of total temperature. It is possible to draw auxiliary scales superimposed on such a plot in order to relate $(S_a / \sqrt{T_{t_2}})$ to η_c and equivalence ratio. Calculated or experimental data are then plotted in terms of engine air flow. Pressure appears in the mass flow parameter, and the effect of temperature is shown by a comparison of separate figures plotted for various appropriate values of total temperature.

Figures 44 through 46 show such experimental test data for a piloted can-type burner operated at inlet total temperatures of 150° , 300° and 450°F respectively, for a wide range of air flow conditions. The required values of $(S_a / \sqrt{T_{t_2}})$, engine air flow, and total temperature can be entered in these curves, interpolating where necessary to determine the equivalence ratio needed to produce the required combustion temperature (measured as S_a). Total fuel flow is computed from the product of air flow into equivalence ratio and from the stoichiometric fuel-to-air ratio. In cases where either test or theoretical data are lacking for the purpose of correlating the equivalence ratio with an actual operating condition, a reasonable approximation to likely performance may be secured by selecting the equivalence ratio required for complete combustion, and then increasing the fuel flow by dividing by a combustion efficiency based upon similar engines operated under comparable conditions. To do this it is necessary to employ the theoretical curve relating S_a to equivalence ratio, as presented in Fig. 43, using a value of S_a determined from the required engine value of $(S_a / \sqrt{T_{t_2}})$ and inlet total temperature, to obtain an equiva-

actual ramjet engine combustion efficiency. This theoretical equivalence ratio is then divided by an efficiency factor to yield the possible actual fuel-to-air ratio.⁵

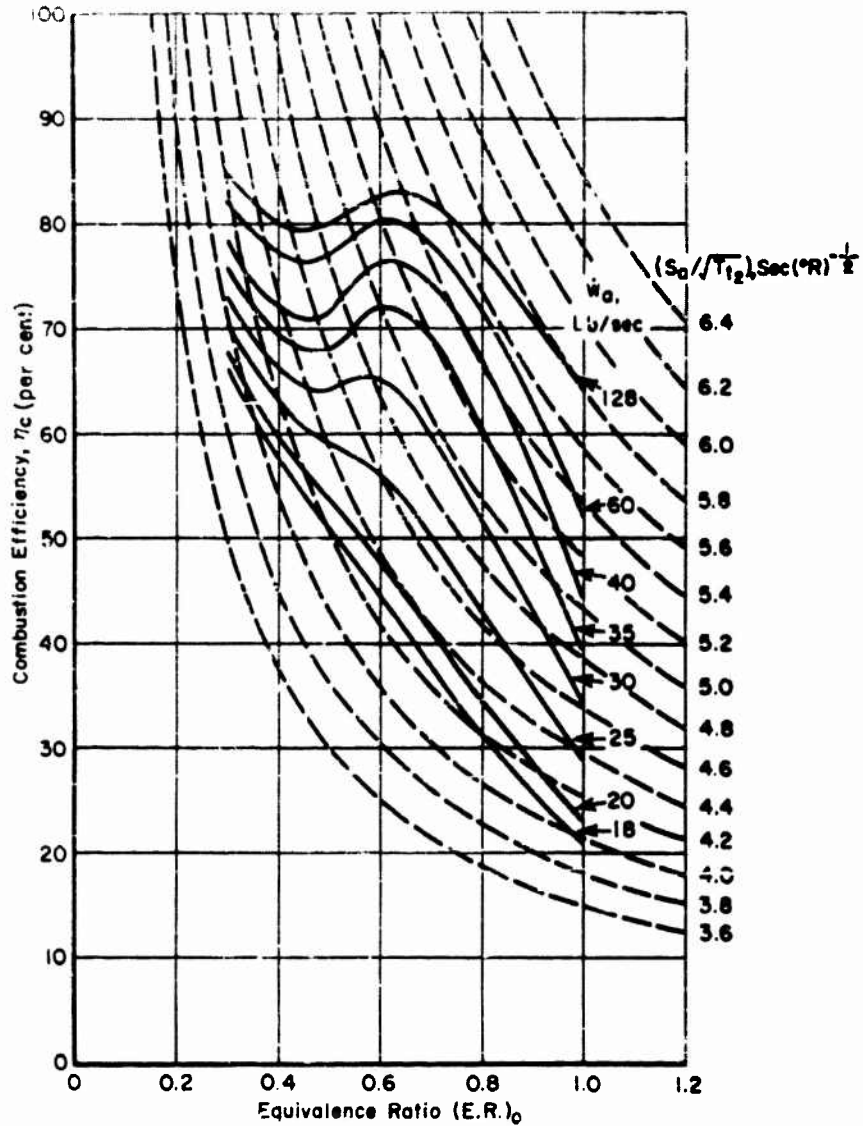


Fig. 44 Typical Combustion Efficiency Correlation for $T_1 = 150^\circ \text{F}$

⁵A recent survey paper by Dugger (Ref. 16) summarizes many of the combustion problems of present-day ramjet engines.

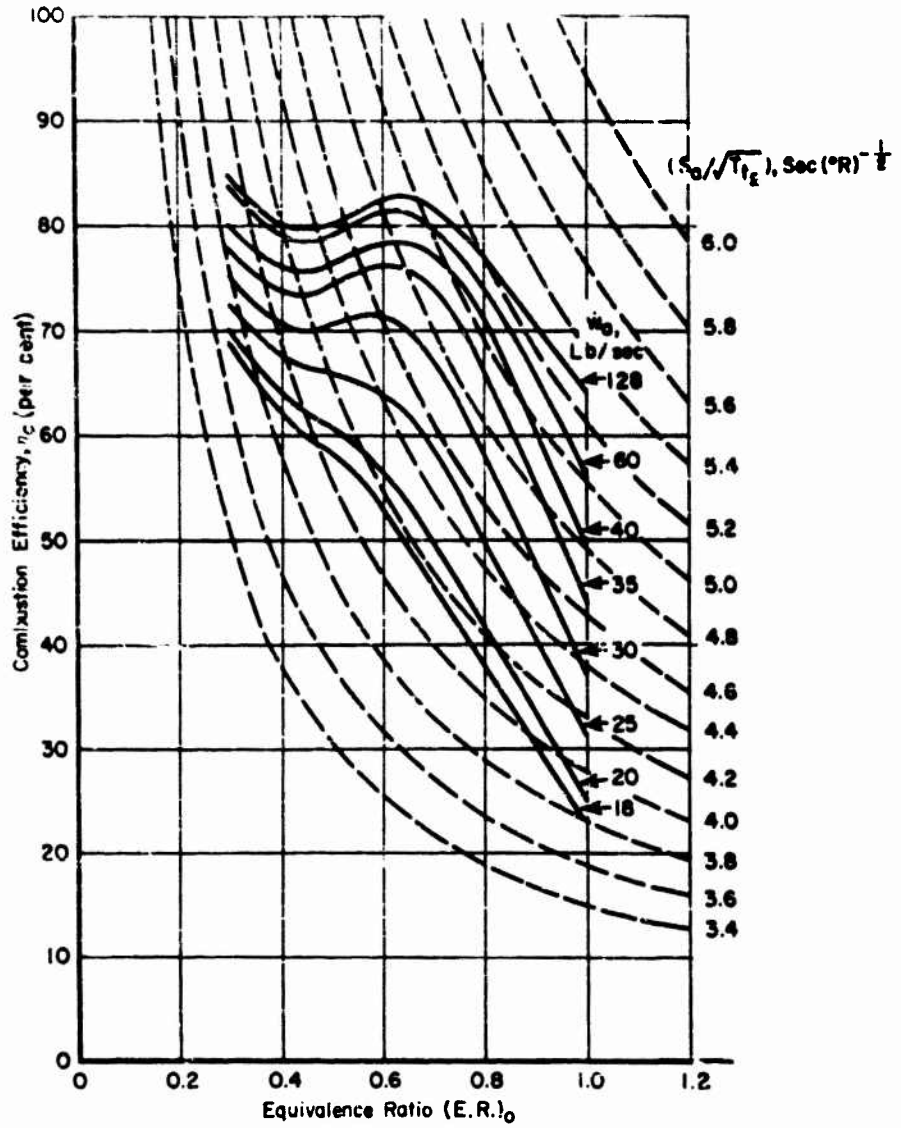


Fig. 45 Typical Combustion Efficiency Correlation for $T_0 = 300^\circ\text{F}$

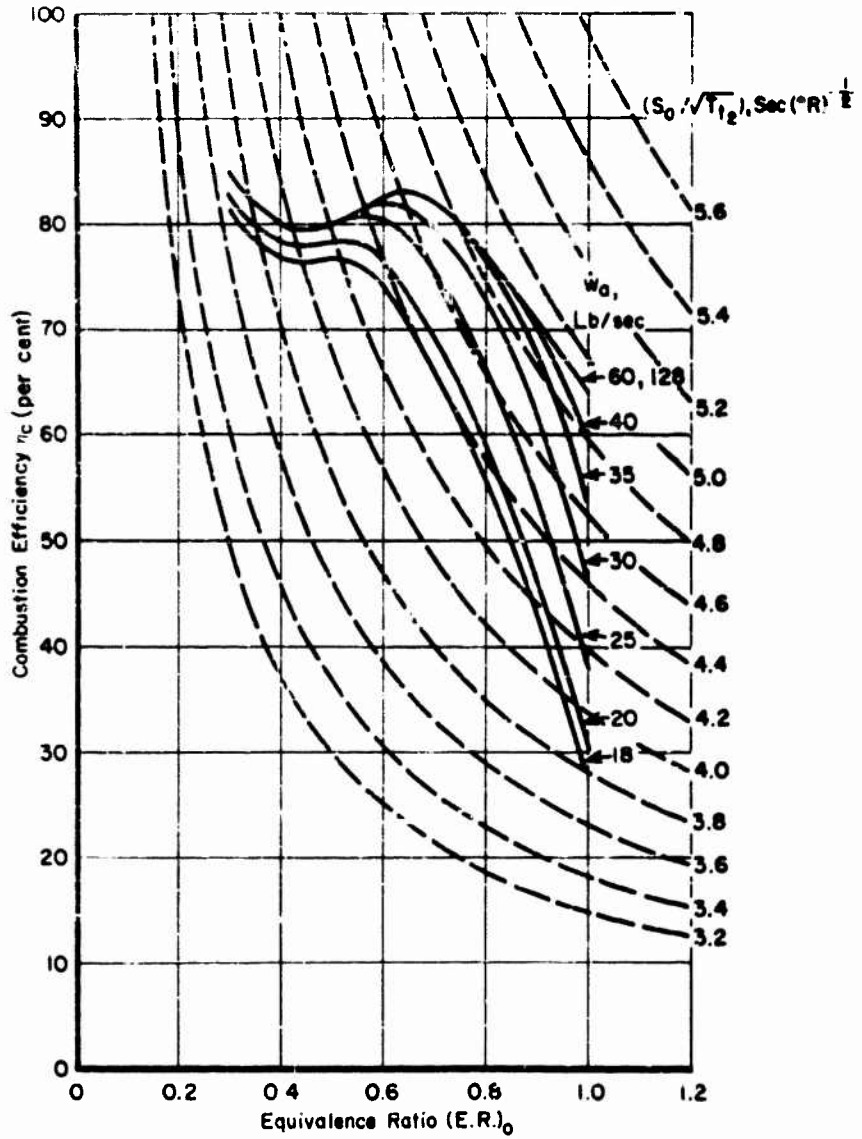


Fig. 45 Typical Combustion Efficiency Correlation for $T_1 = 450^\circ \text{F}$

1.1 The Exit Nozzle

The exit nozzle is generally of the de Laval type, although at times only the convergent part of the nozzle need be used if the exit flow Mach number is only required to be sonic or subsonic. It is essentially a matching device fitted to the discharge end of the combustion chamber and serves to choke the latter by building up pressure to match the available diffuser pressure at the flow conditions of captured air flow and engine exit temperature. The divergent side of the nozzle serves to expand the combustion gases to a supersonic velocity and correspondingly low temperature and pressure, and under such conditions the output of the combustor is independent of downstream atmospheric conditions. In the limiting case, the throat area of the exit nozzle may approach that of the combustion chamber; such an arrangement is known as "straight-tailed" or "unconstricted." (This could correspond to the setting up of a thermal throat.) Flow through the nozzle is nearly isentropic if it is uncooled. For one-dimensional flow the inlet and exit Mach numbers are simply determined by the following Mach number relationships:

$$A_c/A_b = \frac{1}{(A/A^*)_b} \quad (\text{subsonic portion}), \quad (119)$$

and

$$A_c/A_e = \frac{1}{(A/A^*)_e} \quad (\text{supersonic portion}). \quad (120)$$

A value has already been assigned to M_b and thus to $\theta(M)_b$ [Eq. (114)], and this value of M_b , when used in Eq. (119), will define the area ratio of the converging section of the exit nozzle.

The realization of the overexpanded and underexpanded flow previously referred to thus lies in a combination of the effects of heat addition within the ramjet (which affects the pressure upstream of the exit nozzle) and flight altitude (which determines the external pressure). Nozzle shapes for parallel isentropic flow may be computed by various methods, including the "method of characteristics". The resulting designs afford theoretical (ideal) values of exit thrust, apart from the momentum loss due to skin friction, which is approximately 1 per cent of the total, but the minimum length of such an ideal nozzle tends to come out excessive in terms of available space. Since an ideal divergent design is therefore longer than is generally acceptable, the subsonic convergence is often made more rapid than the ideal. This may cause a separation of flow at the throat, leading to a reduced coefficient of discharge with nonuniform flow in the supersonic section. If there were no need for further expansion, a sonic jet would be perfectly efficient, but this is modified by supersonic expansion and may be less efficient than the ideal because of nonuniformity of the entering flow. Figure 47 illustrates the theoretical reduction of efficiency which occurs when a family of supersonic isentropic nozzles are shortened to less than the lengths required to produce parallel flow at the exit.

Since exit nozzles do not in practice give rise to isentropic one-dimensional flow, the coefficient of discharge--which depends to a considerable extent on the inlet geometry--is always less than unity, so that the realizable exit thrust will be below the theoretical value. The principal loss arises from the existence of a radial component in the exit velocity, smaller losses occurring as a result of nonuniformity of the exit velocity and as an effect of skin friction. This drop of actual exit jet thrust below the theoretical value is manifest in a drop of the static pressure acting on the diverging nozzle area. The effectiveness of a nozzle may thus be determined by either a direct experimental measurement of the thrust or of the pressure distribution, or by a calculation of the internal flow field, either within the nozzle or across the exit jet. Figures 48 and 49 illustrate the effect

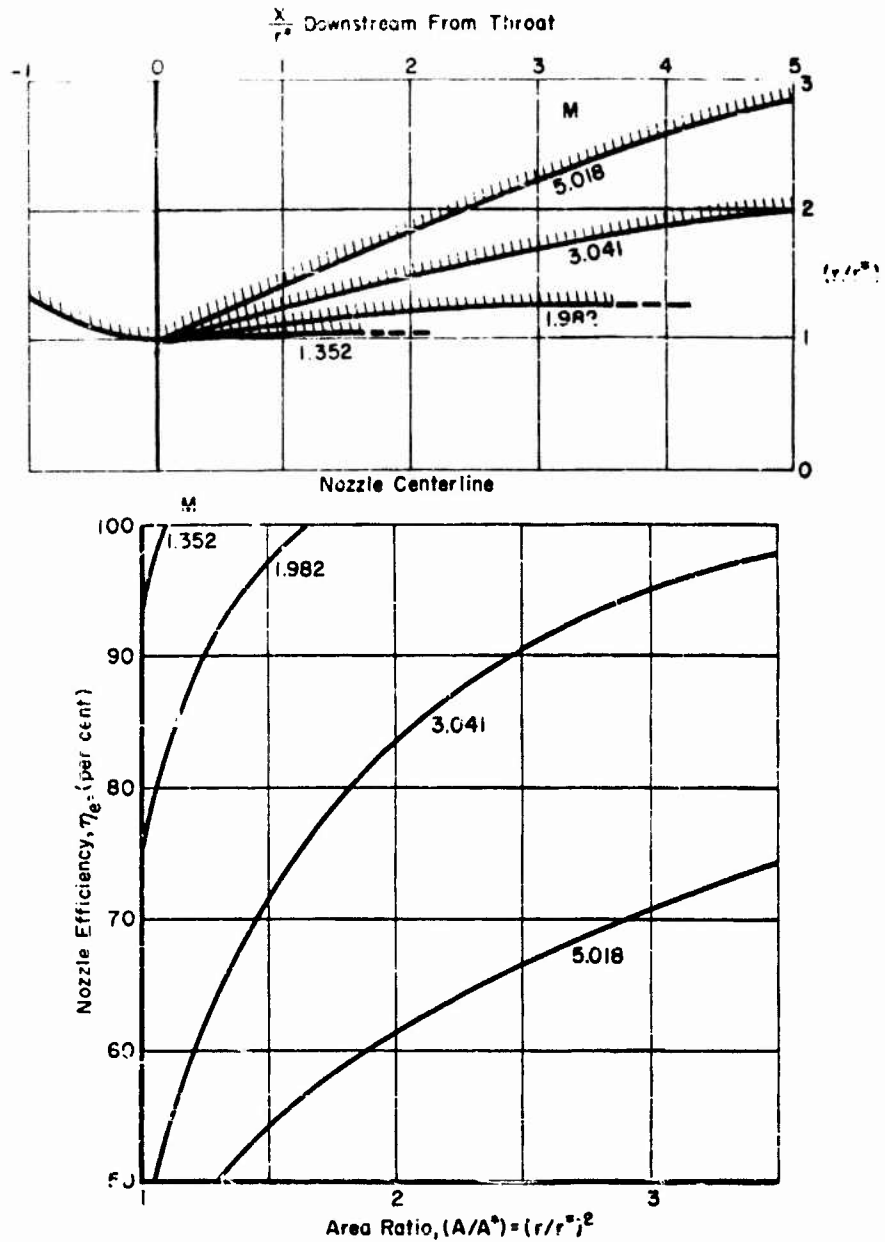


Fig. 47 Theoretical Exit Nozzle Efficiency η_e for Nozzles of Less Than Optimum Length

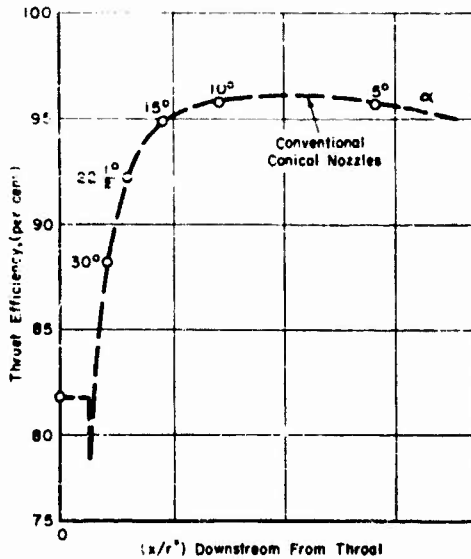
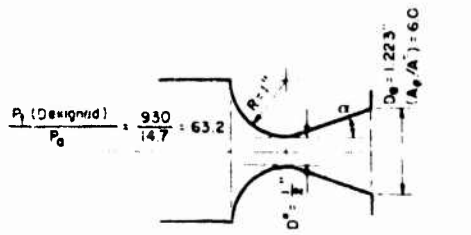


Fig. 48 Actual Variation of Thrust with Length of Conical Nozzle of Fixed Area Ratio
Data taken from Ref. 18.

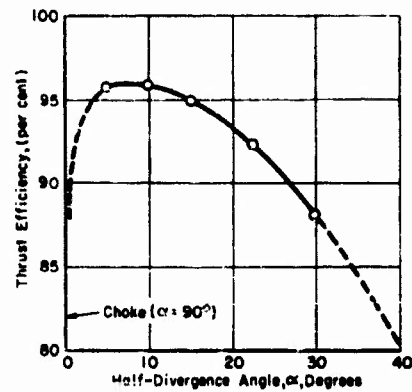
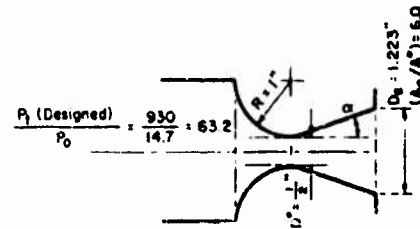


Fig. 49 Actual Variation of Thrust of Conical Nozzle with Divergence Angle
Data taken from Ref. 18.

on actual nozzle thrust efficiency of shortening the nozzle and varying the divergence angle. Further data on the efficiency of practical nozzles will be found in TG 370-13.

The magnitude of the expansion area ratio (A_c/A_e) to yield maximum thrust thus involves the use of an optimum expansion angle which enables a compromise to be struck between excessive friction and excessive expansion losses. In an over-all force balance, the gross forward engine thrust will be made up of the rate of flow of momentum

through the exit nozzle throat together with the forward acting component of the wall gauge pressure summed over the expanding area of the exit nozzle. This latter force attains a maximum when the expansion nozzle area is extended until the gauge pressure acting on the added area reduces to zero. External drag considerations, however, modify the optimum size of the exit nozzle since, for example, a gain of thrust at the expense of an equal increase of drag obviously provides no net improvement. The external drag will be a minimum if the nozzle exit area is the same as the combustion chamber, thereby avoiding the setting up of base or wave drag. In this case, $(A_e/A_c) = (A_b/A_c)$. It is impossible to satisfy this requirement for all possible flight altitudes, unless a variable geometry nozzle is employed, so that expansion to an arbitrary area different from A_b results in the exit static pressure differing in general from the ambient pressure. The simplest type of variable geometry design is an inverted nozzle, having a movable center body; such a design is associated with difficulties in the way both of cooling and of rigidity. If an expansion to ambient pressure is required, the exit total pressure must first be obtained by following the total pressure change through the diffuser and the combustor; the ratio of the exit static to the total pressure then determines the exit Mach number, which in turn fixes the expansion ratio from nozzle throat to exit:

$$(P/P_t)_e = (P_0/P_{t_c}) ,$$

and

$$(A_e/A_c) = (A/A^*)_e .$$

The thrust of the exit jet may then be computed from either Eq. (59) or Eq. (67), as given in Section 2, using Eq. (59) for expansion to the ambient static pressure, and Eq. (67) for expansion to the full area value.

$$F_e = A_e P_e (1 + \gamma M_e^2) \quad (121)$$

$$F_e = \dot{w}_a S_a \theta(M)_e = P_0 A_0 \frac{\rho}{w_0} (S_a / \sqrt{T_{t_0}}) \theta(M)_e \quad (122)$$

These thrust values are expressed on an absolute basis. If they are required on a gauge basis, a force ($A_e P_0$), equal to the product of the ambient static pressure into the exit area, must be deducted from the right hand side. Engine net thrust on a gauge basis may be found from a difference of the exit and inlet forces.

The additional loss of engine thrust arising from nonuniformity of thermal energy (total temperature) in the exit stream has been discussed by Bader (Ref. 19). There are likely to be regions of varying fuel-air ratio or combustion efficiency in the burnt gas stream flowing from the combustor. A stream which has burned at a leaner than average fuel-air mixture or which has less than average combustion efficiency will thus have a lower value of S_a or of total temperature. Similarly, regions of greater heat release will have a higher S_a or total temperature. An approximate calculation of this effect may be made by considering a set of concentric streams differing stepwise from each other in respect of total temperature or of S_a . The loss of thrust may easily be demonstrated qualitatively for the case when the exit jet is considered to consist of a hot and a cold stream both at the same Mach number as the inlet flow. The exit gauge thrust caused by the cold gas will be equal to or less than its inlet thrust and it will make no net contribution to engine thrust other than drag (corresponding to diffuser losses and burner drag). The engine will then operate with less than the optimum air flow and at a higher equivalence ratio and will accordingly be less efficient. The over-all fuel specific impulse of the engine will approximate, but will be lower than,

Since the flow is assumed to be uniform over the portion of the combustor cross-section actually burned, and since this case of nonone-dimensionality arises from the combustor, it is simplest to treat it as a reduction of combustor temperature. The total energy of a nonuniform stream of constant static pressure and Mach number may be determined by finding the sum of the contributions of the stream tubes of constant local total temperature, which equals the product of the average total temperature \bar{T}_t and the heat capacity of the total flow:

$$\sum \dot{m}_i = \sum_i c_{p_i} T_{t_i} \dot{m}_i = \bar{T}_t \sum_i \dot{m}_i c_{p_i} .$$

whence

$$\bar{T}_t = \frac{\sum_i c_{p_i} T_{t_i} \dot{m}_i}{\sum_i \dot{m}_i c_{p_i}} . \quad (123)$$

The mass flow \dot{m}_i per unit time may be expressed in terms of Mach number, static pressure, and total temperature as follows:

$$\dot{m}_i = \frac{A_i P^0}{\sigma \sqrt{T_{t_i}}} ,$$

so that

$$\bar{T}_t = \frac{P^0 \sum_i c_{p_i} A_i \sqrt{T_{t_i}}}{P^0 \sum_i c_{p_i} A_i (1/\sqrt{T_{t_i}})} = \frac{\sum_i c_{p_i} A_i \sqrt{T_{t_i}}}{\sum_i c_{p_i} A_i (1/\sqrt{T_{t_i}})} . \quad (124)$$

The thrust of the air stream may be obtained by summing the thrust contributions of the stream tubes:

$$L.F. = \sum_i \theta(M)_c \dot{m}_i = \sum_i \dot{m}_i (S_{a_i}) \theta(M)_c .$$

then

$$S_a = \frac{\sum_i P A_i \frac{Q(S_a/\sqrt{T_t})}{\rho(M)_e} \rho(M)_e}{P \rho(M)_e \sum_i A_i (1/\sqrt{T_{t_i}})}$$

but $(S_a/\sqrt{T_t})$ is a function made up largely of gas constants since

$$S_a = \sqrt{\frac{2(\gamma + 1) R T_t}{\gamma}} \left(\frac{1 + \gamma}{g}\right);$$

therefore

$$S_a = \frac{\sum_i A_i \left(\frac{1 + \gamma}{g}\right) \sqrt{\left[\frac{2(\gamma + 1) R}{\gamma}\right]_i}{\sum_i A_i (1/\sqrt{T_{t_i}})}$$

This expression may be simplified if γ , c_p , R , and γ are considered constant:

$$\therefore S_a = \frac{A_e \left(\frac{1 + \gamma}{g}\right) \sqrt{\frac{2(\gamma + 1) R}{\gamma}}}{\sum_i A_i (1/\sqrt{T_{t_i}})} \quad (125)$$

If Eq. (124) is divided by $\sqrt{T_t}$, there follows

$$\sqrt{T_t} = \frac{\sum_i A_i \sqrt{T_{t_i}/T_t}}{\sum_i A_i (1/\sqrt{T_{t_i}})}$$

If this latter equation is now divided into Eq. (125), there results the ratio of the actual thrust to that produced by a one-dimensional stream of the same energy:

$$\frac{\bar{S}_a}{S_{a_{unh}}} = \frac{1}{\sum_1 (A_1/A_0) \sqrt{T_{t1}/\bar{T}_t}} \quad (126)$$

One may see the effect on a gross temperature profile when, for example, one half of the exit jet area is at twice the mean temperature while the other half is at half the mean temperature, thus satisfying Eq. (124) in regard to constancy of heat release. Entering these values into Eq. (124),

$$\frac{\bar{S}_a}{S_{a_{unh}}} = \frac{1}{(1/2)(\sqrt{2} + \sqrt{0.5})} = \frac{1}{1.061}$$

Thus there is approximately a 6 per cent loss of thrust in this simple case. Calculation of the thrust loss for actual combustion systems is further complicated by dissociation phenomena that occur during burning at elevated temperatures and by changes in the values of γ , c_p , and R with temperature and gas composition, as indicated earlier.

The equations presented so far are useful only when total temperature distributions are known. If it is desired to calculate the effective thrust available from burning known amounts of fuel in various parts of the air stream, the following procedure needs to be followed in order to deduce the stream temperatures and stream thrusts from the local equivalence ratios. It is assumed that the combustor has been designed on a one-dimensional flow basis and that all flow areas and Mach numbers and the equivalence ratio are fixed. The thrust having been determined for one-dimensional flow, it is desired to calculate the thrust loss that would result if the hot burned gases were not mixed with the remaining throughput. Nominal one-dimensional values exist for T_{t0} , η_c , (E.R.), M_e , and σ (the fraction of the throughput initially heated); the nominal value of $S_{a_{unh}}$ corresponds to η_c (E.R.). The heat, however, is added to only a fraction σ of the flow and this fraction burns at an equivalence ratio of (E.R.)₀/ σ .

The ratio of exit thrusts may now be found from

$$F_{uni} = \dot{w}_a \beta(M)_e S_{a_{uni}}, \quad \text{and}$$

$$F_{actual} = \dot{w}_a \beta(M)_e \left[\sigma S_{a_{uni}} + (1 - \sigma)(2.382 \sqrt{T_{t_0}}) \right],$$

whence

$$\frac{F_{actual}}{F_{uni}} = \frac{\sigma S_{a_{uni}} + 2.382 \sqrt{T_{t_0}} (1 - \sigma)}{S_{a_{uni}}} \quad (127)$$

This reduction of effective thrust can be regarded as a reduction in effective combustion efficiency for a particular chosen engine operating condition. Figure 50 shows this loss of effective combustion efficiency in a combustion system burning kerosene at an inlet

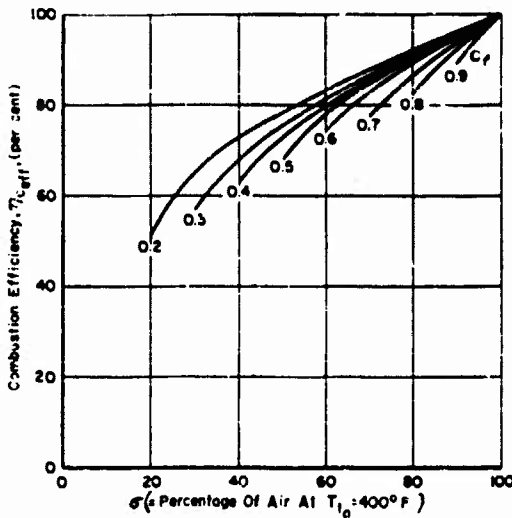


Fig. 50 Percentage Loss of Apparent Combustion Efficiency Due to Nonmixed Exit Jet

total temperature of 400°F. The effective thrust loss is greatest for engines operating at low equivalence ratios where only a small fraction of the over-all flow, numerically equal to the equivalence ratio, is

needed for combustion. The residue of the air not involved in combustion is normally by-passed around the combustion space and mixed with the products of combustion, the process being similar to that occurring in a turbojet combustion system. It may be noted that this reduction of combustion efficiency is a factor to be applied to a calculated fuel specific impulse or combustion efficiency. For lean mixtures, in spite of a certain amount of loss due to nonmixing, the fuel specific impulses usually optimize at values of ϕ less than stoichiometric so that an optimum engine design will still be similar to one with uniform exit flow.

No compensation factor is needed for nonone-dimensionality of the exit stream when the exit jet thrust is measured directly for the determination of combustion efficiency. In the case of experimental combustion efficiency evaluation from thrust, the thrust losses from jet nonone-dimensionality of all kinds are included in the combustion efficiency.

A further problem in the design of the exit nozzle results from the fact that the high temperature of the gases leaving the combustion chamber exposes the nozzle to a considerable flux of heat from both convection and radiation, which may cause it to fail structurally. Considerable effort has therefore been expended in an endeavor to develop suitable nozzle materials to withstand the high temperatures of the gases issuing from the combustion chamber. For example, while a nickel-cobalt steel alloy may melt in the range 2500-2600°F, while retaining its strength up to 2000°F, the melting point of molybdenum is approximately 4750°F, with an upper stress limit at about 3000°F. Another approach is to increase the reflectivity of the subsonic and throat sections by coating them with such metals as gold or platinum. Alternatively, a combustion chamber cooling shroud may be designed to afford relief by spilling an annulus of cooler air onto the nozzle, but this arrangement may result in a reduction of the effective throat.

V RAMJET PERFORMANCE CALCULATIONS

The object of this section is to show how the basic thermodynamic calculations of a ramjet engine are made. The various engine arrangements which can be chosen for specific requirements are first considered, and from these the one having the best figure of merit is picked. Some arrangements may be found which will produce high fuel economy only at the design point, others will provide an acceptable performance over a wide range of speeds or power outputs. The main requirements and indices of merit for engine performance will arise from considerations of engine application presented in a later chapter. Typical requirements will be stated here without extensive discussion, as there are a number of inevitable compromises that arise in the design of engines for any purpose. These arise from requirements of usage, from problems of installation and from the conflicting requirements for high performance presented by the various major components.

5.1 Thrust Performance

The useful output of a ramjet engine is the net difference between the forward-acting reaction on the engine set up by the ejection of the exhaust gases and the drag associated with the air flow capture at inlet. This result is expressed either as a net thrust or as a dimensionless coefficient C_F , the main inlet and exit flow relations having been developed in Sections 2 and 3. Application of these relations requires the selection of values for the two independent gas dynamic variables, flight Mach number M_0 and temperature parameter $(S_a/\sqrt{T_{t_0}})$, in addition to the need to detail the engine geometry. These relations, together with the ambient conditions, determine conditions within the combustor, and allow the selected temperature parameter to be translated into an operating fuel-to-air ratio by means of

the characteristics of the burner which relate the combustion efficiency to the stream flow state.

The mechanics of calculation proceed in a straightforward manner from the junction of the diffuser and combustor, using theoretical relations or test results such as those shown in Figs. 36 to 38 for the diffuser, and Figs. 40, 41 and 44 to 46 for the combustor. A relationship such as that of Eq. (114), or test results such as those shown in Fig. 39, will yield the required relationship between the diffuser exit Mach number M_2 and the temperature parameter. One may then determine the air flow capture by means of Eq. (96), or from test results such as those shown in Fig. 38. The air capture determines the inlet drag, as given by Eq. (98) or by experimental results, as shown in Fig. 37. The exit force is determined from the selected value of $(S_a/\sqrt{T_t})$, the air capture is found for the diffuser, and the exit nozzle performance is then found from Eq. (120). The exit and inlet forces may be converted to a gauge basis by subtraction of the ambient static pressure force on the projected surfaces, or expressed as coefficients by division by the product of a reference area into the dynamic pressure; they are thus functions of the flight Mach number, $(S_2/\sqrt{T_{t0}})$, and the external pressure level, but normalizing them by dividing by q_0 results in values which are independent of the pressure level. Different ways of plotting these three variables of flight Mach number, thrust coefficient and air capture ratio, are shown in Figs 51 and 52. Each figure thus completely represents the gas dynamic behavior of the engine under all conditions, but neither includes any information as to how the exit gas temperature is to be obtained.

It is clear from an inspection of Fig. 51 that the thrust coefficient varies weakly with the freestream Mach number and strongly with the value of $(S_a/\sqrt{T_{t0}})$. In addition, the lines of constant $(S_a/\sqrt{T_{t0}})$ relating M_0 to C_F show three types of engine inlet aerodynamic behavior. Above the line $(A_0/A_1)_{max} = 1$ the thrust rises only slightly because of the reduction of engine air flow due to inlet spillover with an increase in $(S_a/\sqrt{T_{t0}})$. Below this curve the

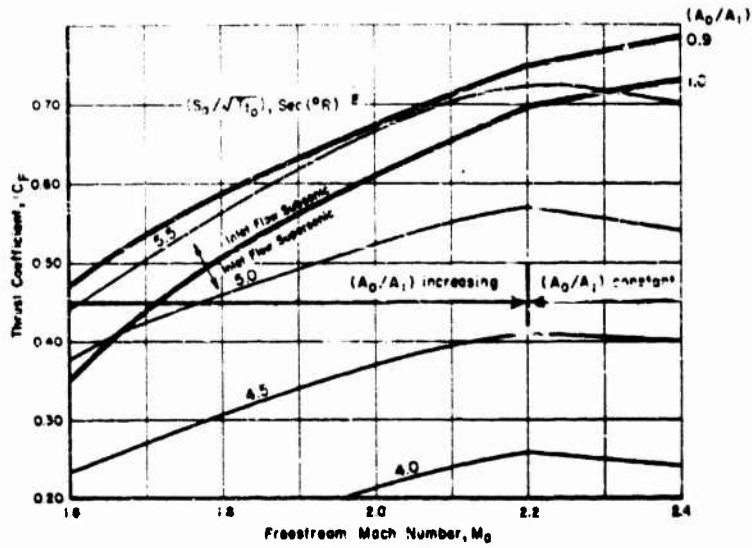


Fig 51 Effect of Freestream Mach Number and Engine Temperature Parameter on Thrust Coefficient

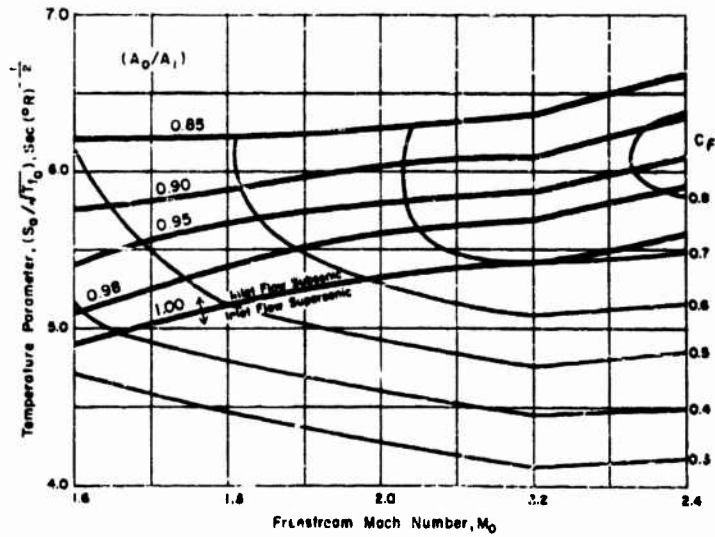


Fig. 52 Effect of Freestream Mach Number and Engine Temperature Parameter on Thrust Coefficient and Airflow Capture Area Ratio

$(S_a / \sqrt{T_{t0}})$ curves exhibit two types of behavior, depending on whether or not the flight speed is above or below the value for which the oblique shock from the spike tip just falls within the inlet. As long as the oblique shock is α of the inlet, an increase in the Mach number reduces spillover between the oblique shock and the inlet lip, so that the air flow captured increases more rapidly than does the speed. This increase is reflected in the rise of exit thrust or thrust coefficient with Mach number until full air flow capture is obtained. Above this speed no supersonic spillover occurs, and the inlet capture area becomes fixed, leading to only a linear increase in the air flow with increasing speed. As the dynamic pressure increases as the square of the speed, the net thrust coefficient drops off in the ratio of the increase of air flow with dynamic pressure, or inversely as the Mach number. This simplified picture is somewhat complicated by the relationship between inlet drag and mass flow capture so that as one moves above the $(A_0/A_1)_{max} = 1$ line the air flow and inlet force coefficient both fall off. For most diffusers, this fall in the inlet force coefficient is enough to offset the thrust reduction caused by lessened air capture, and a small, but at times useful, increase in thrust is obtained by subcritical diffuser operation. Figure 52 thus shows the aerodynamic aspects of the engine behavior better than Fig. 51, as it is easier to show the variation of subsonic inlet flow with the temperature parameter $(S_a / \sqrt{T_{t0}})$ which largely determines $(A_0/A_1)_{max}$; this results in lines of constant thrust coefficient becoming lines sloping in general down to the lower right from the upper left, with breaks in slope and spacing on passing through regions of different rates of air flow change. Figure 51 is simpler to interpret from the thrust output point of view, while Fig. 52 represents the aerodynamic and thermodynamic picture more directly.

Pressure and temperature (in addition to the temperature parameter) must be fixed in order to set the fuel flow or the equivalence ratio required to produce a given value of $(S_a / \sqrt{T_{t0}})$. If combustion were always perfect with no changes due to dissociation, one could obtain a correlation between S_a and the equivalence ratio as shown in

Fig. 44, and would thus need to fix only T_0 , M_0 , and $(S_a/\sqrt{T_{t_0}})$ to obtain the fuel-air ratio needed to produce a given thrust coefficient. Since combustion efficiencies are in fact somewhat pressure-sensitive, one must also fix the ambient pressure P_0 , which thus enables the combustion pressure to be determined from the relationship between ambient pressure, flight Mach number, and the diffuser recovery. If, for instance, one were to set the ambient pressure and temperature to that corresponding to NACA Standard Day conditions at an altitude of 30,000 feet, one could combine the relationship between $(S_a/\sqrt{T_0})$ and the equivalence ratio shown in Figs. 44, 45, and 46 with Figs. 51 or 52 to obtain the thrust coefficient in terms of equivalence ratio. If the given values for $(S_a/\sqrt{T_{t_0}})$, T_{t_0} , and the air weight flow are entered into Figs. 44, 45, or 46, the corresponding equivalence ratio may be derived, as shown in Fig. 53 for the given conditions. These equivalence ratio curves could also have been plotted on Fig. 52 but for the

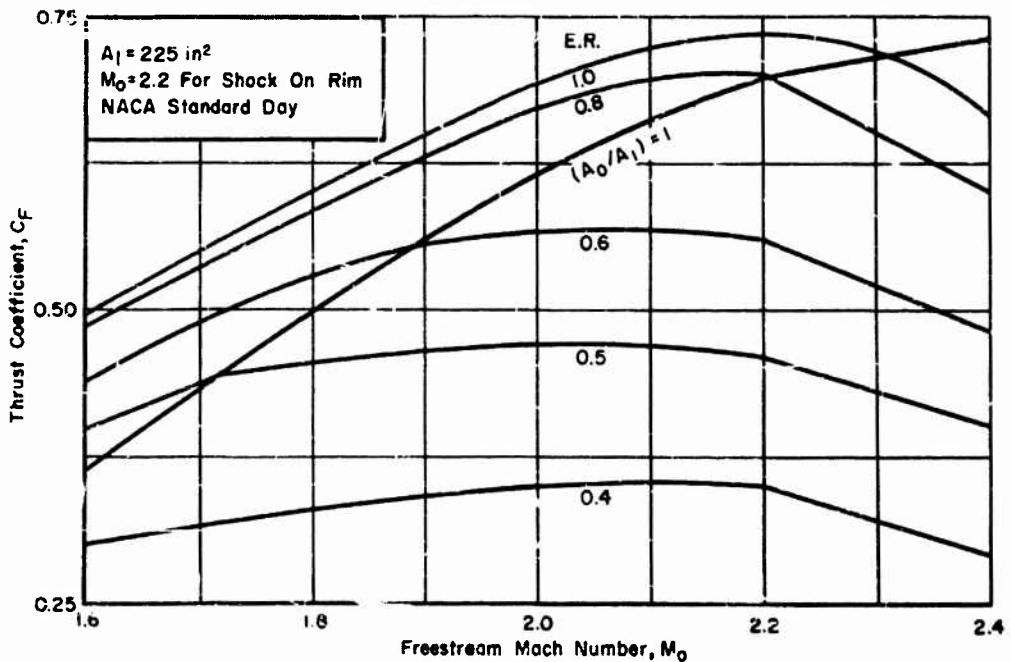


Fig. 53 Relationship of Equivalence Ratio to Thrust Coefficient

Ramjet Performance Calculations

resulting multiplicity of grid lines. If the temperature level at the given flight altitude were changed, engine thrust would be affected because of the effect of inlet temperature on S_a for burning at a fixed equivalence ratio, resulting from the change of combustion efficiency and the increase of T_{t_0} in $(S_a/\sqrt{T_{t_0}})$. The general result is that while S_a increases slightly as the inlet total temperature is varied, the thrust falls because of the correspondingly greater increase of the root of the inlet total temperature in the denominator of the temperature parameter term. Figure 54 shows the over-all effect

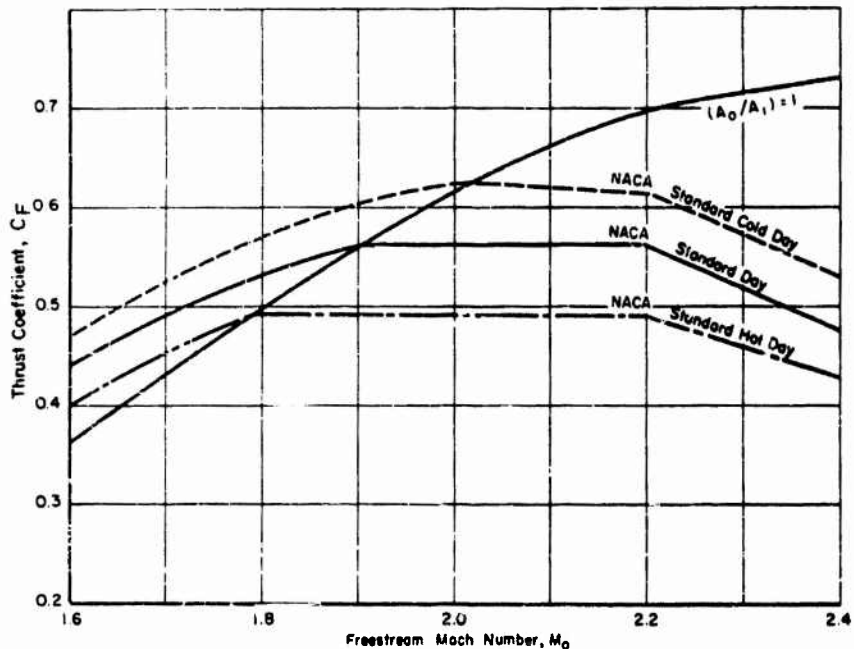


Fig. 54 Effect of Ambient Temperature on Thrust Coefficient at Constant Altitude of 30,000 Feet and Equivalence Ratio of 0.8

of ambient temperature on the engine described in Figs. 51 through 53, as obtained by contrasting the thrust coefficient for a constant equivalence ratio of 0.8 under Standard Hot, Standard Cold, and Standard

Day conditions at 30,000 feet. This effect is large and can be quite serious for marginal power plants. When the engine operating altitude is changed, two effects ensue, caused respectively by pressure level and ambient temperature. At low altitude, higher temperatures generally occur together with higher pressures; combustion at low altitude is also generally more efficient because of the high pressure level, but the value of $(S_a / \sqrt{T_{t0}})$ is lower because of the greater proportional increase of T_{t0} over that of S_a which generally leads to a reduction of the thrust coefficient at sea level as compared to the value at the base of the stratosphere. An increase of altitude above the base of the stratosphere results in lower combustion pressures attended by reduced values of combustion efficiency and S_a without any reduction in T_{t0} so that the thrust again falls. These further effects are shown in Fig. 55 for equivalence ratios of 0.3 and 0.8. Of note is the rapid decrease in thrust coefficient for reduced flight speed at an altitude

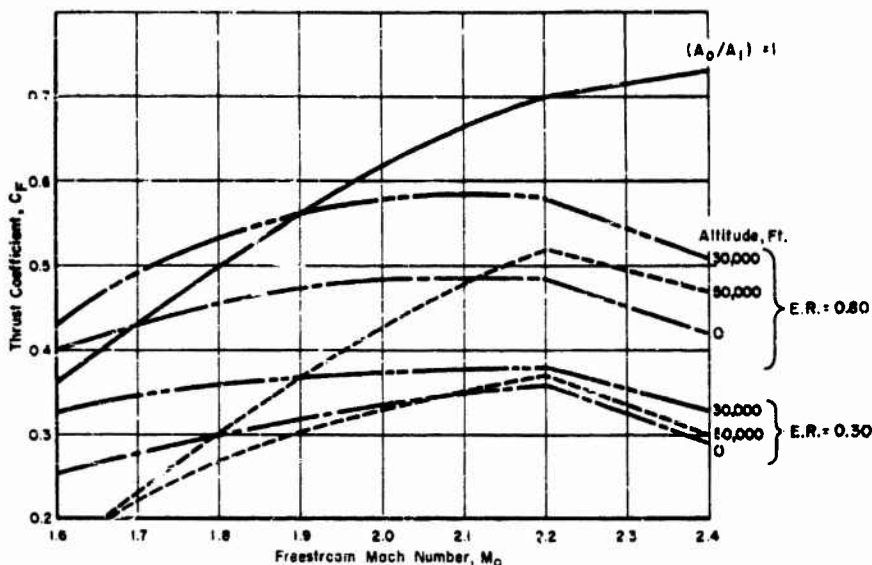
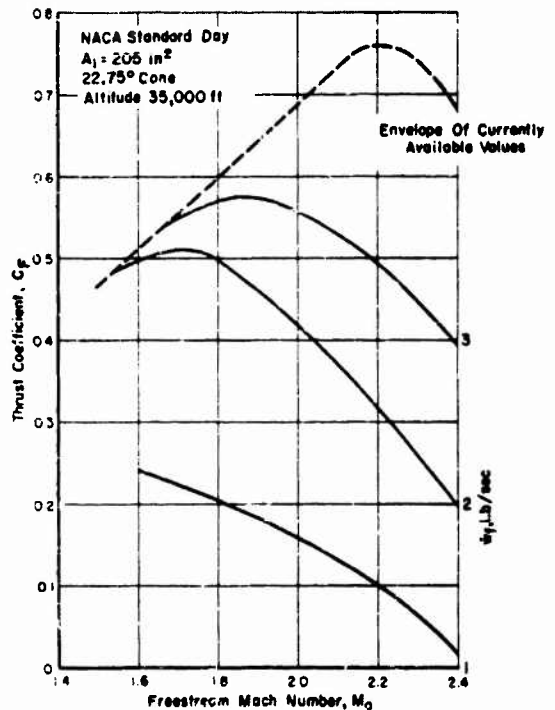


Fig. 55 Effect of Altitude on Thrust Coefficient for NACA Standard Day, at Constant Equivalence Ratio

of 50,000 feet and an equivalence ratio of 0.8, due to the fact that the fall in combustion efficiency is thus large for a change of mass flow or combustion pressure. The change of combustion efficiency with altitude is less pronounced at an equivalence ratio of 0.3 and the slopes of the corresponding C_F curves are more nearly the same.

One may compute ramjet engine air flows at suitable points, and also values of fuel flow from the air flow and the equivalence ratio, as indicated by curves such as those of Fig. 53. The resulting relations between fuel flow, flight Mach number and thrust may be plotted as in Fig. 56 to give the final engine performance relationships re-

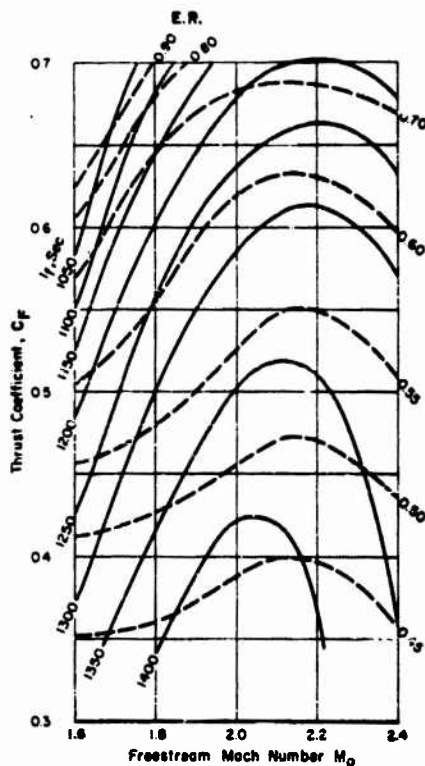
Fig. 56
Thrust Coefficient for Various
Fuel Flows w_f at Constant Altitude



quired. Associated with each point on Fig. 56 are a thrust and a fuel rate. From the quotient of these parameters a figure of merit, I_T ,

tion took place at maximum efficiency. The choice, however, was dictated by the possibility of obtaining greater thrust, by operating the combustor at an equivalence ratio corresponding to higher than optimum combustion efficiency. Maximum thrust is secured by matching the diffuser inlet and combustor exit areas to the maximum available heat release, rather than by achieving the most efficient combustion. A whole series of engine designs may thus be assembled from a combustor and a diffuser of given performance by adjusting inlet and exit areas to optimize economy at various points. Figure 58 shows optimum fuel

Fig. 58 Fuel Specific Impulse for Typical Engine with Variable Inlet and Exit Geometry



specific impulses associated with various values of design thrusts for engines having the diffuser and combustor performance shown in the preceding figures, but with inlet and exit areas adjusted for optimum

efficiency at each point. This figure thus represents the performance of a variable geometry engine--if such could be built. A comparison of Figs. 57 and 58 shows in effect the penalty paid by a fixed geometry engine for off-design performance. The fuel specific impulses for the fixed geometry engine approach those for the variable geometry one at the optimum point, but fall 20 to 30 per cent below them at the extreme values of thrust coefficient and Mach number.

5.2 Optimum Fuel Specific Impulse

To find the optimum of the parameter of fuel specific impulse, it is first necessary to maximize the expression

$$I_f = F_{net} / \dot{w}_f$$

by specifying the thrust value F_{net} ; \dot{w}_f , the fuel flow, is thus regarded as the variable. Since \dot{w}_f is in turn a product of the engine air flow and the fuel-to-air ratio y ,

$$I_f = \frac{F_{net}}{\dot{w}_a y}$$

The two terms in the denominator must be related to each other through the medium of the thrust coefficient equation and the internal flow relationships for particular engine designs as characterized by their geometrical features. These are implicit relations so that the characteristic design features must be such that values can be arbitrarily assigned to them in order to evaluate the required functions. The derivations given below will show that these features are the diffuser exit Mach number, M_2 , and the ratio of nozzle exit area to combustion chamber area, (A_e/A_2) . These are related to the equations for thrust coefficient, diffuser flow, combustion chamber momentum balance, and exit nozzle flow, as follows:

$$C_F = \frac{\bar{w}_0 A_1}{(q/P)_0 A_2} \frac{S_a}{\sqrt{T_{t_0}}} \eta_e \vartheta(M)_e - 2 \frac{A_1}{A_2} - \frac{A_e}{A_2 (q/P)_0} \quad (128)$$

$$A_1 \left[\frac{(P/P_t) \bar{w}}{P_{t_0}} \right]_0 = A_2 \left[\frac{(P/P_t) \bar{w}}{P_{t_2}} \right]_2 \quad (129)$$

$$\frac{1 - (C_{D_b} - 2)(q/P)_2}{\bar{w}_2} = (S_a / \sqrt{T_{t_0}}) \vartheta(M)_b \quad (130)$$

and

$$A_e = \mu A_2 \quad (131)$$

One may evaluate (A_1/A_2) from Eq. (129) in order to express it in terms of functions of M_0 , M_2 , and η_d :

$$\frac{A_1}{A_2} = \frac{P_{t_2}}{P_{t_0}} \frac{\left[\frac{(P/P_t) \bar{w}}{P_{t_2}} \right]_2}{\left[\frac{(P/P_t) \bar{w}}{P_{t_0}} \right]_0} = \eta_d \frac{\left[\frac{(P/P_t) \bar{w}}{P_{t_2}} \right]_2}{\left[\frac{(P/P_t) \bar{w}}{P_{t_0}} \right]_0}$$

Solving for $(S_a / \sqrt{T_{t_0}})$ in Eq. (130),

$$(S_a / \sqrt{T_{t_0}}) = \left(\frac{1}{\vartheta(M)_b} \right) \frac{1 - (C_{D_b} - 2)(q/P)_2}{\bar{w}_2}$$

Entering this value into Eq. (128), along with Eq. (131), there follows

$$C_F (q/P)_0 = \frac{\bar{w}_0 \eta_d \left[\frac{(P/P_t) \bar{w}}{P_{t_2}} \right]_2}{\left[\frac{(P/P_t) \bar{w}}{P_{t_0}} \right]_0} \left[\frac{1 - (C_{D_b} - 2)(q/P)_2}{\vartheta(M)_b \bar{w}_2} \right] \vartheta(M)_e \eta_e$$

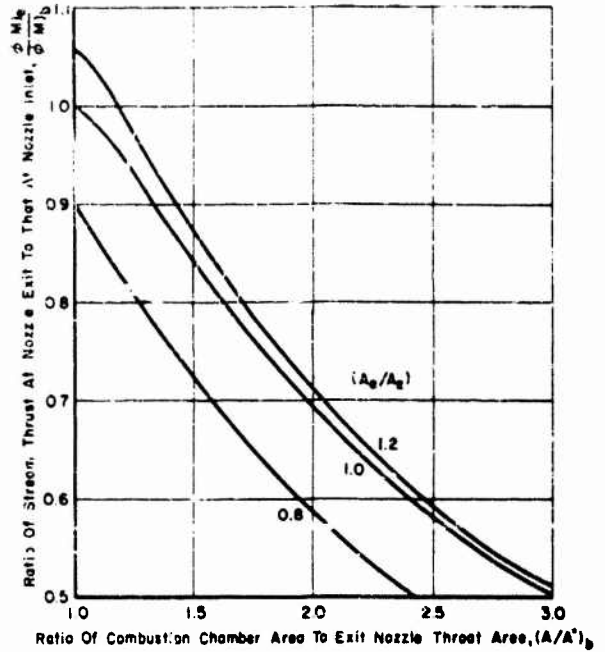
$$- 2(q/P)_0 \eta_d \frac{\left[\frac{(P/P_t)_0}{(P/P_t)_2} \right]_2}{\left[\frac{(P/P_t)_0}{(P/P_t)_2} \right]_0} - \mu.$$

This may be solved for $\vartheta(M)_e/\vartheta(M)_b$ to obtain

$$\frac{\vartheta(M)_e}{\vartheta(M)_b} = \frac{(P/P_t)_0}{\eta_e \eta_d (P/P_t)_2 \left[1 - (C_{D_b} - 2)(q/P)_2 \right]} \left[(q/P)_0 C_F \right. \\ \left. + 2 \eta_d \frac{\left[\frac{(P/P_t)_0}{(P/P_t)_2} \right]_2}{\left[\frac{(P/P_t)_0}{(P/P_t)_2} \right]_0} \left(\frac{q}{P} \right)_0 + \mu \right]. \quad (132)$$

Since μ , C_{D_b} , C_F , M_0 , M_2 , η_d , and η_e have been fixed, the right hand side of Eq. (132) may be evaluated by defining the particular relationship between $\vartheta(M)_e$ and $\vartheta(M)_b$ that must be met if the engine is to produce the required C_F at these conditions. This relationship implicitly determines the throat area ratio (A_2/A_c) because particular values for $\vartheta(M)_e$ and $\vartheta(M)_b$ correspond to each value of (A_e/A_c) and (A_2/A_c). (Either one ratio or the other will have been fixed so that they both change together as A_c is varied.) As A_c is reduced below A_e , the exit stream becomes supersonic, and $\vartheta(M)_e$ also increases with M_e , but its rate of increase is slow. The subsonic value of $\vartheta(M)_b$ likewise increases with decreasing M_b but does so more rapidly; the ratio of $\vartheta(M)_e/\vartheta(M)_b$ is therefore unity for $A_e = A_c = A_2$, and decreases as A_c diminishes. Figure 59 shows this ratio plotted against the combustion chamber to exit nozzle area ratio, as obtained from Eq. (132). From the abscissa of this figure may be determined the exit nozzle contraction ratio for the chosen value of (A_c/A_2). The value of M_b which corresponds to this value of (A/A^*) may then be found from Mach number tables in order to evaluate $\vartheta(M)_b$, which is then inserted into Eq. (130) to determine the value of ($S_a/\sqrt{T_{t_2}}$) associated with the operating

Fig. 59
 Engine Exit Nozzle Stream Thrust Ratio
 of Specified Values of the Ratio of
 Combustion Chamber to Exit Nozzle
 Throat Areas



value of M_2 to give the prescribed C_F . A set of such calculations must be performed for various values of M_2 to obtain corresponding values of the temperature parameter. Air flows for each engine design are computed from the respective values of M_2 by means of Eq. (129), and the corresponding fuel-to-air ratios are deduced from the values of $(S_a/\sqrt{T_{t_2}})$, as obtained above. The value of the fuel specific impulse is then computed for each design, and the values plotted against diffuser Mach number, inlet area capture ratio, equivalence ratio or exit nozzle throat area ratio, in order to find the relation of any one of these to the optimum fuel specific impulse. Other values of the engine design parameters may also be determined from Eqs. (128) through (130). Such an optimum value of I_f is valid only for the selected value of (A_e/A_2) ; if, therefore, (A_e/A_2) is also a variable for optimization purposes, the process needs to be repeated for a range of values to select a further optimum as a function of this ratio.

VI ENGINE OPTIMIZATION PROCEDURES

Preceding sections have treated the general operation of engine components and the equations relating the flow state across each component. It is therefore possible, in principle at least, to combine various diffusers, combustors, and exit nozzles to produce a wide variety of engines which may be operated under various conditions, since the gas dynamic aspects of engine design are more amenable to analysis than are the structural aspects. Although all design is in a sense optimization, the procedure discussed here involves a comparison between various component designs, each optimized with respect to the demands upon it, in order to select the best compromise for the engine as a whole.

The three basic variables affecting the output of a heat engine are an intensive factor, the energy added per unit of working fluid, an extensive factor, the quantity of working fluid handled, and the efficiency of the cycle. Once the choice of a ramjet cycle has been made, various combinations of these factors are possible. The practical variables corresponding to these are the temperature parameter ($S_a / \sqrt{T_t}$) and the diffuser area ratio (A_0/A_n). There are other parameters which also need to be considered when a design is being calculated, but as these are either environmental (such as flight Mach number, pressure, and temperature) or experimental (such as burner drag), they are initially determined constants rather than dependent variables. The discharge area of the exit nozzle occupies a peculiar place in the calculation, as does diffuser cowl drag, in that except for the consideration of external aerodynamic drag, it is at an obvious maximum when the gases have expanded to ambient pressure. If the external drag is not to be considered in the optimization of an engine, all designs will involve an expansion to ambient pressure. On the other hand, since the rate of change of thrust with area is zero when the ambient

combustion efficiency in the course of the optimization procedure since the combustor can be designed for optimum combustion efficiency (the fuel to air ratio indicated by the analysis.) The likely range of diffuser exit Mach numbers will range from 0.250 down to 0.100 for various engine designs, depending on the temperature ratio across the combustor. The pressure ratio across the combustor will also be such as to require expansion of the gases to substantially the full engine area to bring them close to ambient pressure at exit. It will be convenient to consider six values of diffuser exit Mach number from 0.100 to 0.250, at intervals of 0.025, and to evaluate the exit nozzle throat area and the temperature parameter ($S_a / \sqrt{T_t}$) from Eq. (132) for the required value of thrust. Combustor drag values may be chosen to be 2, 6, and 12 combustion chamber inlet velocity heads. These values correspond respectively to the drag range associated with either a huffletype burner at the diffuser exit, a can-type combustor placed wholly in the combustion chamber, or with the latter mounted within the diffuser near its exit.

Six sets of calculations are then performed using the equation referred to, introducing in sequence the six values of M_2 ; values of (A_2/A_c) and M_b for drag coefficients of 2, 6, and 12 are then determined. Since it is assumed that the exhaust gases are to be reexpanded to full engine area, A_e may be set equal to A_2 . The exit forces are next computed, except for the term ψ_a , which is determined when the exit is matched with an inlet corresponding to the assumed values of diffuser exit Mach number M_2 from Eq. (129) for each of the values 0.7, 0.8, and 0.9 for η_d . There are thus nine families of six sets of engine designs requiring various values for the temperature parameter ($S_a / \sqrt{T_t}$) to be determined from values of thrust coefficient, diffuser efficiency, diffuser exit Mach number, and combustor drag. One may now select by interpolation from each set the engine design yielding the desired thrust coefficient, and calculate the fuel flow and fuel specific impulse for the selected thrust coefficient as explained in Section 2, page 34, and Section 5, page 132, and then plot these results to determine the optimum fuel specific impulse for each family. The resultant fuel specific impulse curves are shown in Figs. 60

through 62. (These figures are computed for 100 per cent combustion efficiency but may easily be adjusted to lower values by multiplication of the ordinate and division of the abscissa by any appropriate value of combustion efficiency.)

Fig. 60 Effect of Burner Drag and Equivalence Ratio on Fuel Specific Impulse, $\eta_d = 0.9$

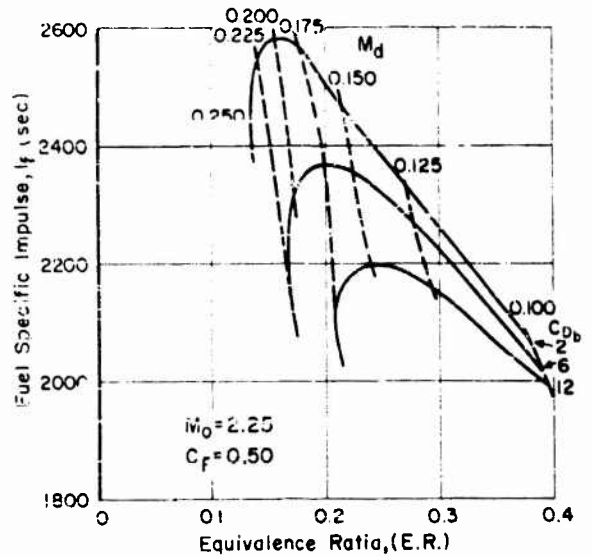
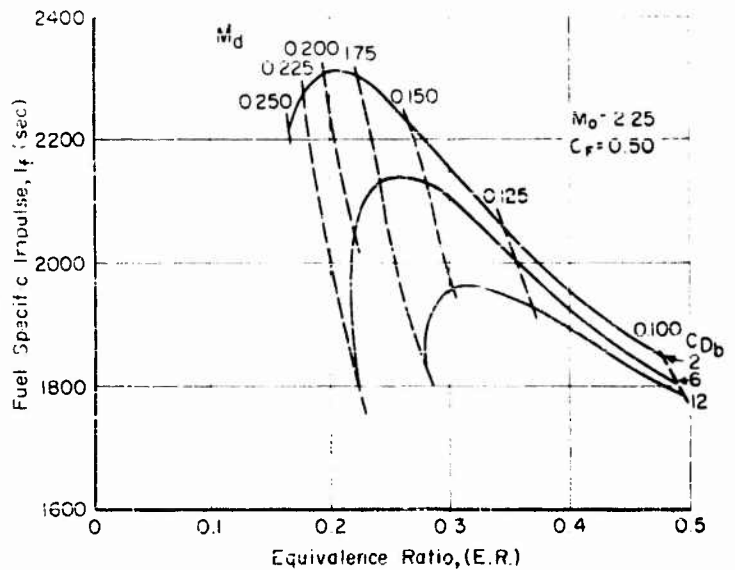


Fig. 61 Effect of Burner Drag and Equivalence Ratio on Fuel Specific Impulse, $\eta_d = 0.8$



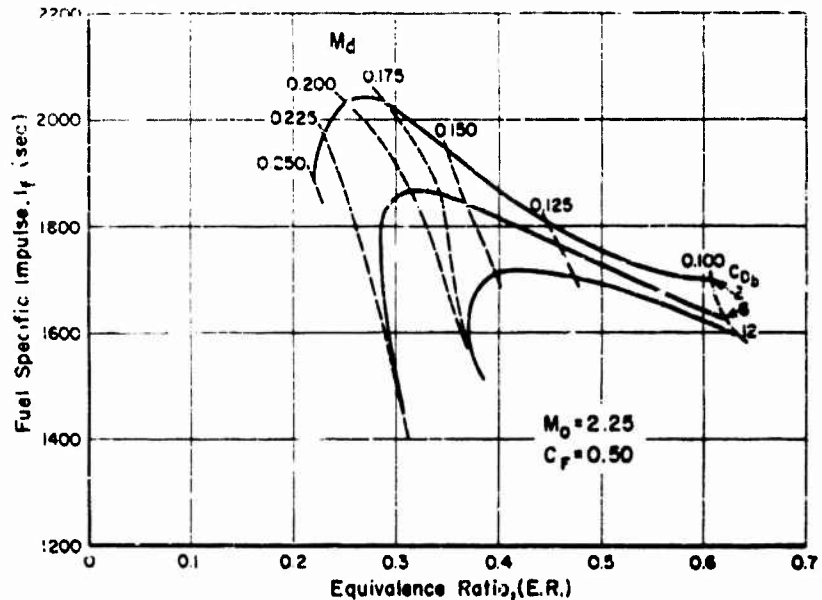


Fig. 62 Effect of Burner Drag and Equivalence Ratio on Fuel Specific Impulse, $\eta_d = 0.7$

The design of an engine for optimum fuel specific impulse with expansion of exit gases to ambient pressure instead of to the fixed nominal engine area would differ only in regard to the selection of the proper value of the area ratio (A_e/A_2) which fixes the exit Mach number. Since μ is needed to obtain the ratio of the throat to combustor area, an approximate value must first be employed to obtain a value for the latter, since changes of μ affect the design less than changes in (A_c/A_2). One may now proceed to determine other features of the engine design that depend on the desired thrust. For example, the exit Mach number may be obtained from

$$(A/A^*)_e = \mu \frac{A_2}{A_c}, \quad (133)$$

and the exit pressure from

$$\frac{P_e}{P_0} = \frac{(A_1/A_2)}{\mu} (S_a/\sqrt{T_{t0}}) \frac{\theta(M)_e (P/P_t)_e}{(f/P_t)_e} \quad (134)$$

The quantities (A_c/A_2) , and $(A_1/A_2)(S_a/\sqrt{T_{t0}})$ were found when the optimum design for selected values of C_F , M_G , and μ was being established. The value of t_0 is found from $(A/A^*)_c$ by means of Eq. (133), and it is used to evaluate the functions of M_e in Eq. (134). The value of (P_e/P_0) is not likely to turn out to be exactly 1.0, corresponding to the case $P_e = P_0$; if $P_e > P_0$, the further expansion required points to the need to select a larger value of μ ; likewise, if $P_e < P_0$, a smaller value of μ is required. A second more accurate trial value of μ , μ' , may then be derived by computing the exit total pressure P_{te} , using values found for M_e , $\theta(M)_e$, and (A_1/A_2) :

$$P_{te} = P_0 \frac{(A_1/A_2)(S_a/\sqrt{T_{t0}}) \theta(M)_e \frac{Q}{\mu}}{(f/P_t)_e} \quad (135)$$

Having found P_{te} from this equation, one may next compute (P_0/P_{te}) to yield the exit Mach number M'_e for nozzle expansion down to atmospheric pressure. This value of M'_e also yields $(A/A^*)'_e$, the new value for (A_e/A_c) , and the corresponding value of μ' is then derived from this by multiplying by (A_c/A_2) , so that

$$\mu' = (A/A^*)'_e (A_c/A_2) \quad (136)$$

These calculations are then repeated, using μ' to obtain a second approximation for (A_c/A_2) , (A_1/A_2) , etc. The calculations implicit in Eqs. (133) and (134) are repeated to determine whether the exit static pressure then matches the ambient value.

A question arises concerning the basis for a first estimate for μ , as it varies widely, ranging in value from a quantity of the order:

of unity for high thrust coefficient designs down to much lower values for low thrust designs. The wisdom of using exit areas larger than the combustion chamber is questionable since the gain in thrust on the downstream side of the nozzle is offset by the increased frontal drag produced by increasing the engine diameter from A_2 to A_e . Accordingly, the assumption of $\mu = 1$ is a reasonable first approximation.

Determination of an engine design to provide maximum thrust is in practice more straightforward than that shown in the preceding calculations since only the maximum value of $(S_a / \sqrt{T_{t_0}})$ need be considered. In cases of low burner drag, the engine air flow will be at a maximum, corresponding to sonic discharge from the combustion chamber without an exit nozzle. The calculation proceeds from the momentum balance across the combustion chamber, starting with $M_b = 1$, and $(S_a / \sqrt{T_{t_0}})$ at a maximum; inserting these values into Eq. (135) enables one to determine M_2 . The inlet area ratio is then found from M_d , the diffuser total pressure efficiency, and the weight flow relationship, Eq. (129). Exit and inlet force coefficients may now be computed, and their difference is then the desired thrust coefficient. If the combustor drag is high, it will be found that substantially as much thrust will be obtained using a slightly convergent-divergent exit nozzle ($A_c/A_2 = 0.94$, say) as with an unstricted combustion chamber -- in addition to better fuel economy.

6.2 Typical Results of Engine Optimization Calculations

The procedure outlined in the preceding section has been carried out for some engine design cases of general interest. The approach chosen has been to investigate first the dependence of Mach number on the engine fuel specific impulse. This has then provided a basis for the selection of the design flight speed when it was combined with experimental test data on the parameter of diffuser efficiency as a function of flight Mach number. Other engine performance parameters such as thrust coefficient, burner drag, combustion efficiency, and exit nozzle efficiency may be considered fixed since they are not dependent on the flight Mach number. The next stage of optimization is then

carried out at the selected flight speed and the corresponding available diffuser pressure recovery in order to determine the best compromise between combustion efficiency, burner drag, and exit nozzle efficiency. The study of the compromise between burner drag and exit nozzle efficiency versus combustion efficiency may be carried out most simply if one notes that the effect of combustion efficiency is to alter the amount of fuel to be burned--in an inverse relationship. Accordingly, the values of fuel specific impulse calculated for a combustion efficiency of 100 per cent may be adjusted to any lower combustion efficiency by increasing the fuel flow inversely with the decrease in combustion efficiency. This leads to a new value for the fuel specific impulse equal to the product of the fuel specific impulse for 100 per cent combustion efficiency and the actual combustion efficiency, and to a new optimum equivalence ratio equal to the quotient of the ideal equivalence ratio into the combustion efficiency.

A relationship between engine geometry and the fuel specific impulse is shown in Figs. 63, 64, and 65 for flight Mach numbers of 1.50, 2.25, and 3.50. (Figure 61 is here repeated for convenient reference as Fig. 64.) Equivalence ratio is plotted as the abscissa, and there is a simultaneous change of inlet area ratio (A_1/A_n) and exit nozzle throat size to maintain a constant thrust coefficient. The maximum or

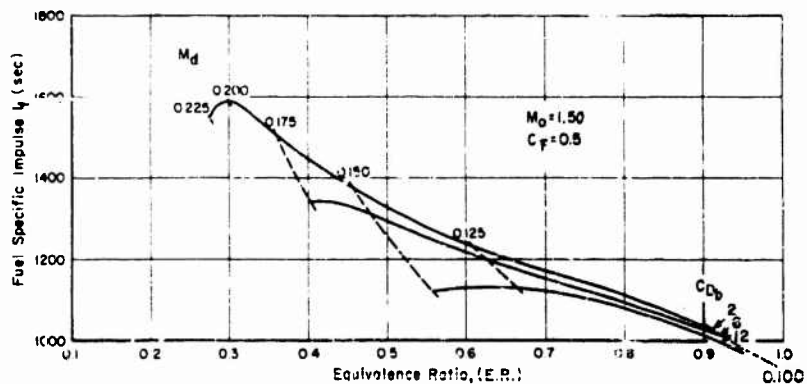


Fig. 63 Effect of Burner Drag and Equivalence Ratio on Fuel Specific Impulse, $\eta_d = 0.9$

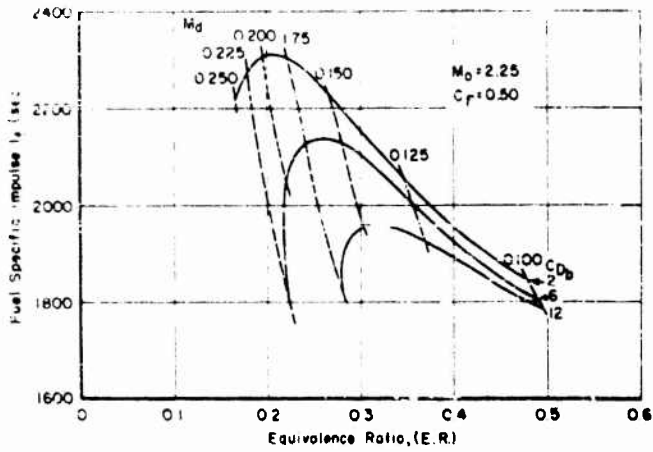


Fig. 64 Effect of Burner Drag and Equivalence Ratio on Fuel Specific Impulse, $\eta_d = 0.8$

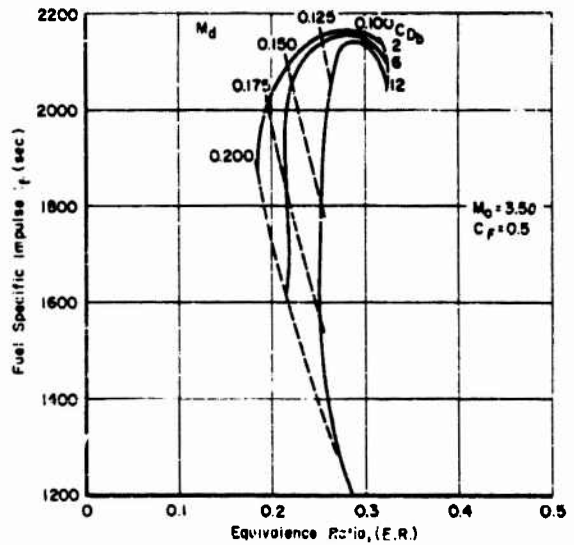


Fig. 65 Effect of Burner Drag and Equivalence Ratio on Fuel Specific Impulse, $\eta_d = 0.5$

this curve determines simultaneously the proper inlet and exit areas as well as the equivalence ratio for optimum performance. A set of such optimization calculations has been made using suitably selected values of diffuser recovery, and resulting values of optimum fuel specific impulse are plotted against the flight Mach number as the abscissa in Fig. 66. This figure is not complete without the insertion of a consideration of the recoveries actually achievable in practical diffusers.

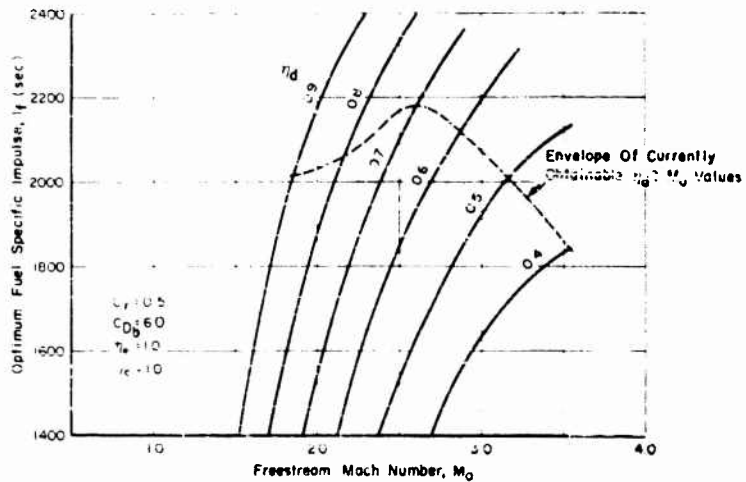


Fig. 66 Effect of Flight Mach Number and Diffuser Efficiency on Fuel Specific Impulse

Reference is made to Fig. 67 which shows conservative values for diffuser efficiency; these are incorporated in Fig. 66 to establish the proper relationship between the optimum fuel specific impulse and the flight Mach number. The fuel specific impulses shown in Fig. 66 were computed on the basis of an assumed exit nozzle efficiency of 100 per cent, a burner drag equal to 6 velocity heads, and 100 per cent combustion efficiency. An assumption of 100 per cent nozzle efficiency is, of course, somewhat optimistic; the burner drag figure is, however, a realistic one. (The combustion efficiency has no bearing on the

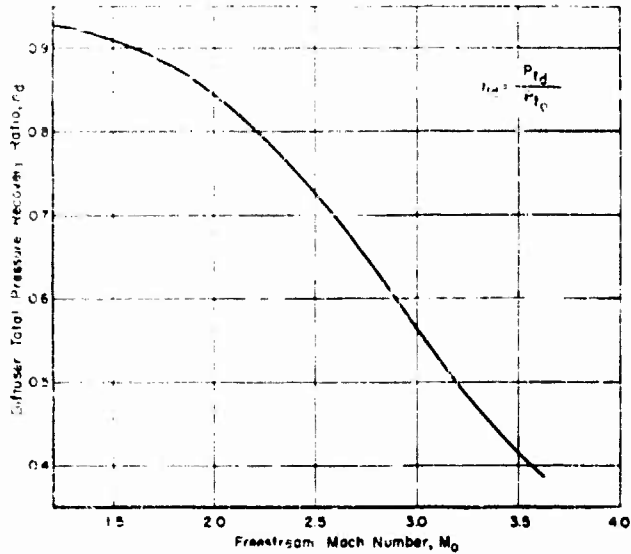


Fig. 67 Experimental Diffuser Recovery Ratios

location of the optimum as long as it can be considered constant.) On these assumptions the flight Mach number for optimum fuel specific impulse will be found to occur at a value of about 2.6. An analysis similar to the above may be performed using the more pessimistic value for the exit nozzle efficiency η_e of 0.67 in order to obtain an increase of exit nozzle thrust above that available from a sonic nozzle; the results of this calculation are presented in Fig. 68. A comparison of Figs. 66 and 68 shows that a loss of exit nozzle efficiency has a large detrimental effect on the magnitude of the available fuel specific impulse for a given diffuser efficiency and flight Mach number, but it does not alter appreciably the flight Mach number at which the optimum impulse is obtained.

The diffuser efficiency strongly affects both the optimum geometry and the operating equivalence ratio, as shown in Figs. 69 and 70. As the diffuser efficiency falls, the fuel specific impulse is optimized by reducing the diffuser air flow, as shown in Fig. 69, at the expense of greater combustor heat addition (Fig. 70) and increased

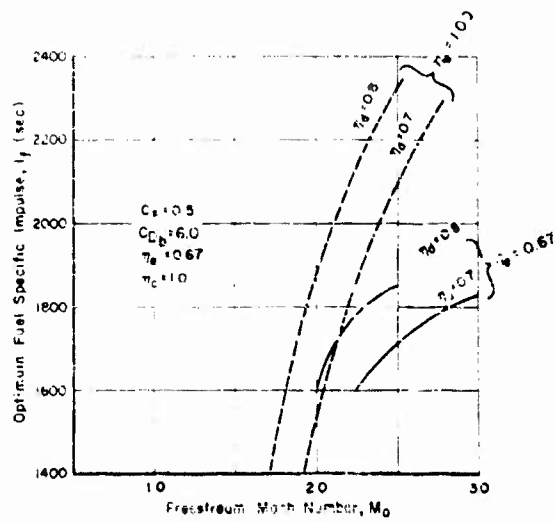


Fig. 68 Comparison of Fuel Specific Impulse on Different Exit Nozzle Efficiencies

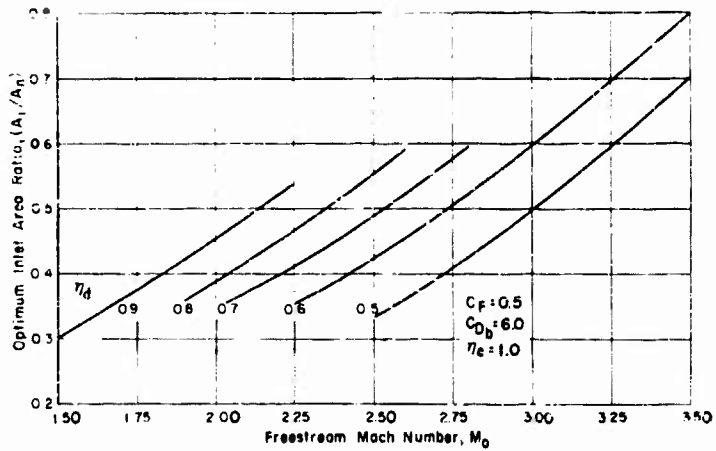


Fig. 69 Optimum Inlet Area Variation with Diffuser Efficiency and Freestream Mach Number

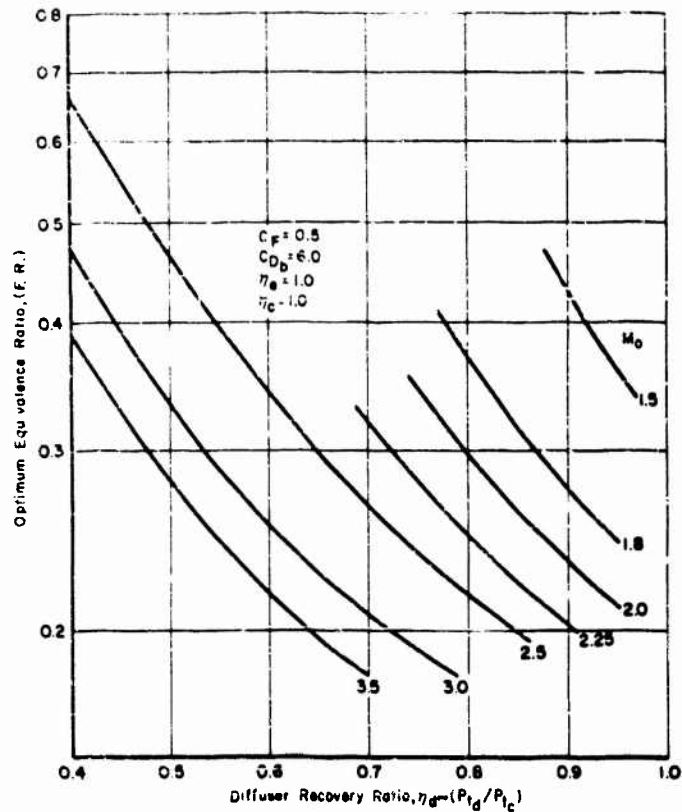


Fig. 70 Variation of Optimum Equivalence Ratio with Freestream Mach Number and Diffuser Efficiency

combustion losses. The effect of η_d on fuel specific impulse has been seen in Figs. 66 and 68. The burner drag losses have an effect similar to that of diffuser pressure losses except that they are related to the local combustion chamber inlet Mach number instead of to the freestream Mach number. Figure 71 shows the reduction of optimum fuel specific impulse with varying burner drag coefficient. The effect will be observed to be large at low flight Mach numbers (1.5 to 2.0) where the diffuser exit velocity head is a significant part of the total pressure loss, but at higher flight Mach numbers from 2.25 to 3.40, the diffuser total

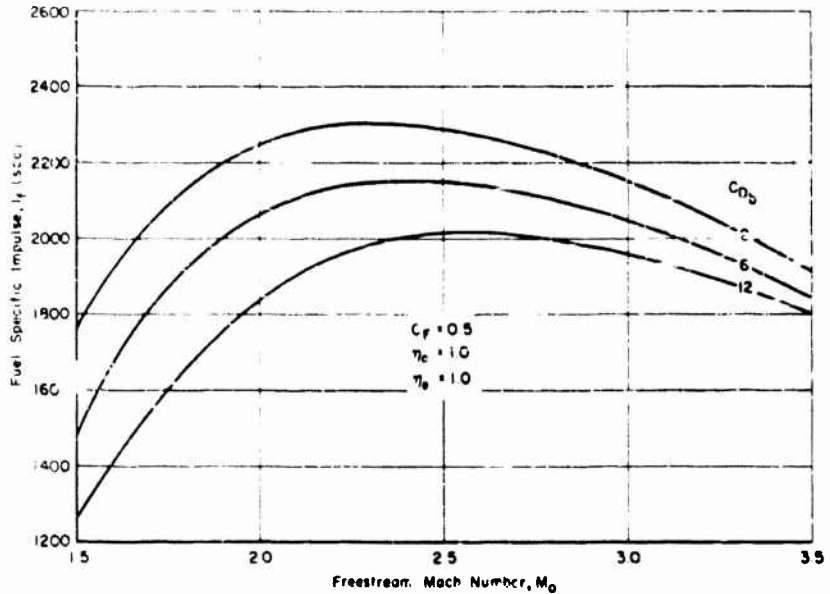


Fig. 71 Effect of Burner Drag on Fuel Specific Impulse

pressure losses increase considerably and so swamp the effect of burner drag. As the flight Mach number increases, the burner Mach number diminishes because of the greater density of the captured air, and internal drag losses are thereby reduced. Because of the relationship of internal drag losses to the diffuser exit Mach number, there is a marked shift of the optimum diffuser Mach number with combustor drag coefficient, as shown in Fig. 72. The overall efficiency in burners of high drag is improved if a lower diffuser Mach number is employed, i.e., the distribution of combustor aerodynamic and thermodynamic losses is readjusted to minimize the sum of these quantities.

The diffuser exit Mach number for optimum fuel specific impulse is relatively insensitive to changes in diffuser efficiency, exit nozzle efficiency, and thrust coefficient. This insensitivity arises from a self-adjusting feature associated with the diffuser and combustor geometry. A reduction of diffuser efficiency, for instance, calls

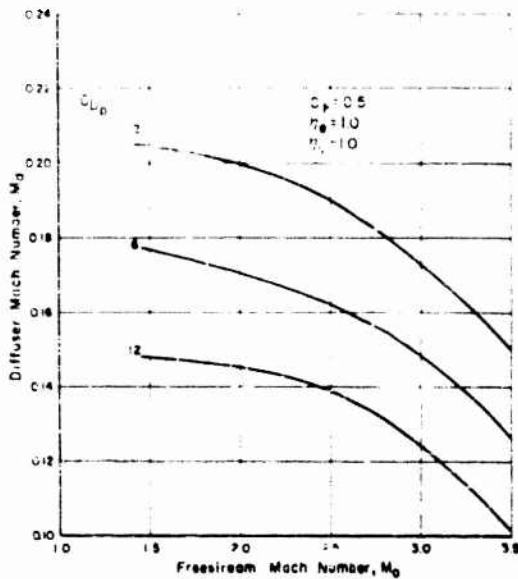


Fig. 72 Variation of Diffuser Mach Number with Burner Drag for Optimum Fuel Specific Impulse

for a lessened capture area ratio which, through the resultant increase in the ratio of diffuser exit to inlet area, offsets the lower pressure recovery and brings the air essentially to a constant Mach number in the diffuser. Similarly, variations in exit nozzle efficiency and design thrust coefficient principally affect the design of the exit nozzle and combustor, together with the value of the over-all specific impulse. This variation of the impulse with exit nozzle efficiency is shown for over-all nozzle efficiencies of 0.975 and 0.950 in Fig. 73 for engines of optimized geometry. The ratio of the impulse loss to the loss of exit momentum is nearly constant with flight Mach number, but the proportion of the former loss becomes greater at the lower specific impulses obtained at lower flight speeds. The fuel flow and the equivalence ratio increase inversely with the change in fuel specific impulse. Exit nozzle efficiency, as explained earlier, is a function of the divergence angle and the exit to throat area ratio. Subsonic and sonic nozzles achieve nearly theoretical values of exit momentum because of their relative uniformity of flow and the absence of flow divergence. Since a supersonic nozzle of fixed length will approach

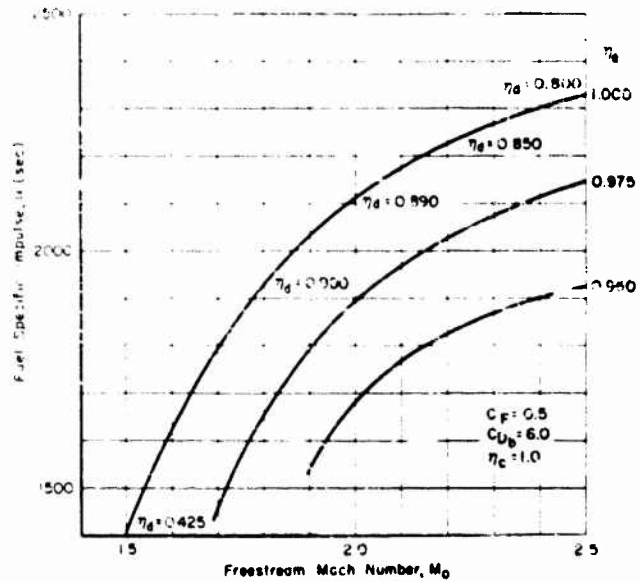


Fig. 73 Effect of Exit Nozzle Efficiency on Optimum Fuel Specific Impulse

the ideal as the area ratio approaches unity, engine design optimization calculations involving such exit nozzles should employ a nozzle efficiency varying with the expansion ratio. A fair approximation to this situation was obtained in the calculations for Figs. 66 and 68 by assuming that the increase of exit momentum above the sonic value for the exit stream was a constant fraction of the ideal. Since the exit momentum is $S_a \psi \theta(M)_{eff}$ and the sonic value is $S_a \psi_a$, the approximation takes the form

$$\theta(M)_{eff} = 1 + [\theta(M)_{ideal} - 1] \eta_e \quad (137)$$

An increase in the value of the design thrust coefficient leads to an increase in the combustion temperature and exit nozzle area, and a fall in the over-all fuel specific impulse with only a slight effect on the optimum diffuser exit Mach number which therefore increases

proportionally at the rate of about only one-tenth of that of the thrust change. The effect of increasing the thrust coefficient on fuel specific impulse and equivalence ratio for three different flight Mach numbers, 1.8, 2.5, and 3.5, is shown in Fig. 74; these curves cover likely regions of thrust and flight speed operation with likely values of diffuser recovery, burner drag, and exit nozzle efficiency. Similar effects occur at other flight speeds.

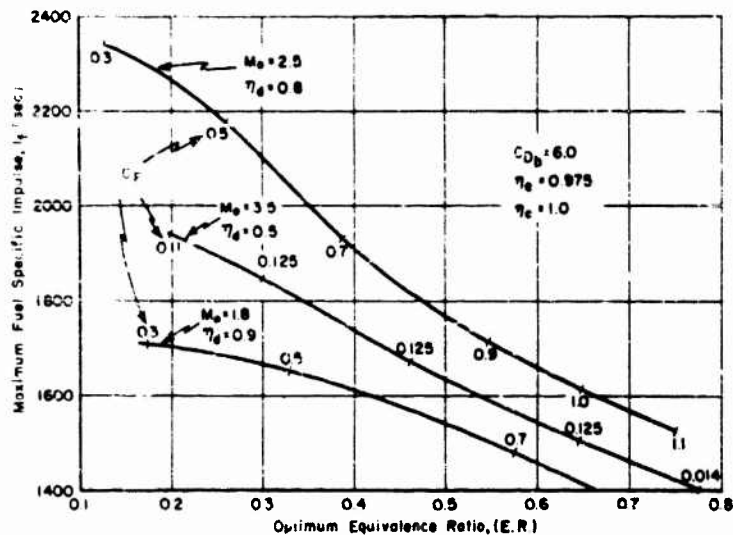


Fig. 74 Effect of Thrust Coefficient on Fuel Specific Impulse and Optimum Equivalence Ratio

In conclusion, it may be said that the most straightforward way of arriving at an optimum engine design configuration is first to assign probable values to the various component performance parameters for use in the indicated calculations. The latter are then repeated using upper and lower limit values in the case of components of uncertain performance in order to determine the variation of optimum proportions and performance within this possible component variation. By this means, one is able to weigh the net performance gains to be made by optimization of one component at the expense of another.

APPENDIX

Tabulation of Mach Number Functions

The flow relationships involving Mach number also involve the value of γ (which decreases with temperature for any given gas, at least up to 5000°F, at all pressures except the lowest), but a change in γ from, say, 7/5 to 9/7 produces a change of only a few per cent in most Mach number functions at any particular value of the Mach number. (The area function (A/A^*) is particularly sensitive to a variation in γ at the higher values of M however.) The Mach number functions tabulated below are presented for comparison at these two values, since they give simple whole number values for such exponents as $\frac{2\gamma}{\gamma-1}$, $\frac{2}{\gamma-1}$, $\frac{\gamma+1}{2(\gamma-1)}$, etc., as indicated in Section 2; these values are respectively 9, 7, and 4 for $\gamma = 9/7$. The value 7/5 corresponds to air at low temperatures (0-500°F), while $\gamma = 9/7$ corresponds to the products of combustion of fuel and air mixtures at more elevated temperatures (about 4000°F). The set of Mach number functions for $\gamma = 7/5$ may thus be used to describe flow into a combustion system, while those for $\gamma = 9/7$ describe flow out of a combustion system. For low heat releases, however, it may be more appropriate to use the 7/5 value for both such streams.

The functions listed below are intended to be uniform with Refs. 22 and 23 and the present text. Other tabulations may be found in Ref. 21 and in some texts listed in the Bibliography. Quantities are all dimensionless unless otherwise stated. Figures A-1 through A-17 illustrate the variation with Mach number of the various functions for values of the latter up to 5. (It has not seemed worthwhile to extend the relationships beyond this value owing to the need to incorporate real gas effects at higher Mach numbers.) To avoid confusion with the curve of (T_t/T_t^*) , the function (ρ_t^*/ρ_t) has been plotted separately. Constant specific heat values are assumed in the derivations.

Appendix: Mach Number Functions

| Function | Units | Plotted in Fig. | Derived in Eq. |
|---|--|-----------------|----------------|
| $K = 1 + \frac{\gamma - 1}{2} M^2$ | - | A-1 | 12 |
| <u>Isentropic</u> | | | |
| $P/P_t = K^{-\frac{\gamma}{\gamma-1}}$ | - | A-2 | 16 |
| $\rho/\rho_t = K^{-\frac{1}{\gamma-1}}$ | - | A-3 | 17 |
| $T/T_t = K^{-1}$ (also across shock wave) | - | A-4 | 13 |
| $f/P = 1 + \gamma M^2 = 1 + \frac{2q}{P}$ | - | A-5 | 59 |
| $f/P_t = (1 + \gamma M^2) K^{\frac{\gamma}{\gamma-1}}$ | - | A-6 | - |
| $\theta(M) = \gamma/\gamma^* = \frac{1 + \gamma M^2}{M \sqrt{2(1 + \gamma) K}}$ | - | A-7 | 68 |
| $\omega = gM \left[\frac{\gamma K}{R} \right]^{1/2}$ | sec ⁻¹ (^o R) ^{1/2} | A-8 | 24 |
| $\frac{P}{P_t} \omega = gM \left[\frac{\gamma}{R} \right]^{1/2} K^{-\frac{\gamma+1}{2(\gamma-1)}}$ | sec ⁻¹ (^o R) ^{1/2} | A-9 | 26 |
| $q/P = \frac{\gamma}{2} M^2$ | - | A-10 | - |
| $A/A^* = \frac{1}{M} \left(\frac{K}{K^*} \right)^{\frac{\gamma+1}{2(\gamma-1)}}$ | - | A-11 | 20 |

| Function | Units | Plotted in Fig. | Derived in Eq. |
|---|-------|--------------------|-------------------|
| <u>Normal Shock (Adiabatic)</u> | | | |
| $M_2^2 = \frac{2K_1}{2\gamma M_1^2 - \gamma + 1}$ | - | A-12 | 37 |
| $\frac{P_1}{P_{t2}} = \frac{1}{K^* M_1^2} \left[\frac{2\gamma M_1^2 - \gamma + 1}{2 K^{*2} M_1^2} \right]^{\frac{1}{\gamma-1}}$ | - | A-13 | 43 |
| $\frac{P_{t2}}{P_{t1}} = \frac{K^* M_1^2}{\frac{\gamma}{K^{\gamma-1}}} \left[\frac{2 K^{*2} M_1^2}{2\gamma M_1^2 - \gamma + 1} \right]^{\frac{1}{\gamma-1}}$ | - | A-14 | - |
| <u>Diabatic</u> | | | |
| $\frac{P}{P^*} = \frac{1 + \gamma}{1 + \gamma M^2}$ | - | A-15, A-16 | 51 |
| $\frac{P_t}{P_t^*} = \frac{1 + \gamma}{1 + \gamma M^2} \left[\frac{K}{K^*} \right]^{\frac{\gamma}{\gamma-1}}$ | - | A-15, A-16 | 52 |
| $\frac{T}{T^*} = \frac{M^2(1 + \gamma)}{(1 + \gamma M^2)^2}$ | - | A-15, A-16 | 53 |
| $\frac{T_t}{T_t^*} = \frac{2 M^2 \times (1 + \gamma)}{(1 + \gamma M^2)^2}$ | - | A-15, A-16 | 54 |

$$\frac{V}{V^*} = \frac{c^*}{c} = \frac{M^2(1+\gamma)}{1+\gamma M^2} \quad - \quad \begin{array}{l} \text{A-15,} \\ \text{A-16} \end{array} \quad 55$$

$$\frac{\rho_t^*}{\rho_t} = \frac{M^2(1+\gamma)}{1+\gamma M^2} \left[\frac{K^*}{K} \right]^{\frac{\gamma}{\gamma-1}} \quad - \quad \text{A-17} \quad 56$$

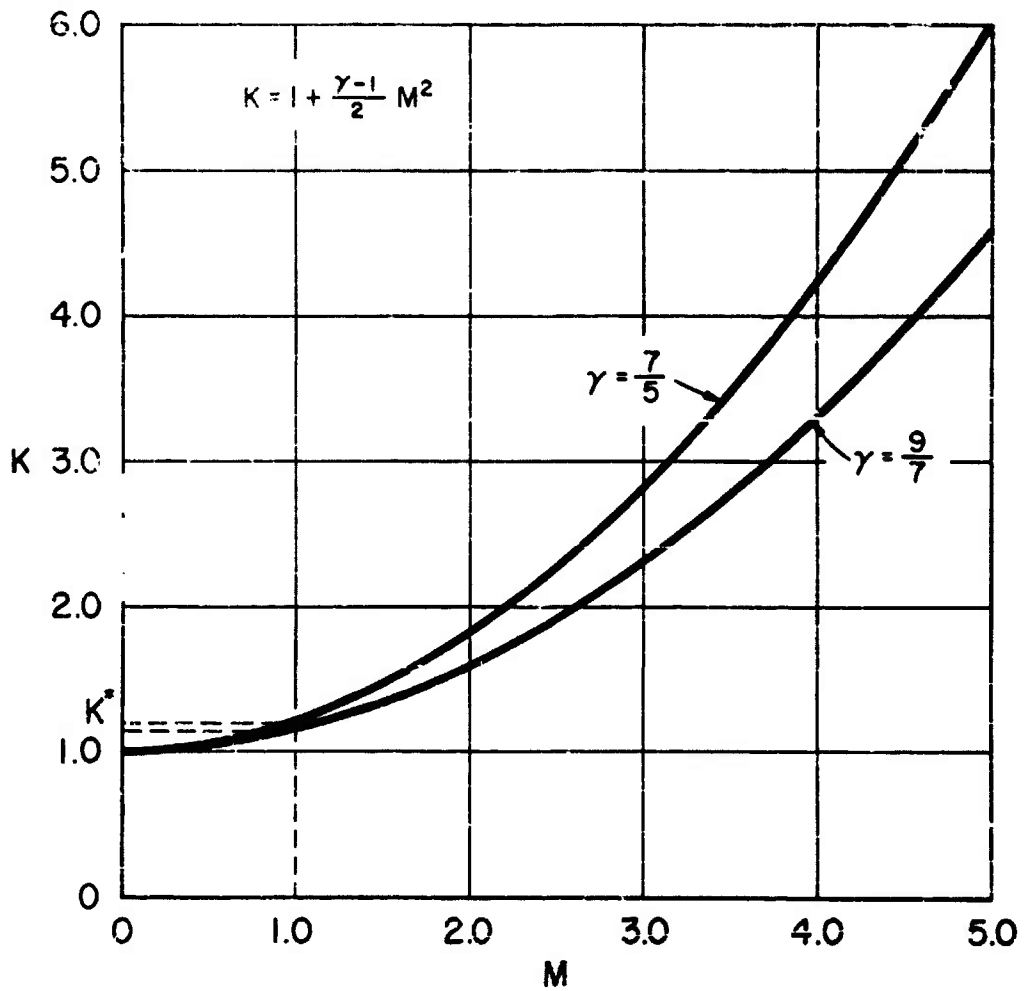


Fig. A-1

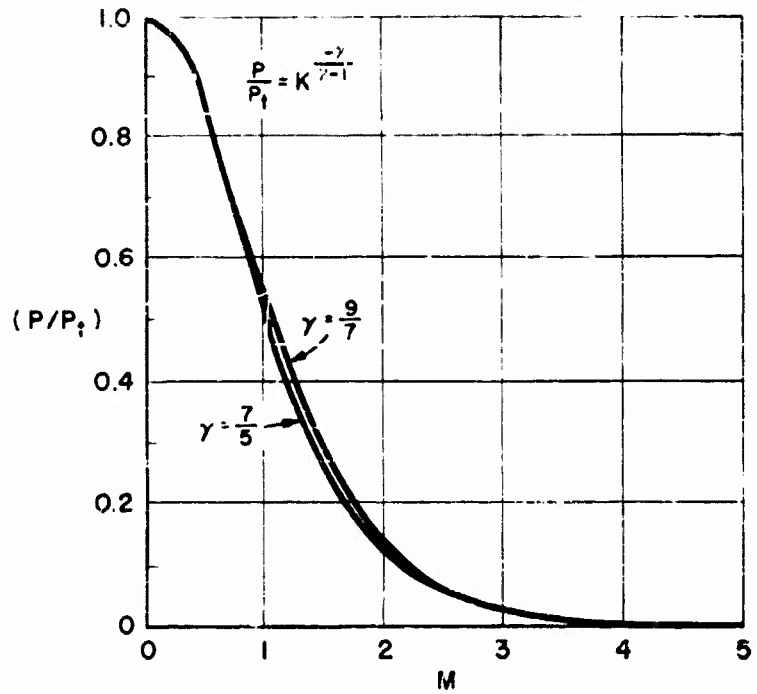


Fig. A-2

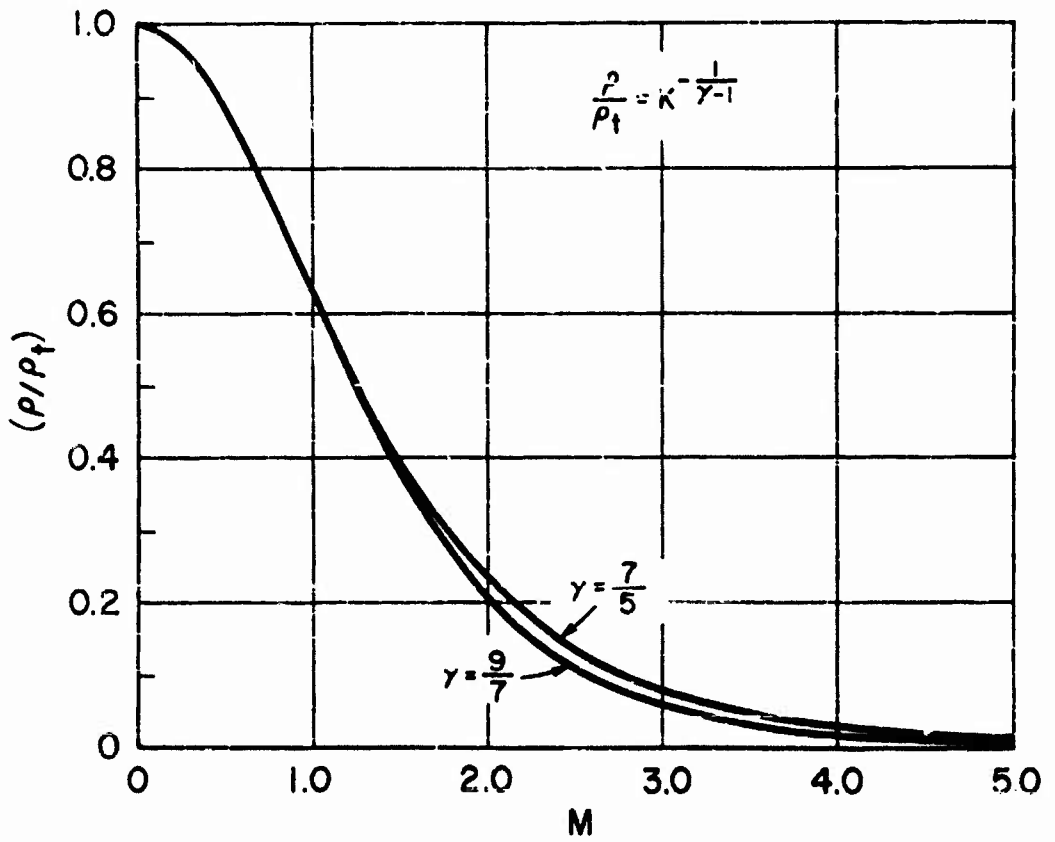


Fig. A-3

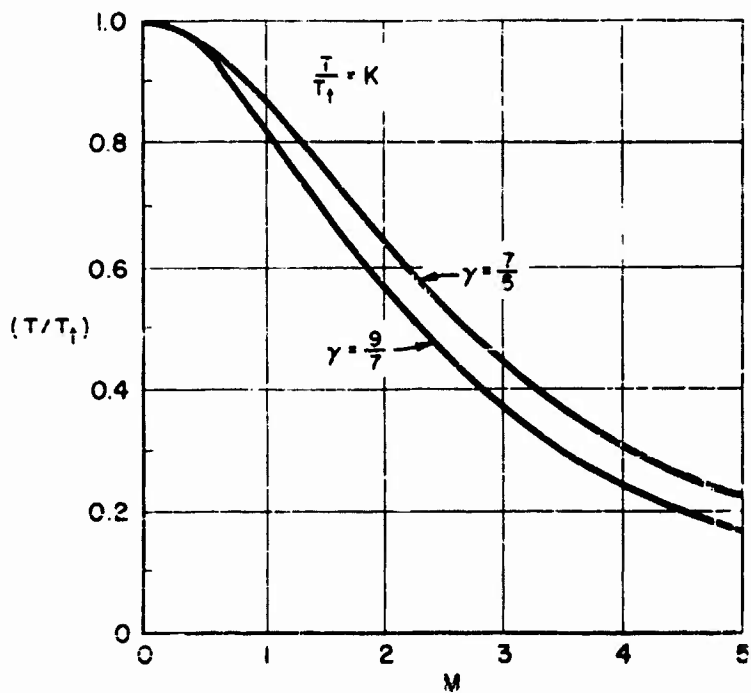


Fig. A-4

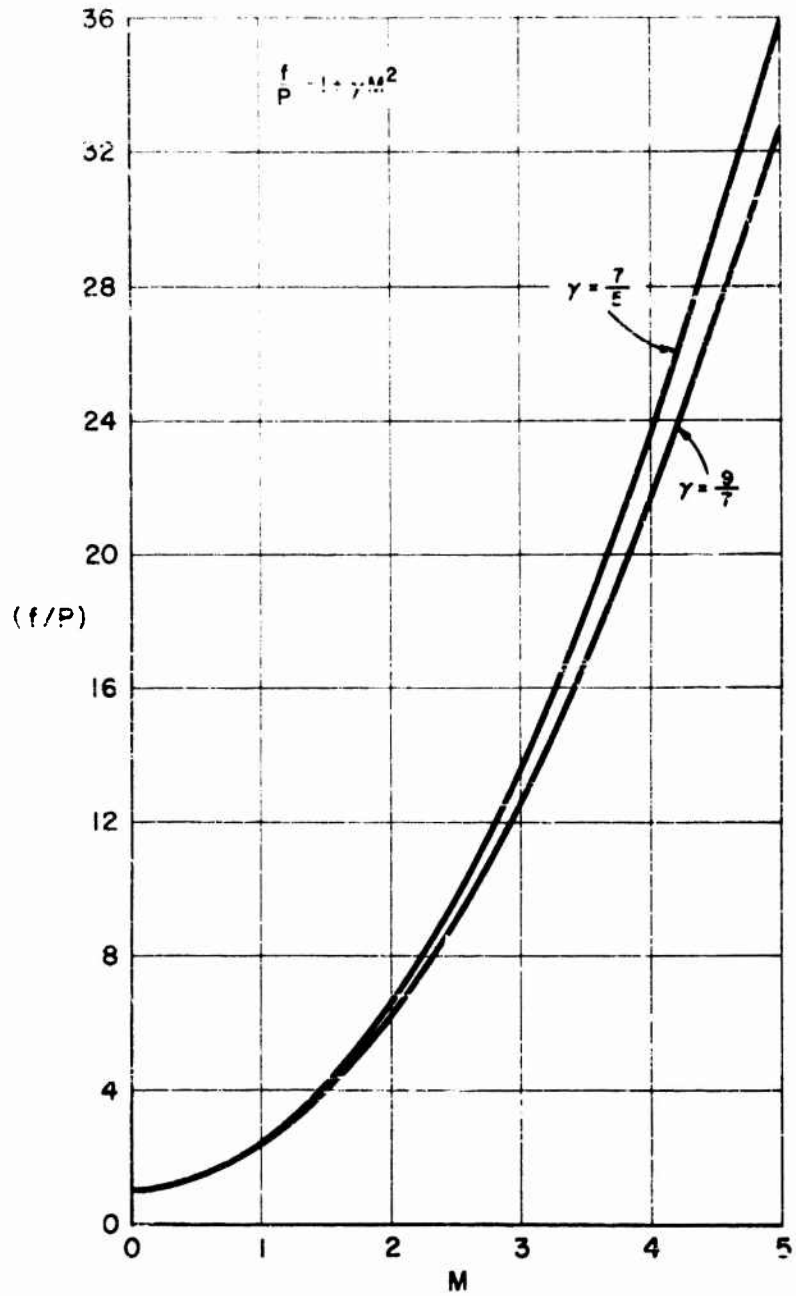


Fig. A-5

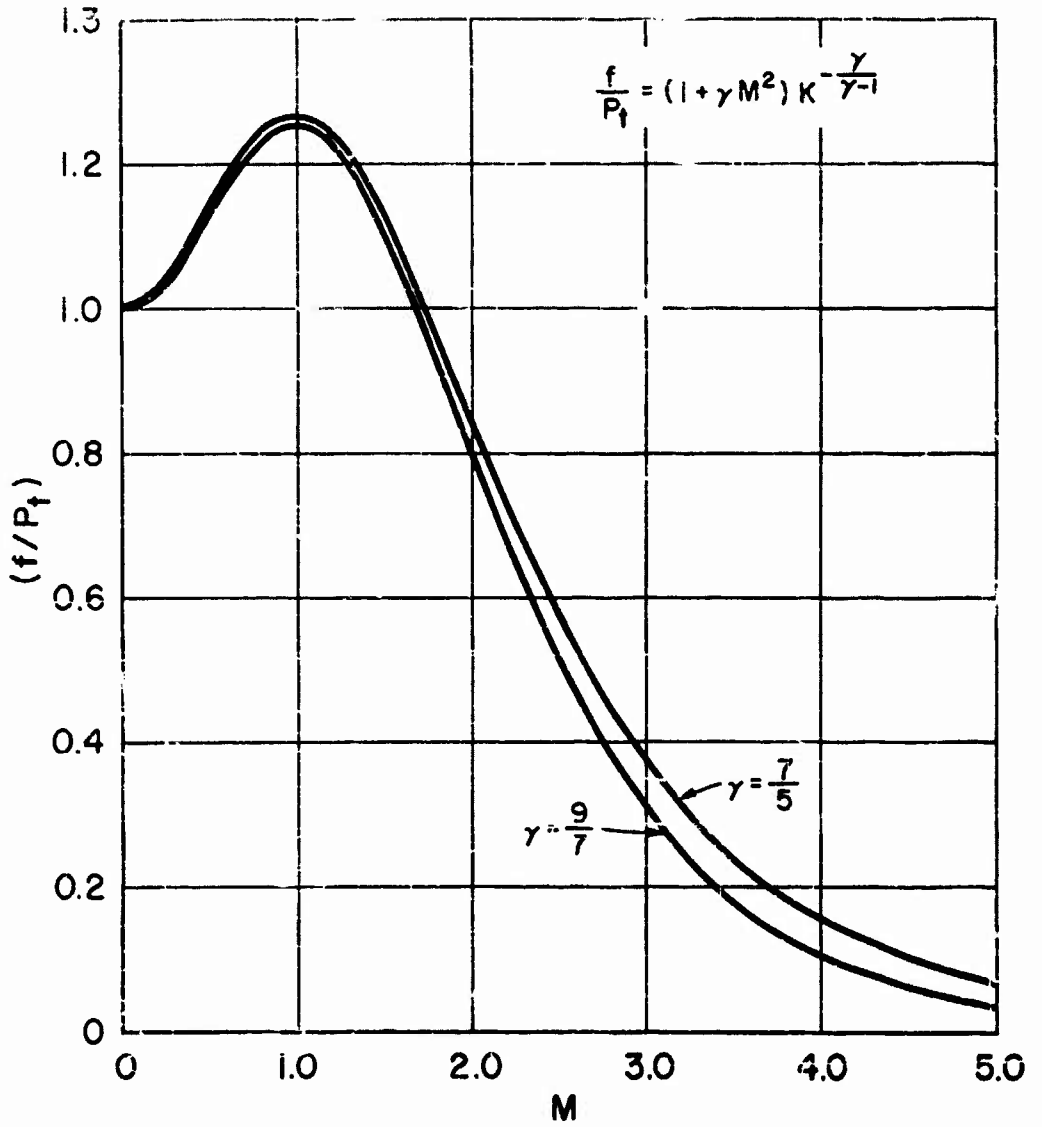


Fig. A-6

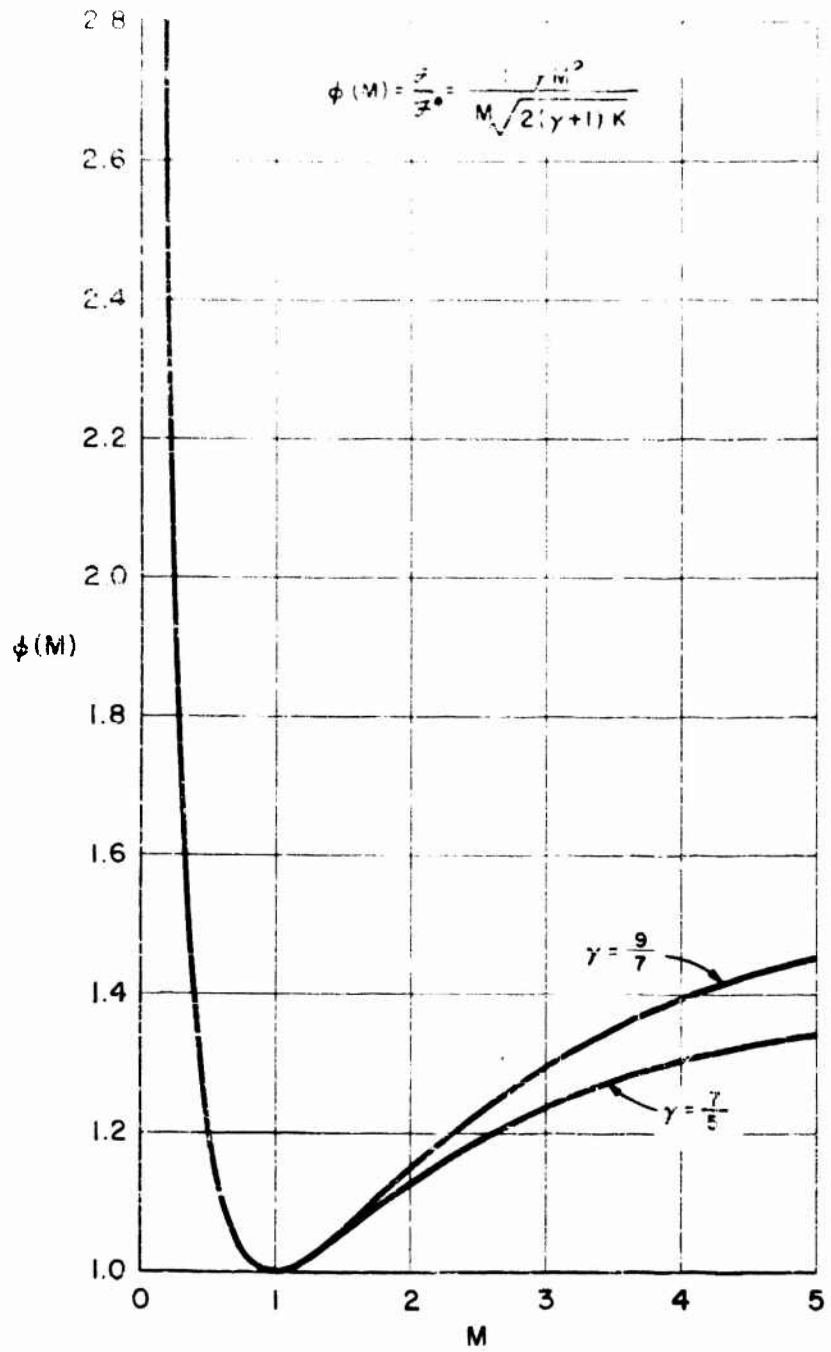


Fig. A-7

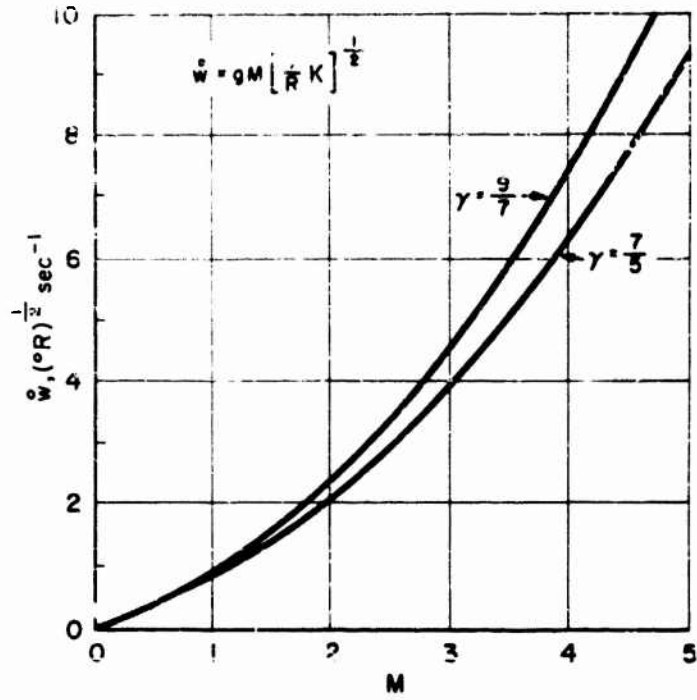


Fig. A-8

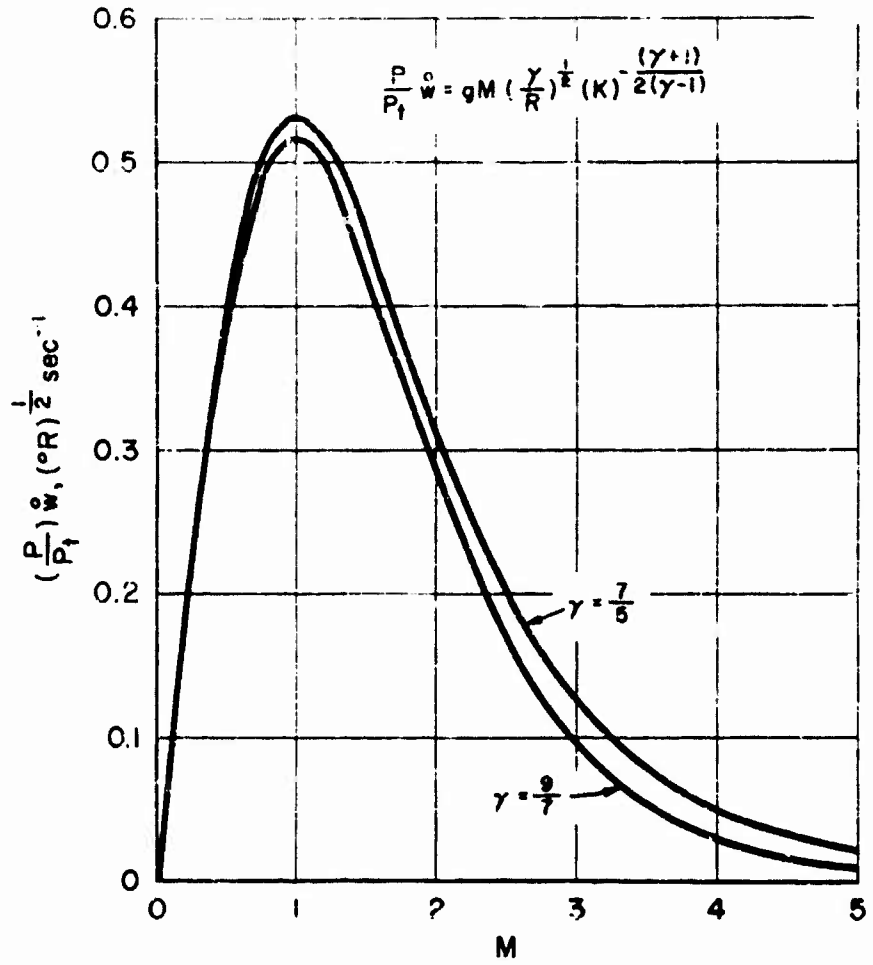


Fig. A-9

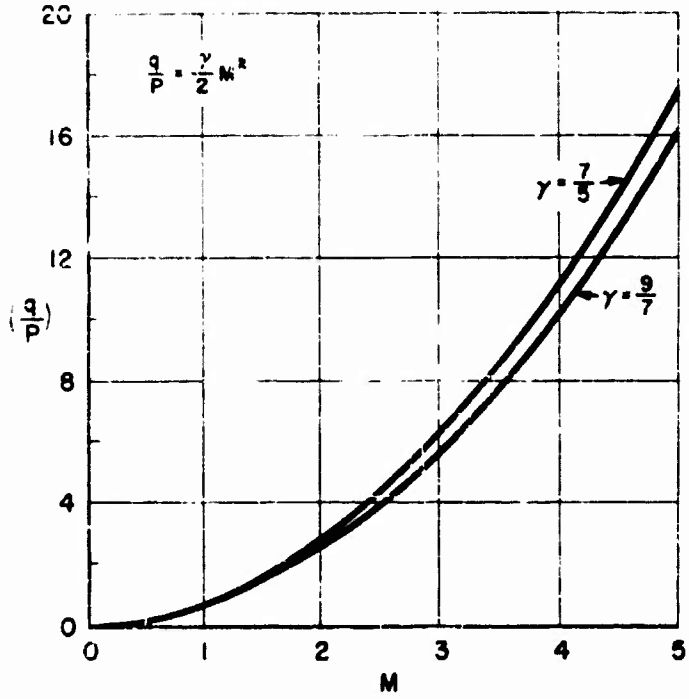


Fig. A-10

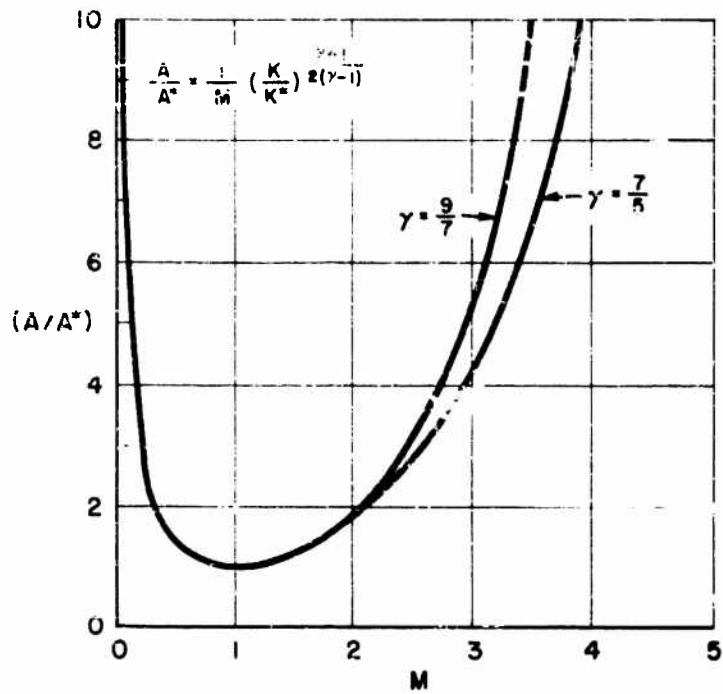


Fig. A-11

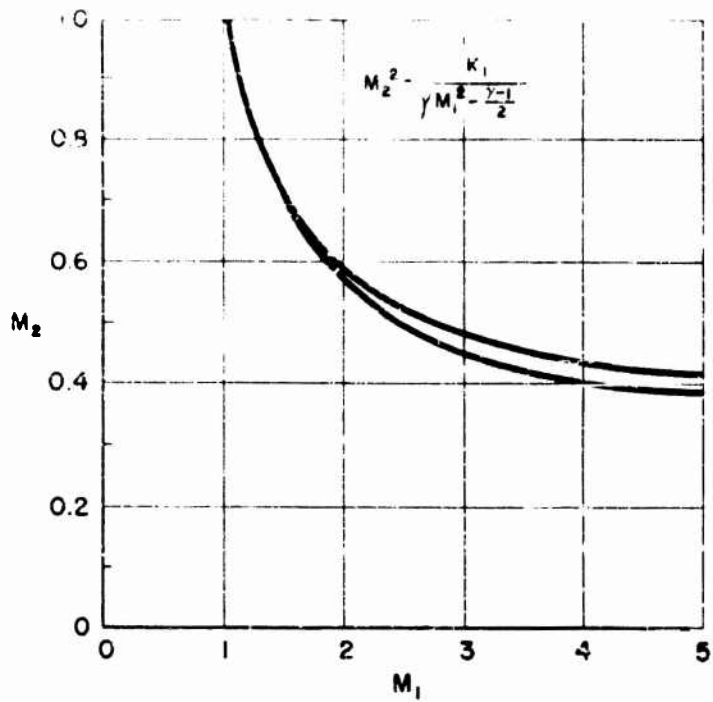


Fig. A-12

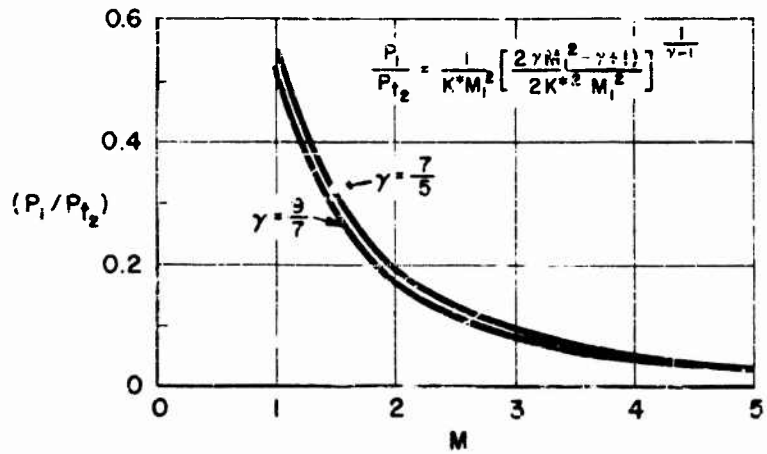


Fig. A-13

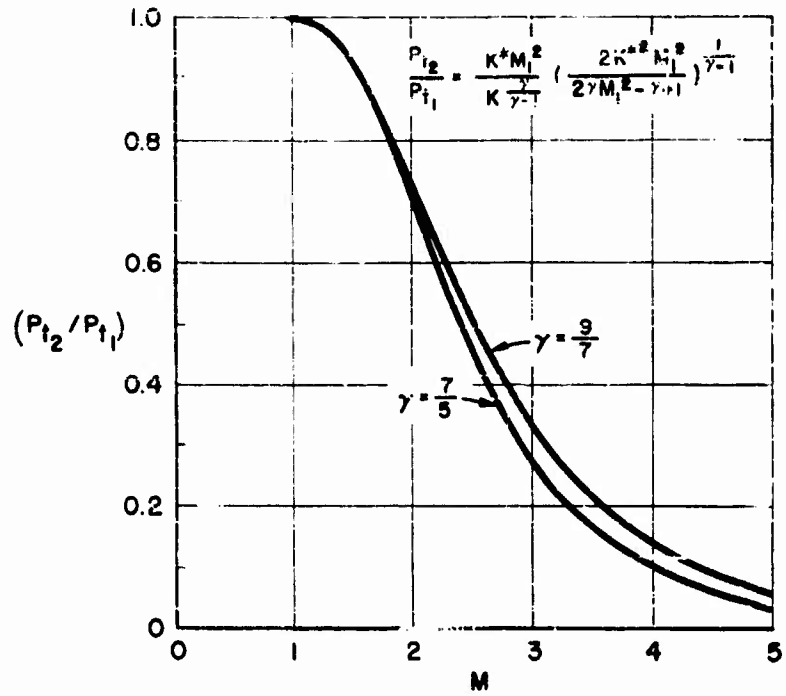


Fig. A 14

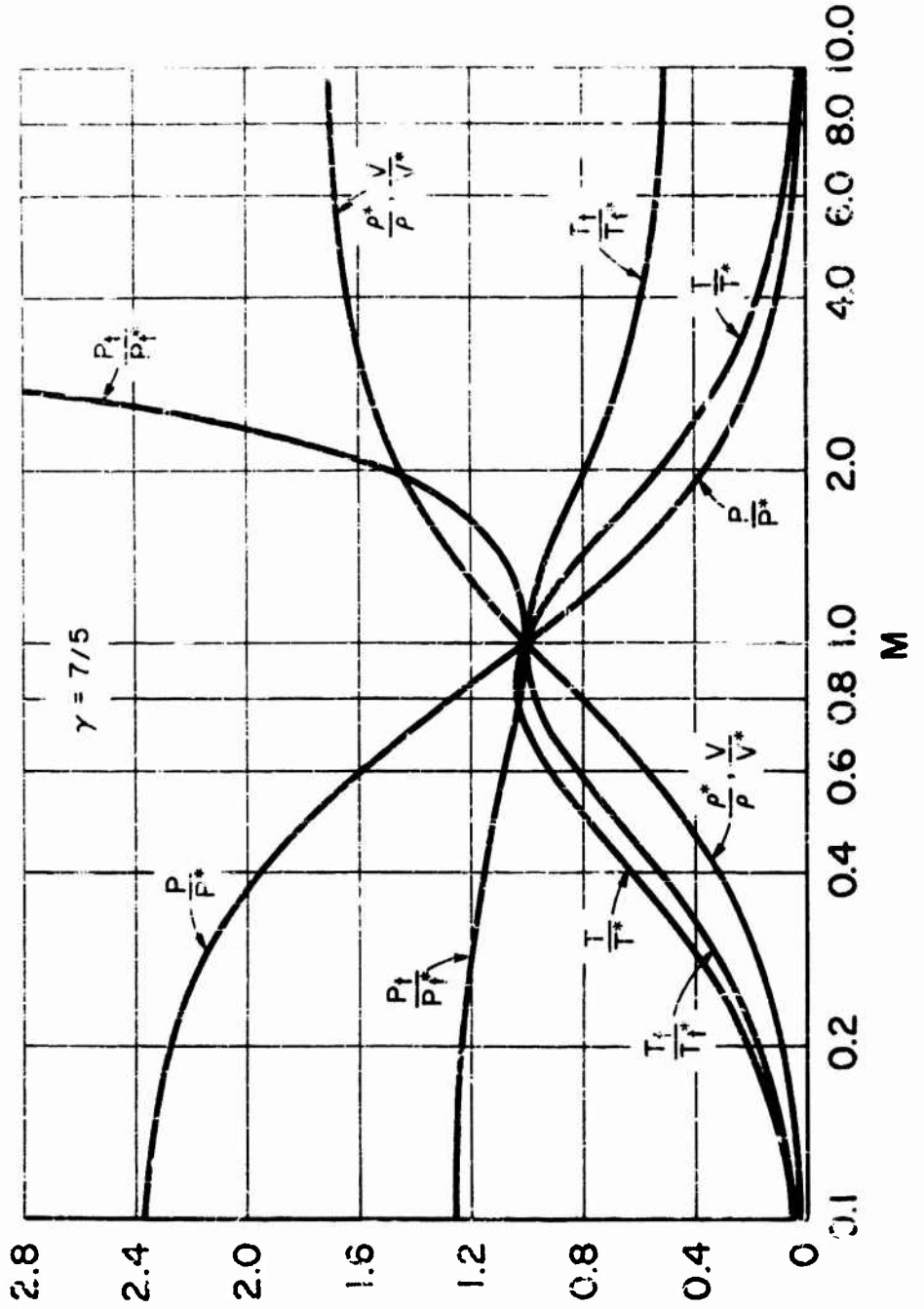


Fig. A-15

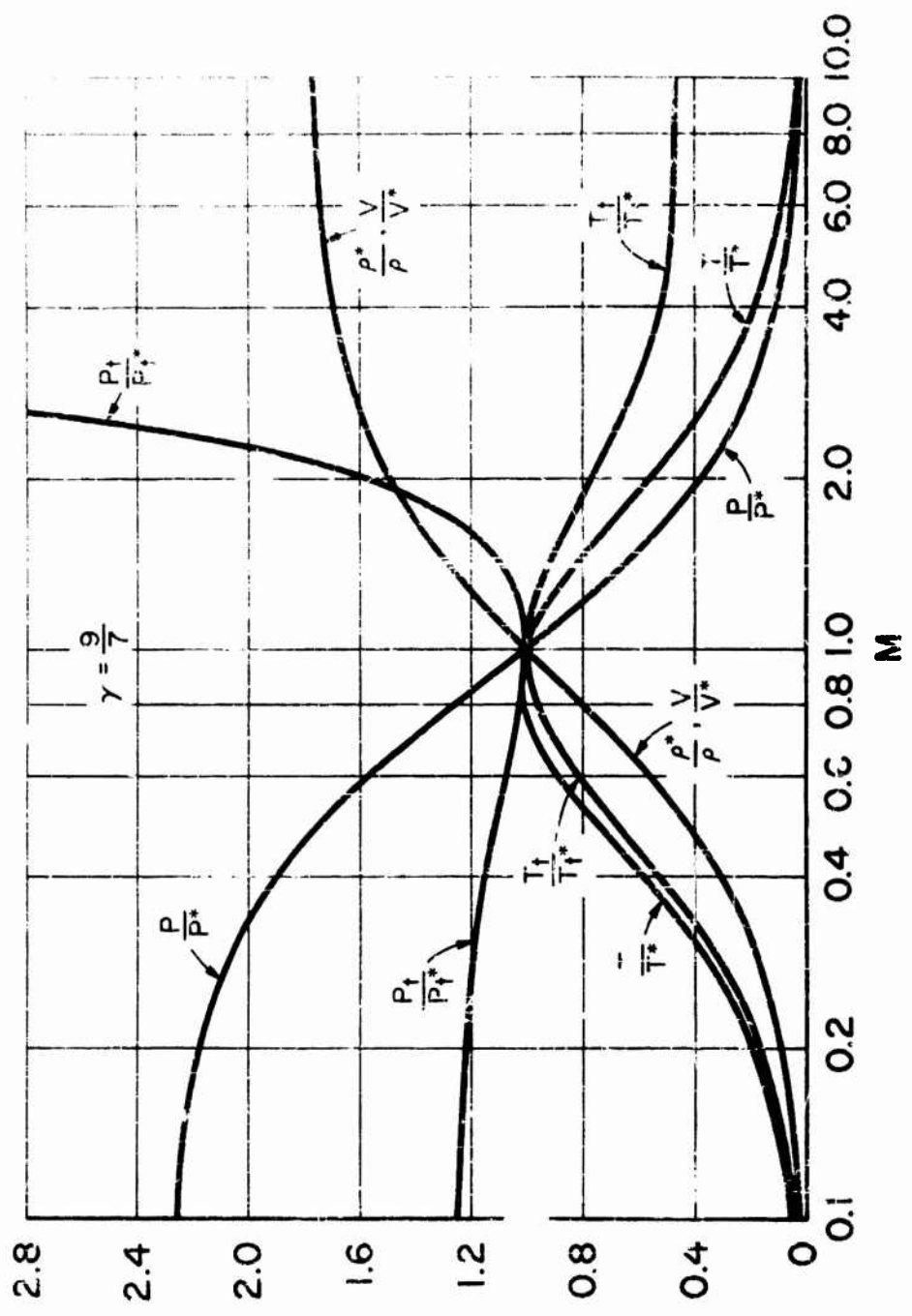


Fig. A-16

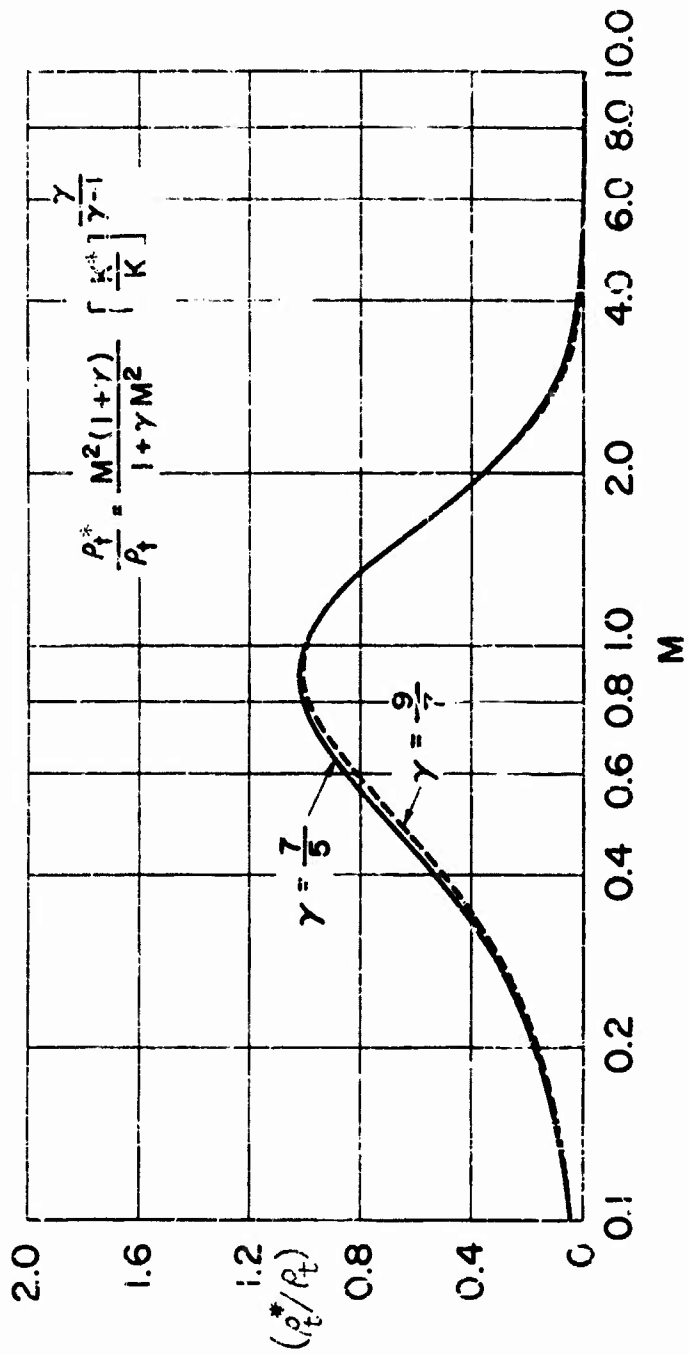


Fig. A-17

REFERENCES

1. C. F. Hansen, Approximations for the Thermodynamic and Transport Properties of High-Temperature Air, NASA TR R-50, 1959.
2. W. D. Hayes and F. F. Probst. Hypersonic Flow Theory, New York, Academic Press, 1959.
3. A. H. Shapiro, W. R. Hawthorne, and G. M. Edelman, The Mechanics and Thermodynamics of Steady One-Dimensional Gas Flow with Tables for Numerical Solutions, M. I. T., Meteor Report No. 14, December 1, 1947.
4. A. H. Shapiro, K. R. Wadleigh, B. D. Gavril, and A. A. Fowle, The Aerothermopressor, A Device for Improving the Performance of a Gas Turbine Power Plant, M. I. T., Gas Turbine Laboratory, 1955.
5. P. Rudnick, Momentum Relation in Propulsive Ducts, J. Aero. Sci., 14, 540 (1947).
6. D. E. Wilcox, A. Weir, J. A. Nicholls, and R. Dunlap, Location of Mach Discs and Diamonds in Supersonic Air Jets, J. Aero. Sci., 24, 150 (1957).
7. R. J. Weber and J. S. Mackay, An Analysis of Ramjet Engines Using Supersonic Combustion, NACA Tech. Note No. 1386, 1958.
8. R. A. Gross, Research on Supersonic Combustion, Amer. Rock. Soc. J., 29, 63 (1959).
9. J. A. Nicholls, E. K. Dabora, and R. L. Gealer, Studies in Connection with Stabilized Gaseous Detonation Waves, Seventh Symposium (International) on Combustion, London and Oxford, Butterworths Scientific Publications, 1959. Also, J. A. Nicholls, Stabilized Gaseous Detonation Waves, Amer. Rock. Soc. J., 29, 607 (1959).
10. R. G. Dorsch, J. S. Serafini, E. A. Fletcher, and I. I. Pintel, Experimental Investigation of Aerodynamic Effects of External Combustion in Airstream Below Two-Dimensional Wing at Mach 2.5 and 3.0, NASA Memorandum 1-11-59E, March 1959.
11. H. W. Woolard, Tables of Properties of some Oblique Deflagrations in Supersonic Flows, The Johns Hopkins University, Applied Physics Laboratory, TG-382, September 1960.
12. R. B. Pearce, Causes and Control of Power Plant Surge, Aviation Week, January 16, 1950.

13. Z. Kopal, Tables of Supersonic Flow About Cones, M. I. T., Tech. Report No. 1, 1947.
14. M. S. Bulkin, Theoretical and Experimental Investigation of Additive Drag, NACA RM E-51B13, 1951.
15. J. L. Zelinski, The Design of Combustors for Ramjet Engines (Confidential), The Johns Hopkins University, Applied Physics Laboratory, Bumblebee Report No. 233, 1959.
16. G. D. Dugger, Recent Advances in Ramjet Combustion, Amer. Rock. Soc. J., 22, 819, 1959.
17. General Electric Company, Cincinnati, Properties of Combustion Gases/System: $C_n H_{2n} - Air$, Vol. 1, Thermodynamic Properties, New York, McGraw-Hill, 1955.
18. R. P. Fraser, F. N. Rowe, and M. O. Couiter, Efficiency of Supersonic Nozzles for Rocket and Some Unusual Designs, Proc. I. Mech. Engineers, 171, 553 (1957).
19. F. Bader, Loss of Ramjet Thrust and Fuel Specific Impulse Through Non-Mixing of Exit Streams (Confidential), The Johns Hopkins University, Applied Physics Laboratory, CF-1386, January 1950.
20. A. C. Beer, An Analytical Approach to Ramjet Design Optimization, The Johns Hopkins University, Applied Physics Laboratory, Bumblebee Report No. 108, 1949.
21. Ames Research Staff, Equations, Tables and Charts for Compressible Flow, NACA Report No. 1135, 1953.
22. Ordnance Aerophysics Laboratory, Daingerfield, Texas, New Mach Number Tables for Ramjet Flow Analysis, $\gamma = 7/5$, $\gamma = 9/7$, Report No. CR-1798-A, 1955.
23. Handbook of Supersonic Aerodynamics, NAVORD Report 1488, Washington U. S. Government Printing Office.

BIBLIOGRAPHY

1. L. D. Landau and E. M. Lifshitz, Jet Propulsion Engines, Vol. XII of High Speed Aerodynamics and Jet Propulsion Series, Princeton, Princeton University Press, 1959.
2. M. M. Bondaruk and S. M. Il'yushenko, Ramjet Engines (in Russian), Moscow, State Publishing House of the Defense Industry, 1958.
3. M. J. Zucrow, Aircraft and Missile Propulsion, Vols. I. and II, New York, J. Wiley, 1958.
4. R. B. Dowd, Fundamentals of Advanced Missiles, New York, J. Wiley, 1958.
5. E. Howarth (Ed.), Modern Developments in Fluid Dynamics, High Speed Flow, London, Oxford University Press, 1953.
6. H. S. Liepmann and A. Roshko, Elements of Gas Dynamics, New York, J. Wiley, 1957.
7. D. Köchemann and J. Weber, Aerodynamics of Propulsion, New York, McGraw Hill, 1953.
8. E. A. Donney, M. J. Zucrow, and C. W. Besserer, Aerodynamics, Propulsion, Structures and Design Practice, in Principles of Guided Missile Design Series, New York, Van Nostrand, 1956.
9. J. Ruptash, Supersonic Wind Tunnels - Theory, Design and Performance, University of Toronto, Institute of Aerophysics, Rev. No. 5, 1952.
10. A. B. Cambel and B. H. Jennings, Gas Dynamics, New York, McGraw-Hill, 1958.
11. A. H. Shapiro, The Dynamics and Thermodynamics of Compressible Fluid Flow, New York, Ronald Press, 1953.
12. D. P. Spalding, Some Fundamentals of Combustion, New York, Academic Press, 1955.
13. V. S. Zuev and L. S. Skubachevskii, Combustion Chambers of Jet Engines (in Russian), Moscow, State Publishing House of the Defense Industry, 1958.
14. W. E. Emmons (Ed.), Fundamentals of Gas Dynamics, Vol. III of High Speed Aerodynamics and Jet Propulsion Series, Princeton, Princeton University Press, 1958.

ACKNOWLEDGEMENT

Much of the material presented in this Chapter has arisen as a result of the participation of the Applied Physics Laboratory in a program of guided missile research, and the authors acknowledge the assistance of many past and present members of the Laboratory in the compilation of this material; in particular, Dr. T. Davis and Mr. E. J. Hardgrave, Jr., who performed most of the analytical studies quoted, and Mr. G. Smoot, who calculated many of the other figures.

DISTRIBUTION

Distribution of this document is in accordance with a list on file in the Technical Reports Group of The Johns Hopkins University Applied Physics Laboratory.

NOTICE: When government or other drawings, specifications or other data are used for any purpose other than in connection with a definitely related government procurement operation, the U. S. Government thereby incurs no responsibility, nor obligation whatsoever; and the fact that the Government may have formulated, furnished, or in any way supplied the said drawings, specifications, or other data is not to be regarded by application or otherwise as in any manner licensing the holder or any other person or corporation, or conveying any right or permission to manufacture, use or sell any patented invention that may in any way be related thereto.